Silicone Nanofilaments as Functional Coatings:

Properties, Applications and Modifications

Dissertation

zur

Erlangung der naturwissenschaftlichen Doktorwürde

(Dr. sc. nat.)

vorgelegt der

Mathematisch-naturwissenschaftlichen Fakultät

der

Universität Zürich

von

Jan-Helge Zimmermann

aus

Deutschland

Promotionskomitee

Prof. Dr. Stefan Seeger (Vorsitz)

Prof. Dr. Marcus Textor

Prof. Dr. Heinz Berke

Prof. Dr. Jürg Osterwalder

Zürich, 2008

"He's the Antichrist!... Suspicion will slide off him like, like…whatever it is water slides off of"[1,2]

[1] A demon, in "Good Omens" by Terry Pratchet & Neil Gainman, HarperTorch, 1999.
[2] Which is no wonder considering that "the devil created the interface" (Pauli, 1920).

Acknowledgements

First and foremost I would like to thank Prof. Dr. Stefan Seeger for giving me the opportunity to carry out my thesis in his research group and for giving me the freedom to explore the exciting world of silicone nanofilaments.

Dr. Georg Artus I cannot thank enough for the invaluable help he provided throughout all aspects of my work and for the fruitful collaboration.

Dr. Stefan Jung I have to thank for discovering the silicone nanofilament coating and enabling me to expand on his work.

Prof. Dr. Heinz Berke, Prof. Dr. Jürg Osterwalder and Prof. Dr. Marcus Textor I thank for agreeing to supervise my work as part of the Promotionskomitee. I would especially like to thank Marcus Textor of the Laboratory for Surface Science and Technology at the ETH Zurich for providing the perspective of a "true" material scientist and for offering the capacity of his research group to assist me in my work.

Prof. Nicholas Spencer I would like to thank for the equally generous opportunity to collaborate with researchers in his group and allowing me to use some of the equipment in his labs.

The following researchers and students of the LSST I would like to thank for collaboration, animated discussions or generally making me feel welcome as a fellow material scientist in the Zurich community: Dr. Sara Morgenthaler, Dr. Lukas Bäuerle, Doris Spori, Dr. Venkataraman V. Nagaiyanallur, Mirjam Ochsner, Thomas Blättler and Martina Baumann.

My most sincere gratitude I would like to express towards Dr. Felix Reifler of the Advanced Fibers group at the Empa St. Gallen for the very fruitful collaboration over the last 4 years. In this respect I would like to thank his co workers Ulrich Schrade, Dr. Giuseppino Fortunato, Pierluigi Barbadoro, Lutz-Christian Gerhardt, Käthe Meyer, Marcel Halbeisen and Dr. Jörn Lübben who all contributed to aspects of my work. Also I would like to thank Dr. Rowena Crocket of the Empa Dübendorf for many helpful discussions in the initial stages of my PhD.

Hanspeter Gautschi of the Center for Microscopy and Image Analysis of the University of Zurich I would like to thank for introducing me to the field of electron microscopy and continuous support in sample preparation, imaging and interpretation of the images. The Center

for Microscopy and Image Analysis of the University of Zurich is acknowledged for use of their facilities. Dr. Heinz Gross of the Electron Microscopy Center of the ETH I would like to thank for helpful discussions.

Reto Hess of the IMPAG AG I thank for advice and supplying the detergent solutions employed in the chemical durability tests.

A special thanks goes to Michael Rabe who I had the pleasure of sharing an office and collaborating on several projects.

The whole Seeger group I would like to thank for a relaxed working atmosphere.

I am greatly indebted to the members of the staff and workshops, Chantal Henningsen-Conus, Ueli Feusi, Armin Kühne, Roland Zehnder, Rolf Pfister and Herman Schwarz. It is hard to imagine life as a PhD without their assistance.

My family and my friends I thank for their continuing support and for keeping me balanced. Andrea for saying yes on January 17th and Jula for her first scream on March 8th 2007.

Abstract

Engineering interfaces with unique chemical, physical and mechanical properties has become a major branch of material science. A subject that is currently receiving much attention is the ability to chemically and physically manipulate a solid interface on the micro- and nanometer scale to create surfaces with extreme wetting properties. Of these, surfaces that combine a low surface energy with a high surface roughness, so called superhydrophobic surfaces, are ascribed the greatest potential in terms of their exceptional water repellent properties.

In this work the fabrication process, the properties and possible modifications of a novel type of superhydrophobic surface coating, silicone nanofilaments, are explored. Both a gas and a solvent phase coating setup and procedure were developed to yield reproducible coating results with minimal requirements towards a pre-processing of substrates, require no expensive lab equipment, and can essentially be performed under ambient conditions. The resulting coating is comprised of a dense layer of polymethylsilsesquioxane nanofilaments with a typical thickness of 20-40nm and lengths up to several micrometers. The coatings can be fabricated to be fully transparent in the visible range or even anti reflective combined with a high water repellence with contact angles above 160° and sliding angles below 10°. Several commercially important substrate materials such as glass, silicon, aluminum, silicone and several natural and artificial textile fabrics were successfully coated with the developed techniques.

Extensive studies on the long term chemical stability were performed by immersion in various liquid media over a period of six months. The coating showed an exceptional stability in organic solvents, neutral and mildly acidic aqueous solutions and mildly acidic detergent solutions. The superhydrophobic coating properties are stable for several days in mildly basic and strong acidic solutions but deteriorate fast under strong basic conditions.

Both natural and artificial weathering tests showed promising results for an outdoor application of the coating. The superhydrophobic and anti reflective properties were retained for at least one year of outdoor weathering. Under artificial weathering conditions the coating was impervious to (global) UV radiation and showed a good stability towards the so called Acid Dew and Fog (ADF) Test.

The mechanical properties of the coating were found to be insufficient for even mildly abrasive applications. However by applying the coating to surface with micro scale roughness, such as a woven textile, the superhydrophobic effect is retained even upon continuous abrasion.

To expand the potential of the SNC, silane chemistry was utilized to modify the coating without altering its surface structure. Hydroxyl, fluorine, methyl, amino and carboxyl functionalities were successfully applied to the SNC to create patterned surfaces with arbitrary (super-)wetting properties and surfaces that mimic high surface area ion exchange residues.

Overall the results presented in this work show that the silicone nanofilaments constitute an exciting new approach to fabricating high surface area coatings that could find applications in many areas of surface science and engineering. In regards to superhydrophobicity, the relative ease of fabrication, the optical transparency and the exceptional long term stability of the coating sets it apart from contemporary coating solutions. The equally simple modification of their surface chemistry makes the silicone nanofilaments a versatile toolbox to create coatings with arbitrary (super-)wetting properties or specific functionalities towards catalytic surfaces, biosensor applications or open channel microfluidic devices.

Zusammenfassung

Die Entwicklung neuartiger Oberflächen mit spezifischen chemischen, physikalischen oder mechanischen Eigenschaften ist heute ein wichtiges Gebiet im Bereich der Materialwissenschaften. Ein Aspekt dieser Entwicklung, die gezielte chemische und physikalische Modifizierung einer Festkörperoberfläche auf der Micro- und Nanometerskala zur Herstellung von Oberflächen mit extremen Benetzbarkeitseigenschaften, erhält immer mehr Aufmerksamkeit. Besonders Oberflächen, die eine geringe Oberflächenenergie mit einer hohen Oberflächenrauhigkeit verbinden, sogenannte superhydrophoben Oberflächen, wird viel Potential hinsichtlich ihrer extremen wasserabweisenden Eigenschaften zugeschrieben.

In dieser Arbeit werden der Herstellungsprozess, die Eigenschaften und mögliche Anwendungsgebiete einer neuartigen superhydrophoben Oberflächenbeschichtung, den Silikon Nanofilamenten, erforscht. Zwei Verfahren wurden entwickelt, die eine reproduzierbare Beschichtung in der Gasphase bzw. in einem Lösungsmittel ermöglichen. Beide stellen nur minimale Anforderungen an die Probenvor- und Nachbearbeitung und zeichnen sich durch einen geringen apparativen Aufwand aus. Zusätzlich können sie unter normalen Laborbedingungen angewendet werden. Eine typische Beschichtung besteht aus einer dichten Schicht von Filamenten aus Polymethylsilsesquioxan, die eine Dicke von etwa 20-40nm und eine Länge von bis zu mehreren Mikrometern aufweisen. Die Beschichtung kann so hergestellt werden, dass sie vollständige Transparenz bzw. sogar antireflektive Eigenschaften mit einem sehr hohen Kontaktwinkel von über 160° und Abrollwinkeln von weniger als 10° kombiniert. Mehrere kommerziell wichtige Materialien wie Glas, Silicium, Aluminium, Silikon sowie diverse natürliche und künstliche Textilgewebe konnten mit den entwickelten Methoden erfolgreich beschichtet werden.

Umfangreiche Experimente zur chemischen Stabilität der Schichten wurden durch Eintauchen der Proben in unterschiedliche Flüssigkeiten über einen Zeitraum von 6 Monaten durchgeführt. Die Beschichtung erwies sich als ausgesprochen stabil in organischen Lösungsmitteln, neutralen und leicht sauren wässrigen Lösungen sowie in leicht sauren Tensidlösungen. Die superhydrophoben Eigenschaften der Schicht bleiben in leicht basischen und sauren Lösungen über mehrere Tage erhalten gehen aber in stark basischen Lösungen schnell verloren.

Bewitterungsversuche unter natürlichen sowie unter künstlichen Bedingungen zeigten vielversprechende Resultate hinsichtlich einer Anwendung der Schicht im Aussenbereich. Die superhydrophoben und antireflektiven Eigenschaften der Schicht blieben über mindesten ein Jahr unter natürlichen Bewitterungsverhältnissen erhalten. Unter künstlicher Bewitterung zeigte sich die Schicht stabil gegenüber globaler UV Strahlung und wies eine gute Stabilität im sogenannten Acid Dew and Fog (ADF) test auf.

Die mechanischen Eigenschaften der Beschichtung erwiesen sich als selbst für Anwendungen mit geringer mechanischer Beanspruchung als unzureichend. Jedoch konnte diese geringe intrinsische Stabilität der Nanofilamente durch Auftragen auf eine mikrostrukturierte Oberfläche (z.B. ein Textil) ausgeglichen werden. Auf solchen Oberflächen erwies sich der superhydrophobe Effekt gegen Abrieb stabil.

Eine Erweiterung des Anwendungsbereichs der Beschichtung konnte durch die chemische Modifizierung der Nanofilamente erreicht werden. Hydroxyl-, Fluor-, Methyl-, Amino- und Carboxylfunktionalitäten wurden erfolgreich auf die Silikon Nanofilamente appliziert. Dadurch konnten zum einen Oberflächen mit beliebigen extremen Benetzbarkeiten wie superhydrophob, superhydrophil, superoleophob oder superoleophil hergestellt werden. Zum anderen wurden so Oberflächen erzeugt, die wie ein spezifischer Ionenaustauscher mit hoher Kapazität wirken. Zusätzlich konnte gezeigt werden, dass die Funktionalisierung mit einfachen Methoden bis in den Submillimeterbereich genau durchgeführt werden kann und so 2-D gemusterte Oberflächen mit konstanter Oberflächenstruktur aber unterschiedlichen chemischen Eigenschaften hergestellt werden können.

Im Gesamten zeigen die Ergebnisse dieser Arbeit, dass die Silikon Nanofilamente einen interessanten Ansatz zur Herstellung von Beschichtungen mit hoher spezifischer Oberfläche darstellen, welche Anwendung in verschiedenen Bereichen der Oberflächenforschung und –technik finden könnten. Hinsichtlich der superhydrophoben Eigenschaften zeichnet sich die Beschichtung gegenüber gängigen anderen superhydrophoben Beschichtungen insbesondere durch die Einfachheit der Herstellung, ihre optische Transparenz und eine ausgezeichnete Beständigkeit gegenüber chemischen und Umwelteinflüssen aus. Dank einer einfachen Modifizierbarkeit der Beschichtung stehen vielfältige Möglichkeiten zur Herstellung von Oberflächen mit beliebigen Benetzbarkeiten, oder mit spezifischen Funktionalitäten zur Verfügung. Solche massgeschneiderten Oberflächen könnten neben selbstreinigenden, schmutz- und wasserabweisenden Beschichtungen insbesondere auch im Bereich der Katalyse, der Biosensorik oder der Herstellung von offenwandigen Mikrofluidsystemen Anwendung finden.

List of Publications

Patents

- J. Zimmermann, S. Seeger, G. R. J. Artus, S. Jung
  Superhydrophobic coating composition of reactive silanes and various coated substrates
  WO20040623 (2004)

Invited Journal Publications

- J. Zimmermann, G. R. J. Artus, S. Seeger
  Superhydrophobic Silicone Nanofilament Coatings
  Journal of Adhesion Science and Technology, accepted

Journal Publications

- J. Zimmermann, M. Rabe, G. R. J. Artus, S. Seeger
  Patterned Superfunctional Surfaces based on a Silicone Nanofilament Coating
  Soft Matter 4, 450 (2008)

- J. Zimmermann, M. Rabe, D. Verdes, S. Seeger
  Functionalized Silicone Nanofilaments: A Novel Material for Selective Protein Enrichment
  Langmuir 24, 1053 (2008)

- J. Zimmermann, F. A. Reifler, U. Schrade, G. R. J. Artus, S. Seeger
  Long term environmental durability of a superhydrophobic silicone nanofilament coating
  Colloids and Surfaces A: Physicochemical and Engineering Aspects 302, 204 (2007)

- J. Zimmermann, G. R. J. Artus, S. Seeger
  Long term studies on the chemical stability of a superhydrophobic silicone nanofilament coating
  Applied Surface Science 253, 5972 (2007)

- G. R. J. Artus, S. Jung, J. Zimmermann, H.-P. Gautschi, K. Marquart, S. Seeger
  Silicone Nanofilaments and their Application as Superhydrophobic Coating
  Advanced Materials 18, 2758 (2006)

Manuscripts in Preparation

- J. Zimmermann, F. A. Reifler, G. Fortunato, P. Barbadoro, L.-C. Gerhardt, S. Seeger
  Robust Superhydrophobic Textiles from a Silicone Nanofilament Coating

- M. Rabe, D. Verdes, J. Zimmermann, S. Seeger
  Relation between Layer Structure and Cooperativity during Nonspecific Protein Adsorption Events

Invited Talks

- J. Zimmermann
  Silicone nanocarpets: surface wetting in the extreme
  Unité de chimie des interfaces, Université catholique de Louvain, Belgium, January 2008

- J. Zimmermann
  Silicone nanocarpets: a novel approach to durable superhydrophobic coatings
  Department of Protection & Wellbeing of the Body, Empa St. Gallen, March 27, 2006

- J. Zimmermann
  Silicone Nanofilaments as Superhydrophobic Coatings
  BioInterface Group, ETHZ, May 2, 2005

Posters at Conferences

- J. Zimmermann, F. A. Reifler, G. Fortunato, P. Barbadoro, L.-C. Gerhardt, S. Seeger
  Superhydrophobic Textiles from a Silicone Nanofilament Coating
  NanoEurope, St. Gallen, Switzerland, September 11-13, 2007
  Best Poster Award

- J. F. Lübben, M. Halbeisen, D. Hegemann, J. Zimmermann
  Simulated and measured height distributions of designed micro- and nanostructured surfaces
  NanoEurope, St. Gallen, Switzerland, September 11-13, 2007

- J. Zimmermann, M. Rabe, S. Seeger
  Silicone Nanocarpets as Biointerfaces: from Superhydrophobicity to Selective Protein Enrichment
  BIOSURF VII, Zürich, Switzerland, August 29–31, 2007

- J. Zimmermann, M. Rabe, S. Seeger
  Silicone nanocarpets: from superhydrophobicity to protein enrichment
  ESF-EMBO Conference on Biological Surfaces and Interfaces, Sant Feliu,
  Spain, July 1-6, 2007

- M. Rabe, J. Zimmermann, D. Verdes, S. Seeger
  Specific and Non-Specific Adsorption of Proteins at Interfaces
  2007 NSTI Nanotechnology and Trade Show -Nanotech 2007, Santa Clara, California, USA, May 20-24, 2007

- M. Rabe, J. Zimmermann, D. Verdes, S. Seeger
  Specific and Non-Specific Adsorption of Proteins at Interfaces
  Nanotech Insight, Luxor, Egypt, March 10-17, 2007

- G. R. J. Artus, J. Zimmermann, S. Seeger
  Silicone Nanofilaments as Surface Coating
  Herbsttagung der Schweizer Chemischen Gesellschaft, Zürich, Switzerland, October 13, 2006

- J. Zimmermann, S. Seeger
  Silicone nanocarpets: a novel approach to durable superhydrophobic coatings
  MRC Graduate Symposium, Zürich, Switzerland, June 29, 2006

- G. R. J. Artus, J. Zimmermann, S. Seeger
  Silicone Nanofilaments as Superhydrophobic Coating
  NanoEurope, St. Gallen, Switzerland, April 13-15, 2005

Contents

Abbreviations

Acid Dew and Fog test	ADF test
Aminopropyltriethoxysilane	APTES
2-(carbomethoxy)ethyltrichlorosilane	CETS
Contact angle	CA (θ)
Contact angle hysteresis	CAH
α-Chymotrypsin	α-Chym
Isoelectric point	pI
β-Lactoglobulin	β-Lg
Lysozyme	Lys
Trichloromethylsilane	TCMS
Methyltrimethoxysilane	MTMS
Octadecyltrichlorosilane	OTS
1H,1H,2H,2H-Perfluorooctyltrichlorosilane	PFOTS
Polyethyleneterephthalate	PET
Polymethylsilsesquioxane	PMSQ
Polypropylene	PP
Relative humidity	RH
Scanning electron microscopy/	
Scanning electron micrograph	SEM
Silicone nanofilament coating	SNC
Sliding angle	SA (α)
Supercritical Angle Fluorescence	SAF
Ultra violet	UV
Water shedding angle	WSA (ω)
Weather-Ometer	WOM
X-Ray Photoelectron Spectroscopy	XPS

1 Introduction

1.1 General Introduction

Engineering interfaces with unique chemical, physical and mechanical properties has become a major branch of material science. In this respect the progress in nanotechnology over the last decades and the ability to manipulate surfaces on the nanometer scale has had a great impact in both science and industry. As one aspect of nanoengineered interfaces, surfaces with extreme water-repellent properties have received a lot of attention in the last decade. These surfaces are characterized by a low surface energy combined with a high surface roughness in the micro or nanometer range. Consequently a drop of water remains almost spherical on these surfaces and rolls off at slight inclination. Although the principles for high water repellence have been known for more than half a century [1-3], it was not until the mid 1990s that the scientific community has shown an acute interest in the subject. This is often associated with the work of Barthlott and Neinhuis, who published a paper on the chemical and structural nature of the lotus leaf surface and how this leads to its extraordinary water repellent and self cleaning properties [4]. Ever since, numerous publications have contributed to a better understanding of the superhydrophobic effect [5-10] and even more have presented new methods to create superhydrophobic surfaces (see reviews [11-15]). Primarily, superhydrophobic surfaces are of interest for waterproofing applications, but potential has also been ascribed to them as antifouling and self cleaning surfaces as well as for applications in which low friction flows are desired. A very recent addition to the list has been the ability of some of these surfaces to support a stable gas layer upon immersion in water. This so called plastron layer has been shown to allow for gas exchange and is utilized by some water dwelling species to breathe underwater [16].

Based on the same principle of roughness enhanced wettability as superhydrophobicity, other so called superwetting/-antiwetting surfaces have recently also gained in attention [17]. Accordingly, strategies to create superhydrophobic, superhydrophilic, superoleophobic and superoleophilic surfaces have been published in the past. Also superamphiphobic and superamphiphilic surfaces, that combine superhydrophobicity/-philicity with superoleophobicity/-philicity respectively, have been fabricated [17]. Such surfaces find applications as self-cleaning or anti-fogging coatings (superhydrophilic) [18-20], oil repellent or

anti-soiling coatings (superoleophobic) [21,22] or in water-oil separation strategies (superhydrophobic/superoleophilic) [23].

The ability to pattern a surface with regions of adverse superwettability further expands the potential of these coatings. Patterned surfaces with superhydrophobic and superhydrophilic domains for instance are considered of interest in liquid handling, biochip and water harvesting applications [24]. Furthermore, surfaces with wetting patterns show great potential in the development of open geometry microfluidics devices for lab-on-a-chip applications [25].

In addition to influencing the wettability of a surface, roughness is also associated with enhancing interfacial phenomena. Rough or porous surfaces with high surface/volume aspect ratios are commonly applied in catalysis and analytics. In recent years, rough surfaces have also gained considerable interest in the field of biosensors [26-28]. Micro- and nanoscale roughness has been shown to influence phenomena like cell adhesion and protein adsorption [29,30]. Of special interest are chemically or biochemically modified surfaces in microfluidic devices that primarily serve for biosensor application in various fields of proteomics such as diagnostics, system biology or pharmaceutical research. In these systems the analytical performance is strongly dependent on the contact area between analyte solution and functional surface [26,28]. There are several attempts to create nanostructures that allow for dynamic droplet control [31], manipulation of protein adsorption [32] or immobilization of active biomolecules [27,28].

1.2 Aim of the Thesis

The scope of this thesis centers around a novel type of coating method developed in our lab by which a dense layer of 1-D silicone nanostructures (silicone nanofilaments) can be grown on a substrate surface. Generally speaking the aims were to establish the coating procedure, explore and expand the coating properties as well as to evaluate the coating's potential for application.
The initial part of the thesis therefore concerns itself with the coating procedure and introduces some of the general properties of the silicone nanofilament coating. The objective was to develop a gas phase coating setup which enables a reproducible manufacturing of the SNC while retaining the overall simplicity of the initial coating procedure developed by Stefan Jung [33].

The second, major part of the thesis focuses on the application of the silicone nanofilament layer as superhydrophobic coating. Besides a general characterization of coating properties, both the chemical and environmental durability of the coating was evaluated in a series of long term experiments. Additionally, a first assessment of the SNC in a concrete, industrially relevant application, as a water repellent coating on textiles, was performed. For this purpose a new

method to evaluate the water wetting properties of macroscopically rough surfaces, the “water shedding angle”, was devised.

In the third part, the coating’s potential for other applications besides superhydrophobicity is explored. Surfaces roughness is known to enhance many interfacial phenomena and in this respect the SNC constitutes a template with a high surface roughness which can be readily modified by simple physico-chemical processes. Accordingly the silicone nanofilaments were successfully modified to yield superwetting/-nonwetting coatings, 2-D structured coatings with high wetting contrasts, wettability gradients or selectively functionalized coatings for proteomic applications such as protein enrichment.

The final part of the thesis concerns an alternative coating process to the standard gas phase coating. A solvent phase coating setup was developed that also enables a reproducible coating of substrates with a silicone nanofilament layer and a first characterization of the coating parameters and their influence on the coating properties was performed.

2 Theory

2.1 Silicones

2.1.1 General introduction

The silicone (or polysiloxane) family contains all mixed organic-inorganic polymers that consist of a silicone-oxygen backbone or network, with organic residues attached to the silicon atoms. The first silicones were synthesized at the start of the 20th century by Kipping, but it was not until the German chemist Richard Müller and his American contemporary Eugene G. Rochow independently discovered a way to synthesize methylchlorosilane (an important silicone precursor) on an industrial scale, that silicones and silicone chemistry started to bloom [34]. Today silicone polymers are found in nearly all areas of everyday life, from healthcare products to computer chips. Some of the benefits of silicones include good thermal stability, good environmental stability (oxygen, ozone and sunlight), low chemical reactivity, low toxicity, flexibility and anti adhesive properties [34-36].

Silicone polymer precursors are of the general formula $R_nSiX_{(4-n)}$, where R denotes an organic residue and X a hydrolyzable group such as alkoxy, acyloxy, amine or halogen. These so called silane precursors are generally thermally stable and easily soluble in common solvents. In the presence of water they hydrolyze quickly to form silanols which then condense in a polymerization reaction. Figure 2.1 illustrates the polymerization reaction of one of the most common silicones, polydimethylsiloxane (PDMS):

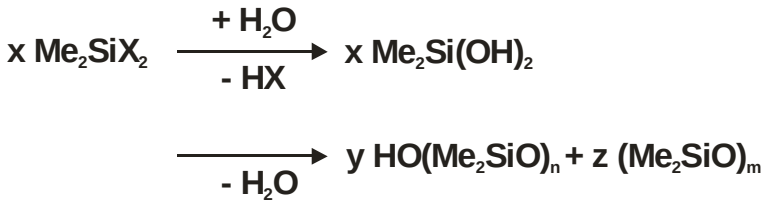

Figure 2.1. Condensation and polymerization reaction of a bifunctional dimethylsilane to form polydimethylsilsesquioxane.

In the initial polymerization reaction, short linear chains (n = 20-40) and small cyclic structures (m = mostly 3 – 6) are obtained which can be further condensed (acid or base catalyzed) to form linear structures of high molecular weight.

Monofunctionalized silanes like trimethylchlorosilane are added as termination units to control the molecular weight and chainlength of the polymer. Tri- or tetra-functionalized silanes can be added as crosslinking agents to form network structures. With varying chainlength, crosslinking and organic sidegroups, silicones with a large variety of properties and compositions can be synthesized. The consistency can vary from liquid to gel to rubber like to hard plastic.

2.1.2 Silsesquioxanes

Silsesquioxanes are a sub species of polysiloxanes with the empirical formula $RSiO_{3/2}$. They are the products of the polymerization of trifunctional silane precursors. Their structure can span from random disordered to extended ladder like structures to ordered, cage like structures with only a small number of atoms [36]. They typically find applications as thin film coatings for protective coatings, electrically insulating coatings, adhesive-related coatings or as resists for microlithography. The various possible structures of the silsesquioxanes are illustrated in Figure 2.2.

2.1.3 Polymethylsilsesquioxane

Polymethylsilsesquioxane (PMSQ) is the silsesquioxane with the shortest organic residue, CH_3, and the empirical formula $CH_3SiO_{3/2}$. It finds widespread application as insulating coatings for optical and electronic devices, as additive powders in cosmetics or ceramic binder [36]. Recently, PMSQ based sol gel foams or aerogels have found applications as superhydrophobic coatings [37,38]. Generally PMSQ is prepared by hydrolysis and condensation of CH_3SiX_3 precursors, where X is either Cl, OCH_3 or OC_2H_5. The structure of PMSQ is not clear but is usually considered to be an amorphous network containing branch, ladder, polyhedral and cage units [39,40]. Depending on the reaction and curing conditions the composition/frequency of these units can vary [40,41].

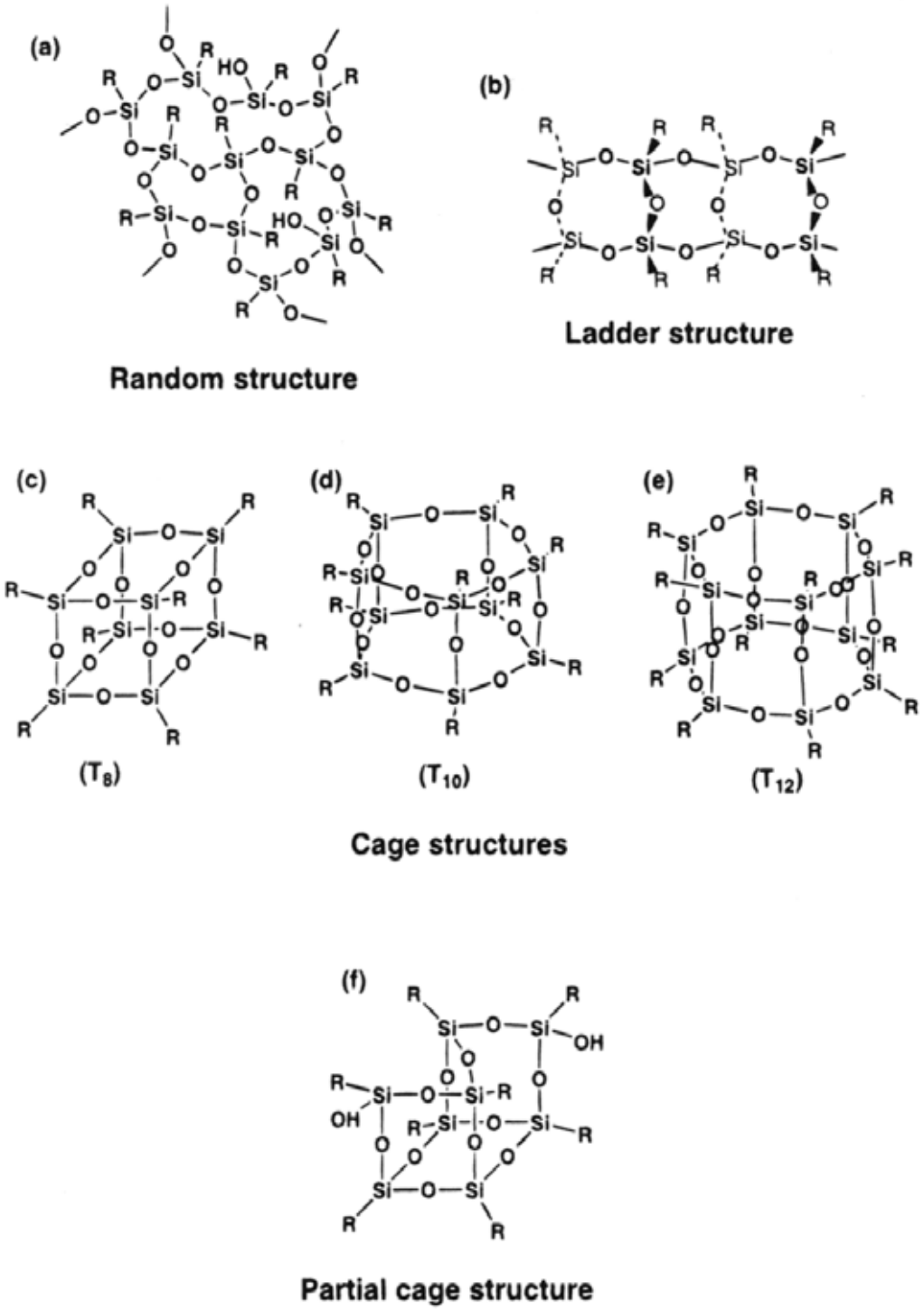

Figure 2.2. The possible structures of silsesquioxanes, taken from Reference [36].

2.1.4 Curing reaction

Typically, as prepared silsesquioxanes like PMSQ contain some degree of unreacted hydroxyl, methoxy or ethoxy groups due to an incomplete hydrolyzation of the initial precursors and an incomplete silanol condensation [36,39,40,42]. Upon curing the reaction product, condensation of these groups can be facilitated, resulting in a higher degree of crosslinking.

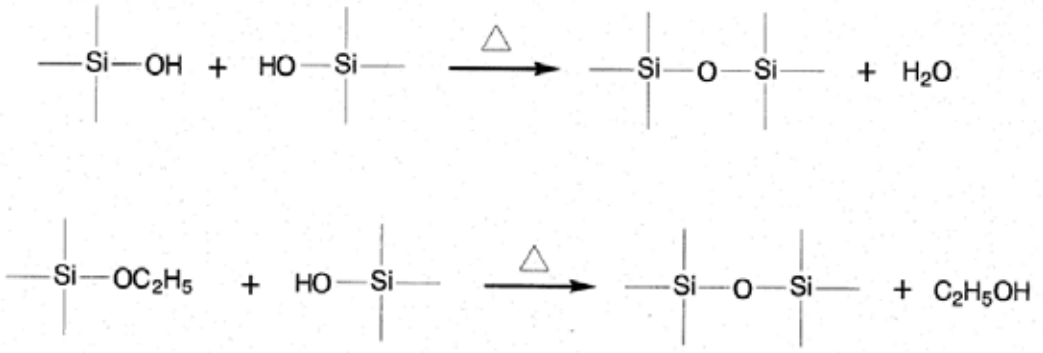

Figure 2.3. Curing reactions of two silanols (top) or a silanol with an ethoxysilane (bottom), taken from Reference [39].

The curing reaction can include the condensation of neighboring reactive groups, ring opening and re-condensation reactions or a general rearrangement of the polymeric structure to allow for further crosslinking.

Depending on the reaction conditions, the initial amount of unreacted groups in the polymer can vary. Maciel *et al.* reported a "substantial amount" of silanol groups in the reaction product of TCMS polymerized by dropwise addition to a large excess of water and subsequent filtration and drying at 55°C [42]. TGA studies on the curing reaction of a PMSQ film produced from a commercial resin revealed a 10% weight loss due to the condensation of silanol and ethoxy groups [39].

2.1.5 Silylation of surfaces

Ever since the pioneering work of Sagiv and co workers, the process of modifying the surface of an inorganic material with a reactive alkylsilane has become widely used in both research and technology and has been studied to great extent [43-52]. When a hydroxyl containing surface such a silica is exposed to reactive silanes, several reaction products can be formed, depending on the reaction conditions [47]. Figure 2.4 illustrates some of the possible reaction products of a silica surface with mono-, di- and trifunctional silanes.

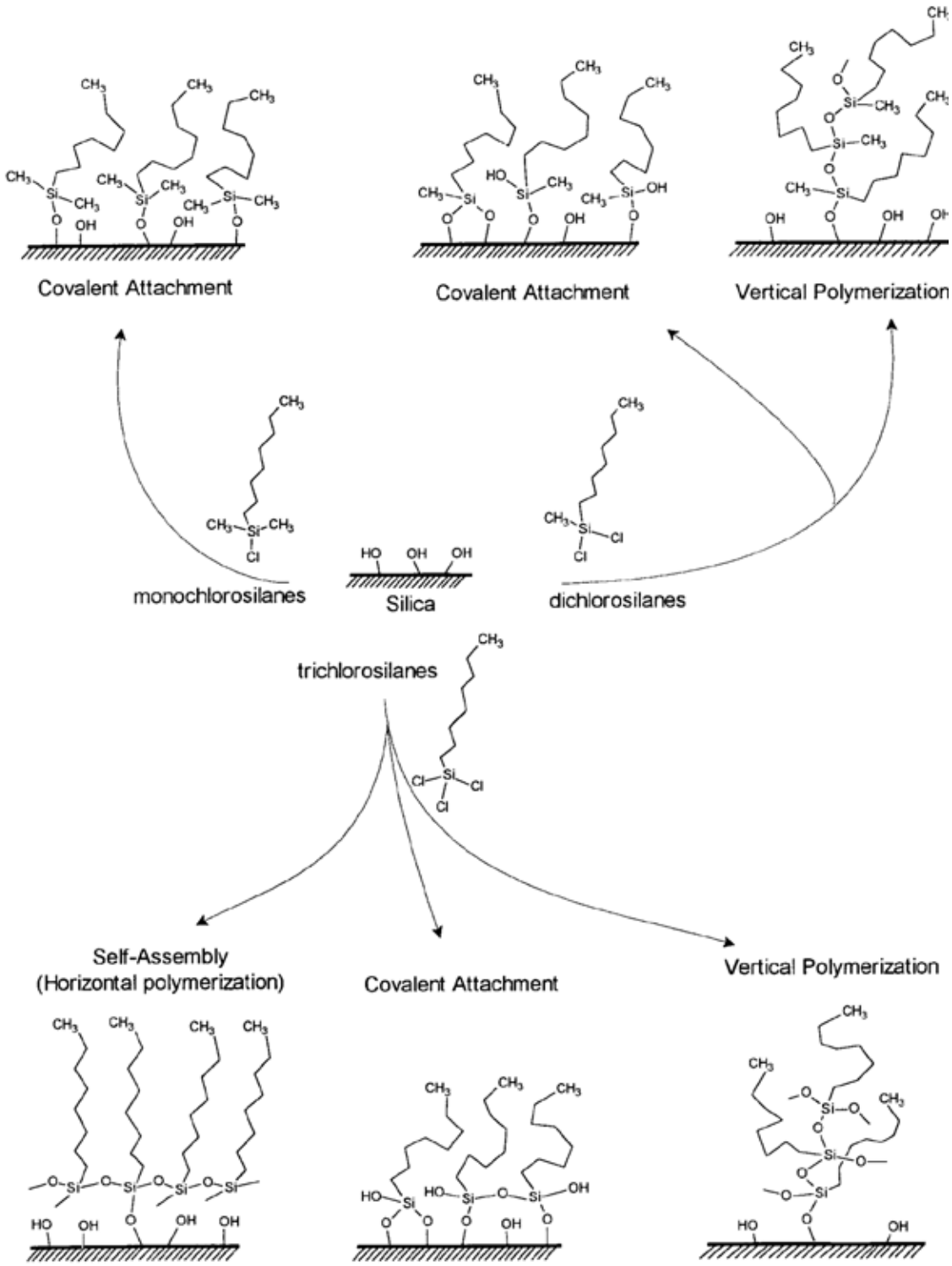

Figure 2.4. Reaction pathways of silanes with a silica surface, taken from Reference [47].

Depending on the chain length and size of the organic residues attached to the silane, monolayer formation (covalent attachment, self-assembly) or a vertical polymerization, leading to multilayer or bulk polymerization, can be favored [47,48]. For most applications, a monolayer type reaction product is desired and therefore silylation reactions are typically performed at low

concentration of silane in a non polar solvent under strict control of the amount of water in the reaction to prevent a bulk polymerization in the solvent phase. Typical substrate materials that are modified with reactive silanes are siliceous materials but stable condensation products can also be formed with other oxides such as aluminum or titanium [49]. Also many organic polymers are susceptible to modification with silanes [53]. Although organosilane monolayers have become a versatile tool to transfer a number of useful interfacial properties to substrate surfaces [52], one of the most widely used applications of the silane-surface reaction remains the alteration of the surface energy or wetting characteristics of the substrate. Typically silanes with unreactive organic residues are applied to substrates to render them water repellent. Fluorosilanes can be utilized to convey a resistance to wetting by non polar liquids.

2.2 Wetting of solid surfaces

2.2.1 Wetting of homogenous planar solid surfaces

When a drop of liquid contacts a solid surface, the interfacial energies of the two phases determine the degree to which the solid is wetted by the liquid. The liquid can either tend to spread on the surface ("wetting") or tend not to spread on the surface ("non wetting"). The extent to which a drop spreads on a surface influences its macroscopic shape. In 1805, Thomas Young derived the basic relationship between the interfacial energies of a liquid drop on a surface and its macroscopic shape [54]:

$$\cos\theta = \frac{\gamma_S - \gamma_{SL}}{\gamma_L} \tag{2.2.1}$$

in which γ_S, γ_{SL} and γ_L are the solid/vapor, solid/liquid and liquid/vapor interfacial energies respectively and θ is the angle at which the liquid contacts the surface at the liquid/air/solid contact line ("three phase contact line"). The so called Young's Equation can be intuitively understood by balancing the surface tension forces acting parallel to the substrate surface on the three phase contact line.

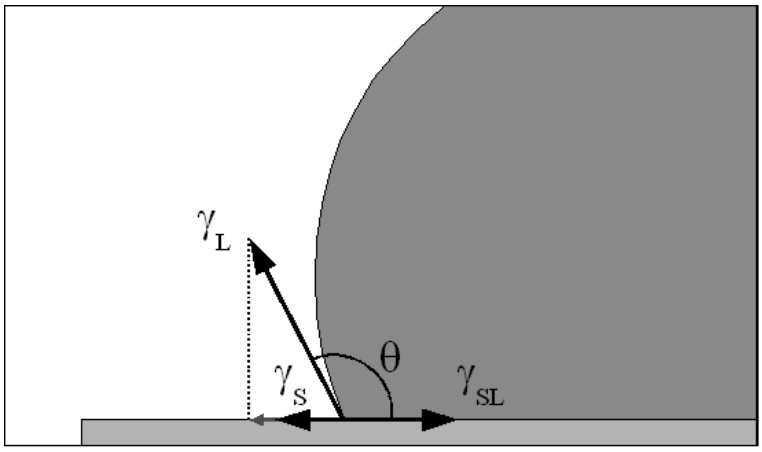

Figure 2.5. Balance of the surface tension forces at the three phase contact line.

Alternatively the total surface energy of the system can be considered:

$$E = A_L\gamma_L + A_{SL}\gamma_{SL} + (A_S - A_{SL})\gamma_S \tag{2.2.2}$$

where A_{IJ} denotes the surface area between the individual phases and A_S is the total surface of the solid [55]. Under the assumption of a small drop volume, gravity can be ignored and the drop shape approximated as a spherical cap. This leads to simple relationships for A_{LV} and A_{SL}. Minimizing E while keeping the drop volume constant results in (2.2.1). A detailed derivation of the Young's equation can be found in textbooks [56].

With the help of this simple relation, the interfacial energies can be directly correlated to an easily accessible, macroscopic measurable property.

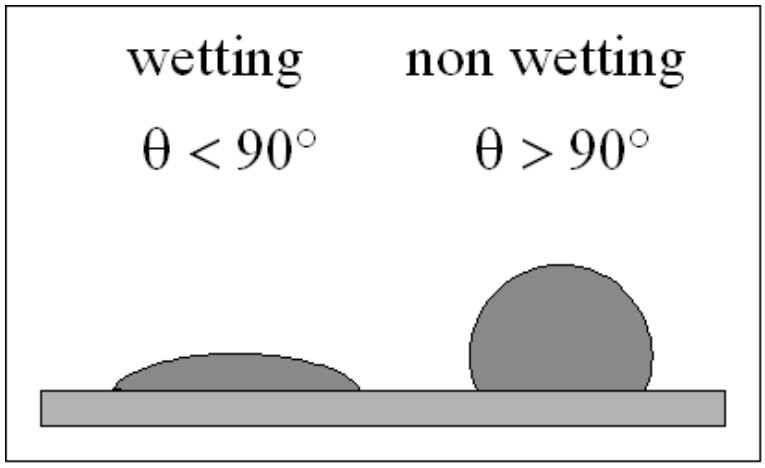

Figure 2.6. Schematic representation of a drop of water on a hydrophilic surface (left) and on a hydrophobic surface (right).

A liquid is considered to wet a surface if the CA is below 90°. If the CA is above 90° the liquid is non wetting in regards to the surface. Accordingly a surface on which water exhibits a CA below 90° is termed hydrophilic, a surface with a water CA above 90° is termed hydrophobic.

In most situations it is not the absolute value of the individual surface tension components that determines the wettability of a solid surface. Especially the solid/liquid surface tension is influenced by the type of interactions that occur. There are several theories that separate the surface energies into individual components. According to Owens and Wendt, surface energies can be divided into a disperse and a polar part [57].

$$\gamma = \gamma^D + \gamma^P \tag{2.2.3}$$

The disperse part of the surface tension is considered to contain all non polar interactions like van der Waals and other non site specific interactions. The polar part accounts for dipole-dipole, dipole-induced dipole, hydrogen bonding and other site specific interactions. According to Good, the solid/liquid surface tension can be approximated as [58]:

$$\gamma_{SL} = \gamma_S + \gamma_L - 2\sqrt{\gamma_L^D \gamma_S^D} - 2\sqrt{\gamma_L^P \gamma_S^P} \tag{2.2.4}$$

Substituting this into Young's equation results in

$$\cos\theta = \frac{-\gamma_L + 2\sqrt{\gamma_L^D \gamma_S^D} + 2\sqrt{\gamma_L^P \gamma_S^P}}{\gamma_L} = -1 + \frac{2\sqrt{\gamma_L^D \gamma_S^D} + 2\sqrt{\gamma_L^P \gamma_S^P}}{\gamma_L} \tag{2.2.5}$$

According to this equation, surface wetting is determined by the interplay of disperse and polar part of the solid and liquid surface tension. A surface that has a low disperse surface tension but high polar part for instance will not be wet by a non polar liquid, which is not evident from the Young's equation alone.

Other approaches consider the adhesive energy between the two phases (Fowkes) [59] or separate the surface tension into three components (van Oss) [60]. For the scope of this work however it is sufficient to consider the Owens and Wendt theory.

2.2.2 Wetting of rough homogeneous solid surfaces

On a rough surface the simple Young's equation is no longer valid because the surface tension balance at the three phase contact line will be changed by the surface roughness.

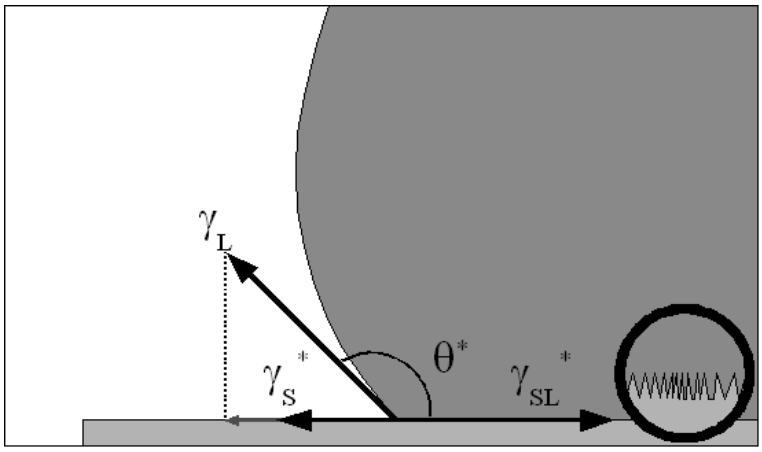

Figure 2.7. Balance of the surface tension forces at the three phase contact line in a Wenzel type wetting state.

If the solid and solid/liquid surface tensions at the three phase contact line are projected parallel to the macroscopic solid interface, as in the derivation of the Young's equation, the surface roughness must be accounted for. To this end, Wenzel introduced the roughness factor r [1]:

$$r = \frac{\text{actual surface}}{\text{geometric surface}} \tag{2.2.6}$$

With this factor, the solid surface tensions projected parallel to the macroscopic solid interface relate to the surface tensions of the flat surface as

$$\gamma^* = r \cdot \gamma \tag{2.2.7}$$

The balance of surface forces now becomes

$$\cos\theta^* = \frac{\gamma_S{}^* - \gamma_{SL}{}^*}{\gamma_L} = \frac{r \cdot \gamma_S - r \cdot \gamma_{SL}}{\gamma_L} = r \cdot \frac{\gamma_S - \gamma_{SL}}{\gamma_L} \tag{2.2.8}$$

And with the Young equation (2.2.1) this becomes

$$\cos\theta^* = r \cdot \cos\theta \tag{2.2.9}$$

the so called Wenzel equation. It relates the apparent contact angle θ^* measured on a rough surface to the intrinsic contact angle θ as it is defined by the material properties.

According to this equation, surface roughness will enhance the intrinsic wetting properties of a material. I.e. a wettable surface will become more wettable if it is roughened and a non wettable surface less wettable.

2.2.3 Wetting of inhomogeneous solid surfaces

Young's equation, or its expansion in the form of the Owens-Wendt equation, considers a solid surface to be perfectly flat and homogeneous in its chemical composition (i.e. the solid surface tension is constant over the whole wetted surface area). To describe the wetting situation on a chemically heterogeneous surface, the Cassie-Baxter equation is often used [2,55]:

$$\cos\theta^* = \sum_i f_i \cos\theta_i \tag{2.2.10}$$

in which f_i denote the solid fractions of the different chemical surface patches that are wetted by the liquid and θ_i the intrinsic contact angles on the individual patches. It relates the macroscopic, apparent contact angle to the microscopic chemical composition of the solid surface.

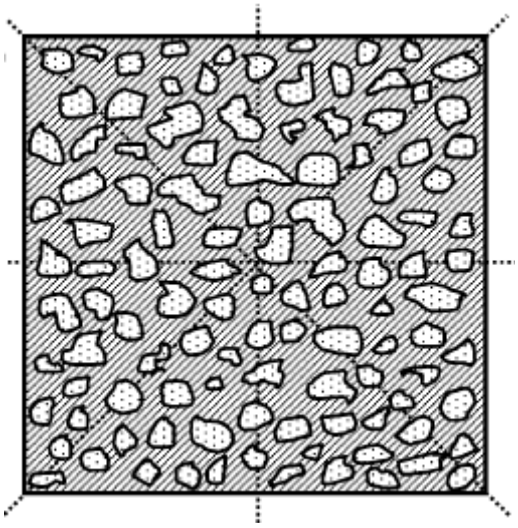

Figure 2.8. A surface having two randomly distributed chemical compositions, taken from Reference [61].

For a system with patches of two chemical compositions (as illustrated in Figure 2.8) the Cassie-Baxter equation becomes

$$\cos\theta^* = f_1 \cos\theta_1 + (1 - f_1)\cos\theta_2 \tag{2.2.11}$$

2.2.4 Superwetting/-nonwetting states

Superwetting or supernonwetting states are referred to situations in which a liquid either completely wets a surface or the surface is completely non wettable by the liquid. The first condition is typically attributed to surface/liquid combinations with contact angles approaching zero, the second to those that exhibit contact angles of more than 150°. The threshold of 150° is somewhat arbitrary and has no real physical basis. It has evolved mainly through the use of the term "superhydrophobic" to describe surfaces that exhibit water contact angles of more than 150°.

On flat surfaces, the Young's equation provides the criteria to achieve a superwetting or –nonwetting state. If $\gamma_S - \gamma_{SL} > \gamma_L$, the CA becomes zero and the drop of liquid will completely spread on the surface (silicone oil for instance spreads completely on most solid surfaces) [55]. The supernonwetting state on the other hand, for which $\gamma_{SL} - \gamma_L > \gamma_L$, is never realized on a flat solid surface. The lowest energy surfaces, fluorinated solids, still exhibit water contact angles of only about 120°. By introducing surface roughness however, both the superwetting and the supernonwetting state can be induced. The Wenzel equation (2.2.9) provides the criteria to transform a wetting into a superwetting or a non wetting into a supernonwetting surface. Technically it even provides the criterion to create a perfectly non wetting surface. Given the intrinsic wettability of a material, it is simple to calculate the surface roughness needed to reach a contact angle of 180°. According to the Wenzel equation for instance a roughness factor of 2 would be sufficient to transform PTFE (θ = 120°) into a perfectly non wetting surface. Experimentally however this situation is never observed because a wetting transition occurs.

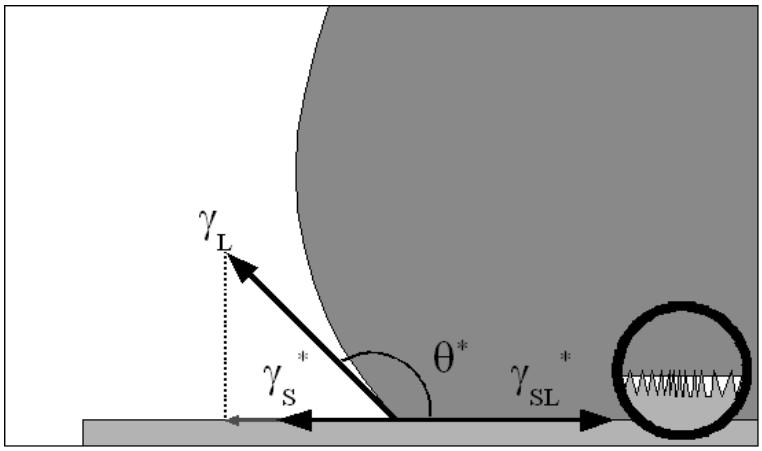

Figure 2.9. Balance of the surface tension forces at the three phase contact line in a Cassie-Baxter type wetting state.

Instead of following the surface structure and completely wetting the solid interface (as assumed for the Wenzel state), the liquid only partially wets the surface and comes to rest on the tops of the surface asperities. A composite liquid/air/solid interface forms which, in this case, is energetically more favorable than the corresponding solid/liquid interface (Figure 2.9).

Here the solid surface tensions projected parallel to the macroscopic solid interface are

$$\gamma^* = f \cdot \gamma \tag{2.2.12}$$

with *f* being the solid surface fraction in contact with water.

For this situation, balancing the surface forces at the three phase contact line becomes

$$\cos\theta^* = \frac{f \cdot \gamma_S - f \cdot \gamma_{SL} - (1-f) \cdot \gamma_L}{\gamma_L} = f\left(\frac{\gamma_S - \gamma_{SL} + \gamma_L}{\gamma_L}\right) - 1 \tag{2.2.13}$$

Taking the Young's equation (2.2.1) into account, this transforms into

$$\cos\theta^* = f(1+\cos\theta) - 1 \tag{2.2.14}$$

The same relation that is received if the surface is described by a two component Cassie-Baxter equation with a contact angle of 180° ($\cos\theta_2 = -1$) for the liquid/air fraction.[3]

At which point the transition between a Wenzel and a Cassie-Baxter wetting state occurs or which state applies for a given surface chemistry and geometry is still a subject of active research. Empirically both Wenzel and Cassie-Baxter type wetting states are observed for surfaces fulfilling the criteria of supernonwettability. Lafuma *et al.* were even able to induce a transition between a Cassie-Baxter to a Wenzel type wetting state by applying external pressure onto a drop of water deposited on a rough surface, showing that a metastable Cassie-Baxter state can occur on a Wenzel type surface [62].

2.2.5 Superhydrophobicity

In textbooks as well as primary literature, the term superhydrophobicity is somewhat ambiguously applied to surfaces exhibiting a water contact angle of more than 150°. Efforts have been made, especially by the McCarthy group, to apply a more rigorous terminology and make a clear distinction between a non wetting surface in a Wenzel state and one in a Cassie-Baxter state [8,63]. This distinction is necessary because while a Wenzel and a Cassie-Baxter state

[3] This is also the actual situation for which Cassie and Baxter derived their equation.

might exhibit the same contact angle, their overall wetting characteristics are very different. In a Wenzel state, the complete surface area underneath the drop is wetted. In a Cassie-Baxter state on the other hand, the solid/liquid interface accounts for only a few percent of the surface area underneath the drop. Amongst others this has a dramatic effect on liquid adhesion and the dynamic wetting characteristics of the surface (see 2.2.6) and should not be neglected in the description of the surface. Unfortunately no terminology has asserted itself yet and the distinction between a Wenzel type and Cassie-Baxter type superhydrophobic surface must be made through supplying additional information on the dynamic wetting properties of a surface.

2.2.6 Dynamic Wetting

When a drop of liquid is placed on a solid substrate and its volume continuously increased, the three phase contact line will advance along the surface with a constant contact angle as the drop grows. When liquid is removed from the drop, the three phase contact line will retract along the surface, also with a constant contact angle. On any real surface, there will be a significant difference in the advancing and the receding contact angle, also known as contact angle hysteresis. This can be attributed to surface inhomogeneities in terms of chemical or structural differences, surface roughness, liquid contamination or line tension forces [56]. A chemical inhomogeneity for instance will hinder either the advancing or receding of the three phase contact line, depending on whether it is more or less wettable than the surrounding area. Macroscopically the CAH will result in a force that keeps the drop of liquid pinned to the surface. If a drop of liquid is suspended on a solid substrate and the substrate is slowly tilted, the CA at the advancing contact line will increase and the CA on the receding line decrease until the advancing/receding CA values are reached. At this point the drop will begin to slide down the surface.

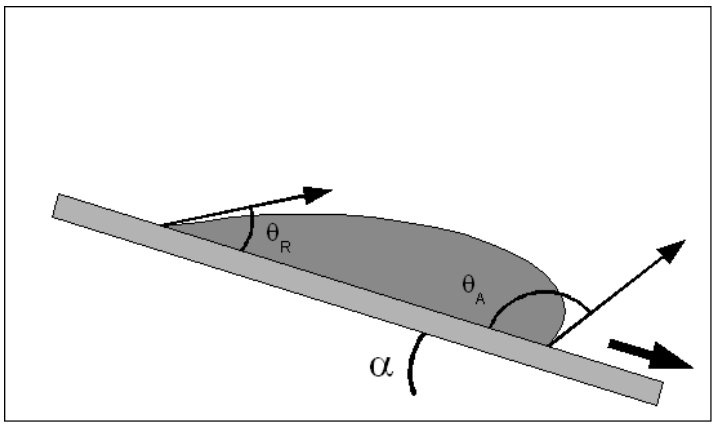

Figure 2.10. A drop of water on a tilted substrate.

The angle at which this occurs is called the sliding angle and can approximately be related to the retention force of the drop on the substrate and accordingly to the contact angle hysteresis [64,65]:

$$\frac{m \cdot g}{w} \cdot \sin \alpha = \gamma_L (\cos \theta_R - \cos \theta_A) \qquad (2.2.15)$$

in which m is the mass of the liquid drop, g is the acceleration due to gravity, w is the drop width, α is the sliding angle and θ_R and θ_A denote receding and advancing contact angle respectively.

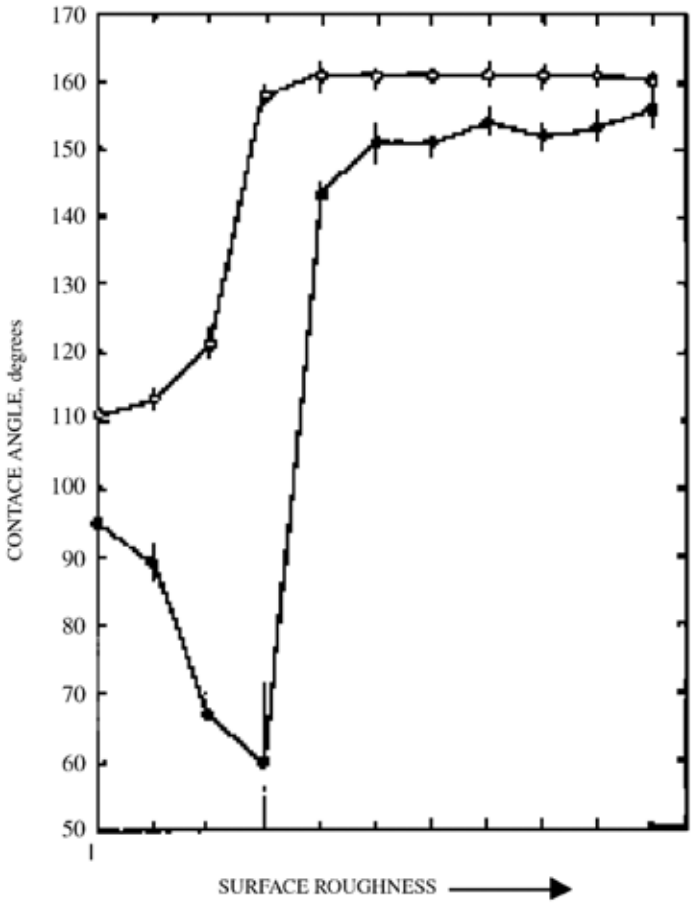

Figure 2.11. Advancing contact angle (top line) and receding contact angle (bottom line) as a function of surface roughness, taken from Reference [3].

On a chemically homogeneous surface, CAH is initially low due to the small number of defects that can cause contact line pinning. With increasing surface roughness, the number of pinning points, and consequently CAH, will increase. This relation holds, as long as the surface is in a Wenzel type wetting state, i.e. the complete surface area underneath the drop is wetted. In the

case of hydrophobic surfaces however, a very high surface roughness can induce a transition from a Wenzel to a Cassie-Baxter type wetting state. As in the Cassie-Baxter wetting state the area beneath the drop can be considered a homogeneous liquid/air interface containing only few defects where the liquid contacts the surface asperities, CAH is generally very low on these surfaces [17]. Figure 2.11 shows the change in advancing and receding CA on a chemically homogeneous surface with increasing surface roughness. The transition from a Wenzel to a Cassie-Baxter type wetting state is clearly evident from the sudden decrease in CAH.

On a Cassie-Baxter type surface, surface asperities in contact with water act as pinning points for the three phase contact line and contribute to CAH. Öner *et al.* have shown that beside the amount of pinning points their shape and distribution affect the CAH for a Cassie-Baxter type surface [8]. The shape of the three phase contact line is determined by the size, shape, density and distribution of the surface asperities. For the contact line to advance or recede on the surface it has to move from one (metastable) state to another. The higher distorted the contact line and the more discontinuous the three phase contact line, the lower will be the energy barrier between these (metastable) states and consequently the contact angle hysteresis. According to this interpretation, a 3-D, random rough surface should exhibit the lowest contact angle hysteresis in a Cassie-Baxter type wetting state [8].

2.2.7 Self cleaning

A term that is generally associated with superhydrophobicity is the so called self cleaning effect or Lotus-Effect®. It refers to the ability of certain (superhydrophobic) plant and animal surfaces to not only remain dry in a very wet environment but to also remain free of contaminations such as dirt particles or spores and bacteria [4,66]. The generally accepted explanation for this phenomenon is that adhesion for macro- and microscopic dirt particles is significantly reduced on nanorough surfaces. If the adhesion of the contaminating particle to water is stronger than to the surface, a drop of water rolling down the surface will “pick up” the particle and remove it from the surface. Essential requirement for a superhydrophobic surface to be self cleaning is therefore that drops of water roll down the surface, i.e. that they exhibit Cassie-Baxter type wetting.

2.3 A note on contact angle measurements

I would like to end this section with a personal remark on contact angle measurement. Contact angle measurement has established itself as a versatile tool to evaluate and determine solid liquid interactions and surface tension forces. As indicated in Chapter 2.2., the macroscopic contact

angle that a drop of liquid forms on a surface is directly related to the surface tension forces of the liquid and the solid as well as the solid/liquid interaction. This is very convenient, since a macroscopic measurable quantity can be related to the microscopic chemical properties of a liquid and a solid surface. Even better, if this macroscopic quantity is as easily accessible as the angle at which the liquid contacts the solid at the three phase contact line. Consequently goniometry has been a standard tool in surface science for decades and has undoubtedly led to many invaluable insights into solid liquid interactions. The procedure however harbors some significant dangers. In the early form of goniometry, still applied in many laboratories today, contact angles are determined by manually placing a tangent at the three phase contact line. To receive consistent and reproducible results this requires considerable expertise on the behalf of the operator. Also comparing the results obtained by different operators/research groups is difficult.

The advances of personal computers and image processing software have helped to eradicate one source of bias. Today, the image of a sessile drop can be recorded with a high resolution CCD camera and directly processed with a few simple mouse clicks to yield contact angle information and surface tension values. Even dynamic contact angle measurements can be performed on line and with high “precision”. The state of the art processing routine performs a least squares fit of a theoretical drop profile to the extracted drop profile (the so called Laplace-Young fitting routine). Technically, with this routine, a systematic error caused by the operator through an over- or underestimation of contact angles when manually fitting a tangent to the drop profile is excluded.

A source of error however remains the optical detection/representation of the drop profile; lighting, contrast and focus influence the optical image of the drop. Also, the three phase contact line for the system needs to be clearly determined, which is typically achieved by slightly tilting the optical axis and setting the three phase contact line at the transition between the drop image and its reflection on the substrate. All these processes again depend on the skill and care of the operator. When evaluating contact angle values in the intermediate range (between 20-140°) the source of error from slightly different adjustments in the optical settings is negligible. For very high contact angles however it becomes increasingly difficult to clearly capture the drop profile near the three phase contact point. Additionally, the substrate baseline must often be set manually because the image processing software fails to find it.

Figure 2.12 illustrates how even slight changes in the optical settings and the position of the baseline influence the contact angle values determined with the automated fitting routine. All images were successively recorded on the same sessile drop.

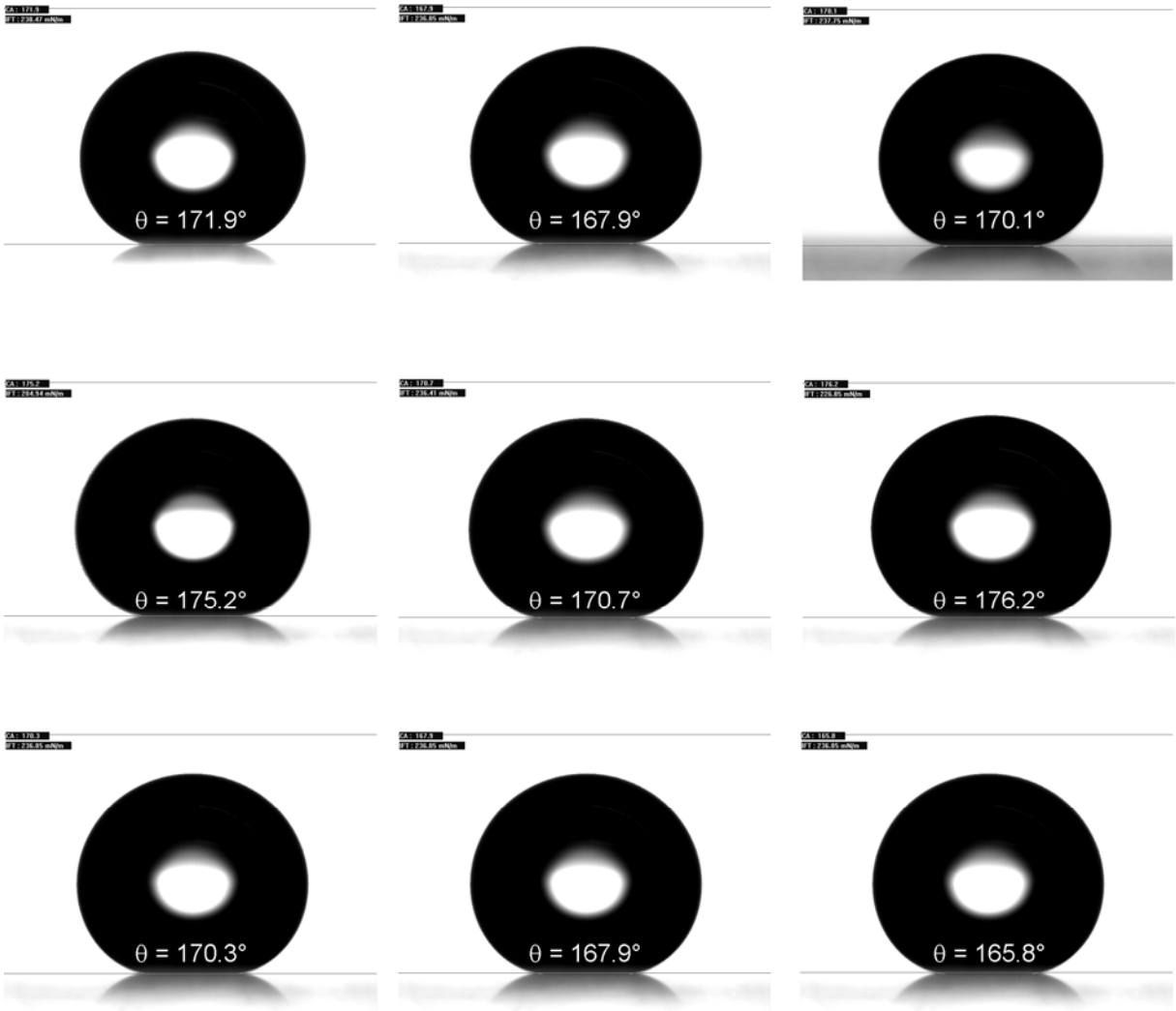

Figure 2.12. Automated contact angle determination performed on the same drop of water under slightly varying settings. Top row: varying lighting conditions. Middle row: varying position of the three phase contact line. Bottom row: varying focus.

The top three images show the drop profile at slightly different lighting conditions. In the middle images, the baseline was successively shifted down by a single pixel from left to right. The bottom three images show the drop profile at slightly different foci. The average contact angle determined from these 9 images is 171 ± 4°. So although technically the automated fitting routine is considered to be able to reproduce a contact angle measurement with an accuracy of ± 0.2° (as opposed to ± 2° for the manual determination) [67], the systematic error caused by the operator can be considerably higher. It is therefore clear that despite recent advances in goniometry, there is still a significant bias inherent in the measuring technique when high contact angles are evaluated. In the worst case, inexperienced performance of an automated contact angle routine and blind trust can produce completely misleading results [68].

Despite these apparent difficulties, many publications regarding superhydrophobic surfaces consistently report contact angle values well above 160° or even 170° with margins of error well below 1° and directly relate these to the results of other research groups. Only few publications indicate an awareness of the difficulties described here [69]. Unfortunately there is currently no alternative procedure available that allows for an equally simple and straightforward determination of contact angles. The automated contact angle determination was therefore also employed in this work. However I would like to stress at this point, that great care was taken to be as consistent as possible in the contact angle evaluation. So while undoubtedly all contact angles reported in this work are biased to some extent, they all contain the same measure of systematic error which still enables a meaningful comparison of the individual values.

Since dynamic contact angles are equally affected by the difficulties of static contact angle measurements and pose some additional, experimental difficulties [12,70], sliding angle values instead of contact angle hysteresis was chosen to act as a qualitative measure of the water adhesive and dynamic wetting properties.

3 Materials

3.1 Chemicals

Table 3.1 List of chemicals (in alphabetical order)

Chemical	Quality	Supplier
Acetic acid	p.a.	Fluka
Acetone	puriss. p.a.	Fluka
Aminopropyltriethoxysilane	97%	ABCR, Germany
Ammonia solution	p.a.	Fluka
2-(carbomethoxy)ethyltrichlorosilane	97%	ABCR, Germany
Chloroform	puriss. p.a.	Fluka
Decane	p.a.	Fluka
Dehyquart A-CA		IMPAG AG, Switzerland
Dehyton K		IMPAG AG, Switzerland
Diiodomethane	p.a.	Fluka
Dodecane	p.a.	Fluka
Ethanol	p.a.	Fluka
Glucopon 215 CS UP		IMPAG AG, Switzerland
Hexadecane	p.a.	Fluka
HYDRANAL-Coulomat AD		Riedel-de Haën
HYDRANAL-Water Standard	0.10	Riedel-de Haën
Hydrochloric acid	p.a.	Fluka
Methyltrimethoxysilane	97%	ABCR, Germany
Octadecyltrichlorosilane	95%	ABCR, Germany
Octane	p.a.	Fluka
1H,1H,2H,2H-Perfluorooctyltrichlorosilane	95%	ABCR, Germany
Sodium hydroxide	purum, pellets, p.a.	Fluka
Texapon NSO BZ		IMPAG AG, Switzerland
Toluene	extra dry, water <50ppm	Acros Organics
Toluene	puriss. p.a.	Fluka
Trichloromethylsilane	98%	ABCR, Germany

3.2 Substrates

Glass coverslips of varying shape and size were purchased from Menzel Gläser (Germany) and cleaned prior to use. Pre-cut silicon wafers were purchased from Crystec (Germany) and cleaned and activated before use. Aluminum and PDMS samples were supplied by the technical workshop and cleaned and activated before coating. The following textile samples were supplied by the Empa St. Gallen and used as received:

Table 3.2 List of textile samples

Empa Testmaterials Sample No.	Chemical composition	Additional information
#211	Cotton “Percale”	bleached, without optical brighteners
#213	Polyester(PET)/Cotton 65/35	bleached, without optical brighteners
#214	Cotton “Body”	without optical brighteners
#402	Wool “Mousseline”	ISO 105-F01
#403	Silk “Crêpe”	ISO 105-F06
#404	Viscose-Fibranne	ISO 105-F02
#405	2,5 Acetate	ISO 105-F07
#407	PET “Dacron”, Type 54	ISO 105-F04
#408	Polyacrylnitrile “Orlon”, Type 75	ISO 105-F05
#413	Cotton for Crockmeter	without optical brighteners ISO 105-F09
#414	Wooltricot	JWS SM29 Hercosett, superwash

4 Methods

4.1 Sample preparation

A prerequisite for good coating results is a clean, homogeneous substrate. The substrate surface should be free of dust and other particles and have a uniform chemical composition to ensure a defect free coating. This is especially important in the field of thin film coatings where mono- or multilayers are applied on a substrate. In these cases it is often necessary to enforce strict cleaning procedures consisting of clean bench/clean room use and a thorough cleaning of all equipment employed in the coating process.

Fortunately the SNC does not require such drastic measures in terms of cleanliness. Only a minimal pre-treatment protocol was necessary to ensure consistent coating results: a cleaning step to remove dirt particles and other contaminants from the surface and an activation step to chemically prepare the surface for coating.

4.1.1 Cleaning procedures

The cleaning procedure for the standard substrate glass was adapted from an online tutorial by Dr. William R. Birch [71]. Samples were cleaned by 30 min ultrasonication (Elmasonic X-tra 70H, Digitana AG, Switzerland) in a 10% solution of “Deconex 11 universal” (Borer Chemie AG, Switzerland) at 50 °C, followed by rinsing with copious amounts of tap and distilled water. Samples were handled with blue PP forceps (Nalgene) and rinsed first holding the top of the slide and then holding the bottom of the slide with a clean forceps to ensure that no surfactant remained between forceps and sample. Samples were then dried in a dry nitrogen stream according to the scheme illustrated in Figure 4.1.

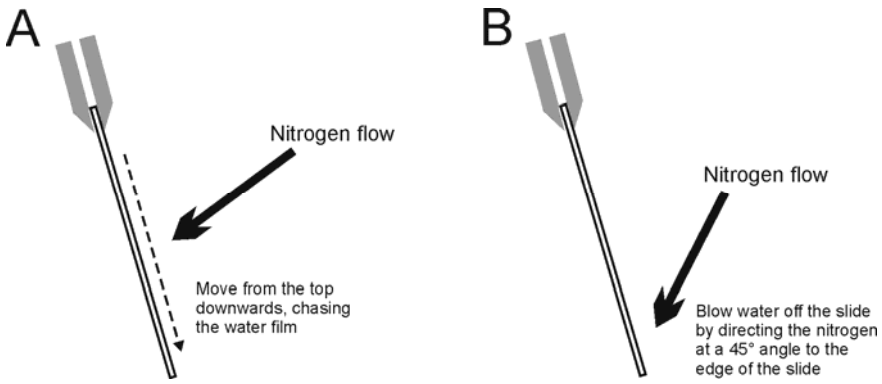

Figure 4.1. Drying flat substrates, adapted from Reference [71].

It is important to avoid water streaks or water drops that rewet already dried areas on the surface as they noticeably influence the coating results.

For thin glass substrates (Menzel reference #1, 0.1mm), the dry nitrogen stream was applied parallel to the side of the substrate to avoid breaking the glass. Glass samples were immediately used after cleaning and required no further activation step. The substrates were fully wetted by water after the cleaning step in basic Deconex solution, indicating a predominantly hydrolyzed surface.

Silicon wafers were cleaned analogous to glass, but required an additional activation step prior to coating. PDMS was cleaned by rinsing with deionized water and subsequently activated. Aluminum samples were cleaned by 15min ultrasonication in chloroform followed by rinsing with deionized water and subsequent activation.

4.1.2 Surface activation

Silicon, PDMS and aluminum substrates were activated in a laboratory plasma machine “Femto” from Diener Electronic (Germany) with oxygen as process gas at 100W (100%) generator power. Substrates were typically activated for 2-10min. For an additional functionalization of the SNC, coated substrates were activated for 5min at 50% generator power. After plasma treatment all substrates were rinsed with deionized water and dried in a nitrogen stream.

4.2 Coating procedures

4.2.1 Gas phase coating procedure

The gas phase coating procedures were developed in close collaboration with Dr. Georg Artus, as an expansion of the procedure employed by Dr. Stefan Jung [33].

4.2.1.1 Setup

The setup developed for the gas phase coating procedure is illustrated in Figure 4.2. The coating setup consists of three central elements: A coating chamber, a humidity adjuster to prepare the gas mixture for flushing the chamber and a remote controlled opening mechanism for the silane vial. A standard vacuum desiccator (Schott DURAN, total volume ~ 6.5L) with an inlet and outlet valve is used as coating chamber. The gas inlet is routed to the bottom of the chamber with glass tubing. The standard perforated ceramic plate supplied with the desiccator acts as the platform for the sample holder and silane vial holder.

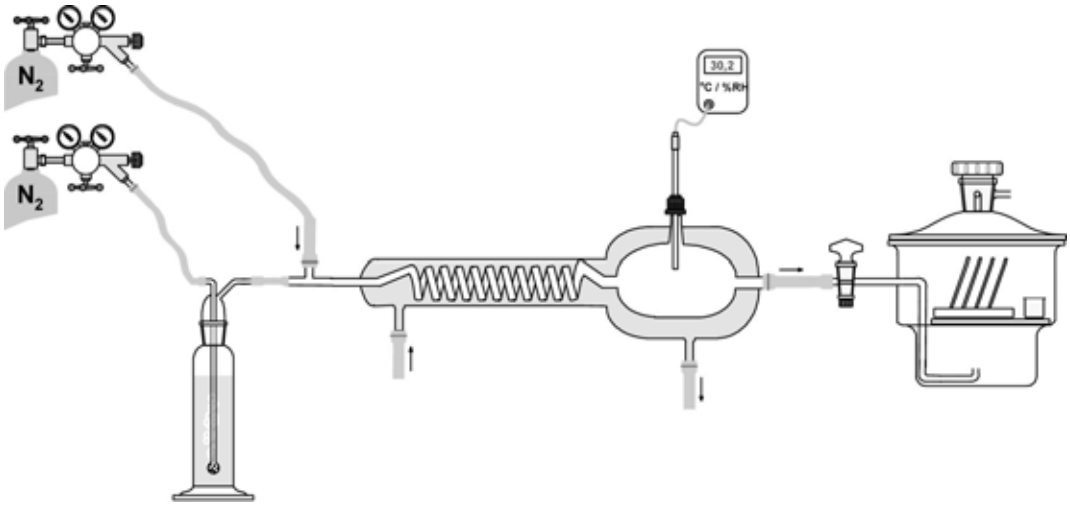

Figure 4.2. The gas phase coating setup.

The humidity adjuster is comprised of a custom built mixing chamber with an inlet for dry and humidified nitrogen. Humidified nitrogen was generated by flushing dry nitrogen through a water filled gas-washing bottle. The humidity of the gas mixture was regulated by controlling the ratio of dry and humidified nitrogen with the help of two flow-meters (WISAG). The temperature inside the mixing chamber was controlled by a water thermostat (Haake FE). Humidity and temperature of the gas mixture was determined with a EE23 hygrometer (E+E Elektronik).

For a controlled release of the reactive silanes inside the reaction chamber, a custom built, remote controlled, spring loaded silane vial holder was fabricated. Silanes were filled into 500µl Eppendorf caps inside a nitrogen flushed dry-box (ITA Spezial, InerTec) using positive displacement pipettes (Microman, Gilson). If required, the amount of silane could additionally be determined with an electronic scale (AB54-S, Mettler Toledo) installed in the dry-box. The closed caps were placed into the vial holder and introduced into the reaction chamber prior to equilibration. To start the reaction, a catch holding the spring could be released from outside of the reaction chamber using a magnet. This triggered the opening mechanism for the vial, enabling the evaporation of the silane inside the reaction chamber.

A Teflon base with 1mm milled slots was used as a sample holder for glass slides. All other substrates could usually be introduced into the reaction chamber without a holder.

4.2.1.2 Protocol I

To yield reproducible coating results, the following coating protocol was followed:

1. Equilibrate mixing chamber at 30°C.
2. Set dry and humidified nitrogen stream ratio to yield the desired humidity of the gas mixture (for a total flux of $2Lmin^{-1}$)
3. Flush coating chamber for at least 1 hour to remove traces of HCl from previous coating processes.
4. Introduce substrates and silane loaded vial holder into the reaction chamber.
5. Equilibrate reaction chamber for 1 hour.
6. Isolate chamber by closing inlet and outlet valve.
7. Start the reaction by triggering the opening mechanism of the vial holder.
8. Wait for 12hrs (overnight).
9. Remove vial holder and samples from reaction chamber and thoroughly flush chamber with a jet of dry nitrogen.
10. Rinse substrates with deionized water.
11. Anneal substrates if required.

In the standard coating procedure, 300±10µl TCMS were used for the coating of 5 clear glass slides (25x76x1mm) at a coating temperature of 24 ±2°C and a RH of 35±2%. This corresponds to roughly equimolar amounts of water and TCMS inside the reaction chamber at the start of the reaction (2.6±0.1mmol TCMS and 2.5±0.2mmol H_2O).

4.2.1.3 Protocol II

For coating substrates that are sensitive to HCl, the coating protocol was adjusted to minimize the development of HCl in the reaction chamber. Instead of TCMS, methyltrimethoxysilane (MTMS) was employed in the coating. Subsequently, methanol instead of HCl develops during hydrolyzation of the precursor molecules. It was found however, that small amounts of TCMS included in the reaction mixture were still necessary for a successful coating. This is probably due to a catalytic effect that traces of HCl have on the hydrolyzation or condensation reaction.

As MTMS possesses a relatively low vapor pressure, the small Eppendorf cap could not be used as silane vials. They would clog with polymerized MTMS very early in the coating process. Instead, 5ml glass vials with stopper were used to introduce the reagents into the reaction chamber. Typically 300µl MTMS and 20µl TCMS were mixed in the vial and placed inside the reaction chamber after equilibration. This involved an opening of the reaction chamber after

equilibration and consequently a loss of control over the exact reaction conditions. Since Protocol II was only employed occasionally and no large number of reproducible coatings was required, the setup was not further optimized for coating with MTMS. Typically the same process and equilibration conditions were used for Protocol II as for Protocol I.

4.2.2 Solvent phase coating procedure

The solvent phase coating setup was developed as an alternative to the gas phase setup.

4.2.2.1 Setup

Figure 4.3 illustrates the solvent phase coating setup.

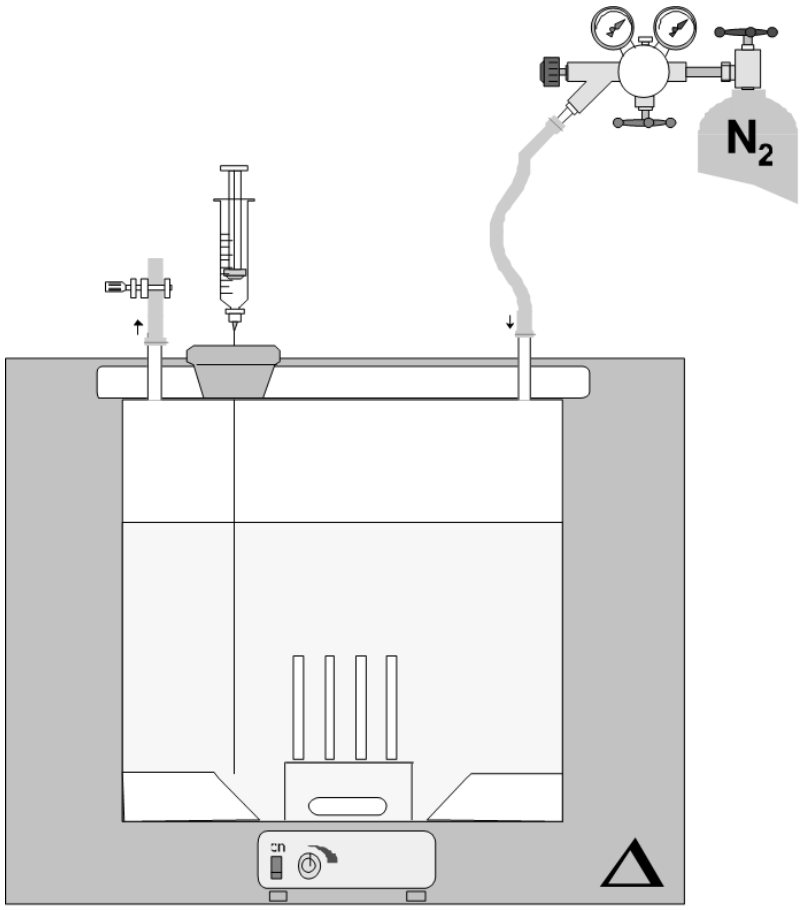

Figure 4.3. The solvent phase setup

The setup consists of a custom built reaction chamber and a thermostat. The reaction chamber, with an inner diameter of 90mm and a depth of 110mm (volume ~700ml), is made of aluminum. The inside of the chamber was coated with 500-1000µm of ECTFE Halar® by EPOSINT (Switzerland). Halar is a fluoro-chloro-hydrocarbon polymer that combines an exceptional

chemical stability with an extremely low water uptake (<0.1% according to the manufacturers specifications). This is important to ensure that the walls of the reaction chamber are inert to the coating reaction. The coating chamber is sealed by a Teflon lid with a gas inlet and outlet valve for flushing the chamber. A Teflon holder was used to fix the samples inside the reaction chamber.

Typically 250ml of toluene (Acros, extra dry) were used as solvent[4]. The water content of the solvent was adjusted inside the reaction chamber by flushing the chamber with dry or humidified nitrogen. A coulometric Karl-Fischer Titrator DL32 (Mettler Toledo) was used to determine the final water content. The reaction temperature was adjusted with a water thermostat Thermomix 1460 (B. Braun) for temperatures above 20°C and a water cooled thermostat HS40 (Huber) for temperatures between 10 and 20°C. TCMS was introduced into the reaction chamber through a septum with a µl syringe (Hamilton). The reaction mixture was stirred with a remote controlled magnetic stirrer (H+P Labortechnik), typically at 240rpm.

4.2.2.2 Protocol

The following protocol was developed to yield reproducible coating results with the solvent phase setup:

1. Place magnetic stirrer and sample holder with cleaned substrates into the reaction chamber.
2. Add 250ml toluene (Acros, extra dry).
3. Close and seal reaction chamber.
4. Place reaction chamber inside thermostat, set at desired temperature.
5. Equilibrate for 30min.
6. Remove 2ml toluene from the reaction chamber (ml syringe) and perform water content determination.
7. Flush chamber with dry or humid nitrogen to adjust toluene water content.
8. Equilibrate for 10min.
9. Repeat steps 6-8 until the desired water content is reached (usually 2-3 cycles).
10. Equilibrate for 1 hour
11. Perform final water content determination.

[4] It was noticed that for some batches of toluene the coating would be unsuccessful. In these cases, TCMS would visibly polymerize in solution, independent of the water content. Changing to a different bottle of toluene would solve the problem. We suspect that small impurities or contaminations of the toluene, that catalyze the polymerization of TCMS, are responsible for this behaviour but the true reason could not be elicited.

12. Add TCMS into the reaction chamber with a µl syringe (rinse syringe at least 3 times with dry toluene before and afterwards to remove traces of water and to prevent polymerization inside the needle and syringe)
13. Wait for chosen time
14. Open reaction chamber and remove samples.
15. Rinse samples with dry toluene, ethanol and deionized water
16. Anneal substrates if required.

The empirical method to adjust the water content of the reaction solution could not be avoided. It was impossible to sufficiently control the humidity and pressure of the nitrogen used to flush the chamber. With experience however, the water content inside of the reaction mixture could be set to the desired water content to within 10ppm after two flushing steps and within 2ppm after the third flushing step. It was also found that the chosen strategy to adjust the water content was the best suited for our purposes. Dry toluene is very hygroscopic and will equilibrate very fast with its environment. Strategies like mixing defined amounts of wet and dry toluene to reach a desired water content are therefore not feasible. It was found for instance that the water content of the dry toluene added to the reaction chamber would differ by as much as 100ppm, depending on the temperature and relative humidity in the lab at the time of filling. A possible alternative strategy to adjust the water content of the toluene would be to add the required amounts of water to the dry toluene inside the reaction chamber and ultrasonication of the mixture to speed up the solving process.

The solvent phase coating was performed for a variety of TCMS concentrations, water contents, reaction times and temperatures. As with the gas phase coating, it was found that equivalent coating results can be achieved with MTMS, provided that catalytic amounts of TCMS or HCl are added to the coating solution.

4.2.3 Annealing

Annealing was performed in a drying oven (Heraeus, Switzerland) under ambient atmosphere. Typically samples were annealed at 200°C overnight. A short assessment of the influence of temperature and annealing time on the wetting properties of the coating was also performed. For this purpose, 5 coated glass samples were placed in the drying oven at 200°C, removed at set intervals and evaluated in terms of contact and sliding angles. The same process was repeated with fresh samples at 100°C.

4.3 Sample processing and evaluation

4.3.1 Chemical Durability

To assess the long term chemical durability of the SNC, several dip tests in a number of organic and aqueous solutions were performed. Typically four annealed samples from different coating batches were evaluated. Coated samples were immersed in a particular solution in sealed glass vessels for a total immersion time of 182 days. At timed intervals, samples were removed, rinsed with water, dried with a nitrogen stream and characterized by static contact angle and sliding angle measurements before being returned to the solution. Each sample was evaluated at four designated positions with subsequent measurements at random control positions to exclude a possible bias. For reference, one non annealed sample was also immersed in the same solution and evaluated accordingly.

The following solutions were prepared and employed in the stability tests: Toluene , acetone and chloroform were used as received. pH 0 solution was produced by diluting hydrochloric acid , pH 3 solution with diluted acetic acid , pH 11 with diluted ammonia solution and pH 13 with diluted sodium hydroxide . pH measurements were performed with an inoLab pH electrode (WTW, Germany). Ammonia and acetic acid were chosen for the mild pH solutions since they are part of many cleaning agent formulations.

The following standard detergents were supplied by IMPAG AG and used in 10%vol solutions: Glucopon 215 CS UP (non-ionic surfactant, pH 12), Dehyton K (amphoteric surfactant, pH 9.5), Texapon NSO BZ (anionic surfactant, pH 4.5), Dehyquart A-CA (cationic surfactant, pH 3.5).

4.3.2 Outdoor weathering

To study the environmental durability of the SNC on glass, an outdoor weathering test was performed. To illustrate the benefits of the superhydrophobic effect on outdoor applications a setup was devised that allowed a continuous visualization and monitoring of the coatings performance. The setup was comprised of two webcams (Monacor, TVCCD-162SCOL) mounted at 70° inclination on the weather side of our lab (facing north-west). A coated and annealed glass slide (∅50mm x 1mm) was fixed in front of one of the webcams and an untreated glass slide in front of the other. Figure 4.4 shows the experimental setup.

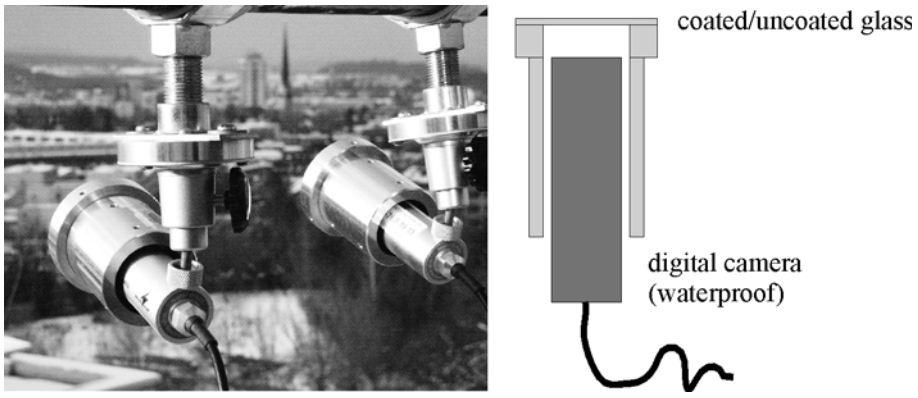

Figure 4.4. Picture of the camera setup for the outdoor weathering experiments (left) and cross section of the aluminum mount to fix the glass slides to the camera.

At regular intervals, especially during rain or snow, pictures or movies were recorded with the webcams. Also CA and SA measurements were performed on a regular basis. The transmittance of the glass slides in the visible range was evaluated before and after the experiment by UV/vis spectroscopy. Changes in the microscopic structure were visualized by SEM. Outdoor exposure was performed for a total duration of 12 months from September 2004 until September 2005.

4.3.3 Artificial weathering

The artificial weathering tests were devised and performed in collaboration with Dr. Felix Reifler and Ulrich Schrade of the AdvancedFibers group at the Empa St. Gallen.

As there are no standard procedures available for the evaluation of weathering effects on thin film coatings, suitable procedures were chosen from other, related fields.

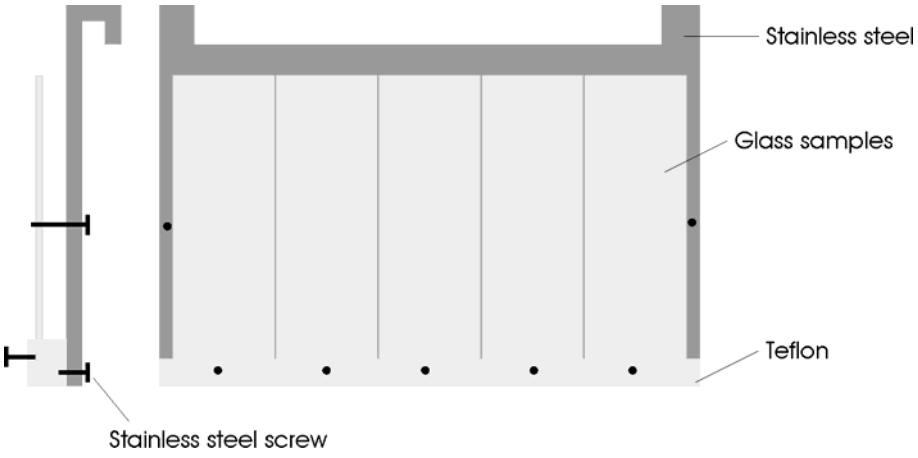

Figure 4.5. Side view (left) and front view (right) of sample holder employed in the artificial weathering experiments.

Laboratory (UV) weathering was performed according to ISO 9022-9:2000-09 [72] and a combined UV and acid rain weathering according to VDI 3958 Part 12 [73].

For mounting the glass samples inside the testing chambers, a custom built sample holder was devised which is illustrated in Figure 4.5. Although Teflon is considered an inert material, it was found that in the vicinity of the Teflon, the coating would haze and loose its superhydrophobic properties. If a second Teflon rim was attached to the top of the slides, rivulets would form on the slides during the acid rain weathering tests (see second to right slide in Figure 4.6). These would originate from the top Teflon rim and cause a hazing of the slides with subsequent loss of superhydrophobicity. To avoid these disturbances, the samples were only fixed at the bottom.

4.3.3.1 Laboratory weathering according to ISO 9022-9:2000-09

Laboratory weathering was performed in a Ci65A Xenon Weather-Ometer (Atlas Material Testing Technology GmbH, Germany) according to ISO 9022-9:2000-09 [72] (degree of aggression 4) using the following operating parameters: water cooled xenon arc lamp (inner and outer filter: borosilicate glass); irradiation: $0.54 Wm^{-2}nm^{-1}$@340nm (corresponding to $625 Wm^{-2}$ @300-800nm, which is in reasonable accordance with ISO 9022-9 requiring an irradiation of $623 Wm^{-2}$ @320-780 nm); black standard temperature: $78 \pm 2°C$; air temperature: $55 \pm 2°C$; relative humidity: $20 \pm 3\%$.

The sample holder with two non annealed and three annealed samples was placed at the height of the middle tier of the specimen rack into the exposure chamber. The total exposure time was 240 hours.

4.3.3.2 Acid Dew and Fog test according to VDI 3958 Part 12

The effect of acid rain on the coating was investigated using the so called "Acid Dew and Fog" test (ADF test) according to VDI 3958 Part 12 [73]. Test variant “C” was chosen to simulate conditions for Central Europe and degree of aggression I (pH 2.5) as recommended for paints and coatings. The samples were mounted in a Global UV testing chamber (systems Weiss type BAM, Weiss Umwelttechnik GmbH, Germany) by means of the custom-made sample holder as illustrated in Figure 4.6.

Figure 4.6. Global UV chamber (left) and sample holder during rain and UV exposure (right).

The 24 h ADF cycle comprised four distinct phases.

1. In a first step (spraying phase, duration: < 5min), the samples were sprayed with an acid solution (mixture of H_2SO_4, HNO_3 and HCl in a mass ratio of 1 : 0.3 : 0.17, diluted with deionized water to a pH of 2.5) using a commercial sprayer as it is used in household applications. One sprayer burst at a distance of approx. 30cm was applied for each group of 5 samples (= one sample holder) to cover the surface of the samples with little droplets (mean diameter: ~60µm), replicating the deposition of acid dew in the early hours of the morning under a clear sky. Due to the superhydrophobic nature of the sample surface, the resulting load (~5g/m^2) was considerably lower than the load specified in VDI 3958 Part 12 (30-40g/m^2).
2. In the following first drying phase, the samples were kept at 35°C and 30% relative humidity (RH) for 9 hours and afterwards at 60°C and <10 % RH for 5 hours.
3. In the following rain phase, the samples were sprinkled with deionized water at 35°C for 4 hours.
4. Finally this was followed by a second drying phase at 60°C and 10% RH for 6 hours.

According to VDI 3958 Part 12, after every 5 complete ADF cycles, there followed 2 cycles with omission of the spraying phase. During steps 2 to 4, the substrates were subjected to UV radiation simulating the global radiation in the range of 290nm to 450nm (UV-A: 36Wm^{-2}; UV-B: 40Wm^{-2}; UV-C: 2.4Wm^{-2}). The intensity of the UV radiation was measured with a UV-Radiometer (Minolta Radio-Meter UM-1) using three different sensors for the UV-A (360-480nm), UV-B (310-400nm) and UV-C (220-390nm) part of the spectrum, respectively.

For the ADF test, a total number of 24 annealed and 8 non annealed samples were exposed for the recommended duration of 4 weeks. Six annealed and two non annealed samples were removed from the chamber after every week to monitor the contact angle and sliding angle

development as well as for scanning electron microscopy and UV/vis studies. To exclude a possible bias due to a samples position relative to the water nozzles, the samples were arranged in the holders and exchanged systematically.

4.3.4 Evaluation of textile samples

Textile evaluation procedures were devised and performed in collaboration with the AdvancedFibers group at the Empa St. Gallen.

4.3.4.1 Tensile strength according to ISO 13934-1:1999

The tensile strength and the elongation at break of coated and uncoated samples were evaluated on a INSTRON 4502 universal testing instrument (Instron Corporation, Norwood, MA, USA) in the style of ISO 13934-1:1999[74] using the following parameters: testing direction: weft; sample width: 23-56mm; initial length of the sample: 50mm; pretension: slack mounting of the samples; rate of extension: 50 mm/min; testing atmosphere: 23+/-1°C, 50+/-2% rel. humidity. Tests were carried out in triplicate. All samples were preconditioned in the testing atmosphere for at least 24 hours before testing.

4.3.4.2 Plastron stability

To evaluate the stability of the gas layer that forms upon immersion of SNC substrates in water, a 2 x 5cm sample of coated PET fabric was placed in a beaker of deionized water and pictures taken over the course of 2 months.

4.3.4.3 Friction test

Frictional load was applied to the samples using a Textile Friction Analyzer (TFA) primarily designed for the instrumental simulation of skin-fabric contact and friction. A skin simulating polyurethane-coated polyamide fleece (Lorica® Soft, Winter Creation AG, Münchenstein, Switzerland) was used as the friction partner for the silicone nanofilament coated glass plates and textile substrates.

The TFA works on the reciprocating sliding principle: the lower friction partner is mounted on a reciprocating sled (metallic block) oscillating with a given frequency and sliding velocity. The upper friction partner is mounted on an elevation arm which provides enhanced friction by applying a vertical load over an adjustable force range. A detailed description of the TFA can be found elsewhere [75].

For the reference measurements, the nanofilament coated glass plates (30mm x 10mm) were mounted as the lower friction partner, with Lorica® mounted on the elevation arm (round swatches, Ø 28mm). In the case of the nanofilament coated textile substrates, the arrangement was vice versa: Lorica® mounted on the reciprocating sled (lower friction partner), and the coated textile fabric (round swatches, Ø28mm) acting as the upper friction partner. There was one PET swatch rubbed along the warp and along the weft direction against the skin equivalent, respectively. All samples were mounted on the sample holders using double-sided adhesive tape.

The friction experiments were carried out using the following experimental parameters: normal load: 5N; oscillating frequency: 1.25Hz; stroke: 20mm; resulting sliding velocity: 62mm/s; number of cycles: 1450; textile standard climate (20±1°C, 65±2% relative humidity). All samples were preconditioned in the testing atmosphere for at least 24 hours before testing. A normal load of 5N (equivalent to an apparent pressure of 7.7kPa) is comparable to the pressure at the skin-mattress interface for a bedridden person.

4.3.4.4 Machine washing according to ISO 6330:2000

Washing was performed according to ISO 6330:2000 [76], procedure 8A (delicate cycle, 30°C, total amount of polyester ballast: 2kg, total amount of washing agent 28g) in a reference washing machine (Wascator FOM 71 Lab; Electrolux Laundry Systems, Hvidovre, Denmark). For the washing process, a 6 x 14cm sample was stitched onto a piece of ballast.

4.3.4.5 Oil resistance test according to ISO 14419:1998

Oil repellency was evaluated according to ISO 14419:1998 [77]. In this test, drops of standard test liquids, consisting of a selected series of hydrocarbons with different surface tensions, are placed on the substrate surface and then observed for absorption, wicking and contact angle. The oil repellency grade is the highest numbered test liquid which is not absorbed by the substrate surface. The tests were performed in textile standard climate (20±1 °C, 65±2% relative humidity). Test specimens were conditioned for 24 h in the test climate prior to testing.

Preliminary tests on various small samples revealed an oil repellency grade lying between 5 and 7. The subsequent evaluation with samples having a greater surface was then limited to this region using n-dodecane, n-decane and n-octane as standard test liquids for oil repellency grades 5, 6 and 7, respectively. Because of sample size limitations, the distance between the individual drops had to be reduced to approx. 1.5 cm.

According to the standard, the drops should be placed on a minimum of five locations representing all physical and color characteristics of the fabric. Since the nanofilament coated

samples have only one physical and color characteristic, it was possible to reduce the amount of drops necessary to a minimum of 2 for each of the test liquids for oil repellency grade 5 to 7.

4.3.5 Chemical Modification

The following procedures were applied to subsequently alter the wetting properties or add specific functionalities to the SNC. Prerequisite for a further functionalization is a plasma activation of the SNC (4.1.2).

To reapply a hydrophobic methyl-functionality to the activated SNC, samples were placed in a 1mmol solution of OTS in anhydrous toluene under a dry nitrogen atmosphere (drybox, custom built) overnight, followed by rinsing with dry toluene, ethanol and deionized water.

The same procedure could be applied to add a fluorine-functionality to the surface. In this case a 1mmol solution of PFOTS was used as coating solution.

To add a carboxyl-functionality to the activated SNC, the above procedure was performed with a 1mmol solution of CETS. After coating the ester was cleaved by treating the surface with alkaline buffer (phosphate buffer, pH 11.5) for 30min to obtain bare carboxyl groups on the surface.

A procedure adapted from the literature was used to add an amino-functionality to the activated SNC [78]. Here the substrates were dipped in a 10mM solution of APTES in anhydrous toluene for 4 hours under dry nitrogen.

Typically 2-5 samples were placed in 60ml of the coating solutions. Essential to good coating results was a very low water content of the anhydrous toluene. If the water content exceeded 10ppm, the coating quality would decrease and the silanes would noticeably polymerize in the solution

4.3.6 Patterning

During plasma treatment of the SNC, regions of the sample could be shielded from the oxygen plasma by covering them with a glass slide. Sub mm structures were activated by applying a thin layer of vacuum grease between the glass slide and the sample to prevent the oxygen plasma from diffusing under the glass slide. The grease could be removed after the activation step by rinsing or ultrasonication in acetone.

In the subsequent functionalization step (4.3.5), only the previously activated areas of the SNC would be coated, even if the whole sample was immersed in the coating solution. In this way, by subsequently activating and coating the SNC, regions of varying functionality could be

generated on a single sample. Scheme 4.1 illustrates the simple procedure to create a trifunctional, patterned surface from a SNC template.

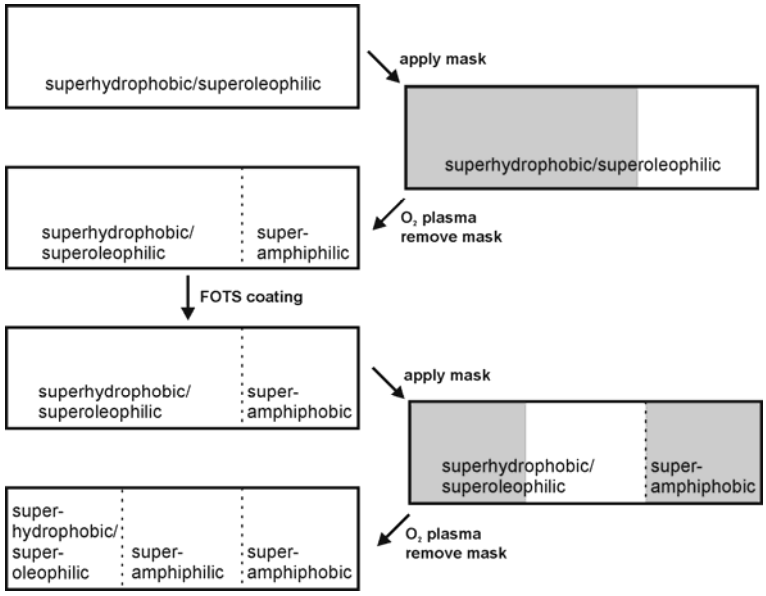

Scheme 4.1. Coating procedure to create a trifunctional surface from a silicone nanofilament template.

4.3.7 Protein adsorption experiments

The protein adsorption experiments were performed in collaboration with Michael Rabe of the Institute of Physical Chemistry at the University of Zurich.

The adsorption of fluorescently labeled β-Lg on the plasma activated as well as on the amino- and carboxyl- functionalized SNC was monitored at pH 3 and pH 6 (citrate buffer, 50mM) in a continuous flow cell setup. The fluorescence count rate generated by the adsorption of labeled proteins to the surface was measured with the super critical angle fluorescence (SAF) biosensor [79,80].

All proteins used in this work were labeled with the fluorescent dye DY-647 according to the manufacturer's protocol and subsequently diluted with an excess of unlabeled proteins to yield a probe in which 10% of all molecules were labeled. A recent study shows no evidence that the fluorescent tag alters the adsorption properties of proteins of this size [81]. A final protein concentration of 1.0×10^{-7}M was obtained by diluting the appropriate volume of the stock solution in buffer. The preparation of the buffer solutions and protein labeling was performed by Michael Rabe. Details on the exact procedures can be found in a recent publication [81].

4.3.8 Wettability gradients

The experiments were performed in collaboration with Sara Morgenthaler from the Surface Science and Technology group at the ETH Zürich. Coated samples were gradually immersed in 2M NaOH solution using a linear motion drive.

4.4 Analytics

4.4.1 Contact/sliding angle measurements

Contact angle measurements were performed on a Contact Angle System OCA and included software (DataPhysics, Germany). For static contact angle measurements, digital drop shape analysis was performed on 10µl sessile drops of test liquids using the Laplace Young fitting routine. Sliding angles were measured on the same drop immediately afterwards with the help of a home built tilting table, also on 10µl drops. All measurements were performed at ambient conditions.

Sliding angle and not contact angle hysteresis was measured because of the experimental difficulties associated with measuring and analyzing advancing and receding contact angles at very high contact angle values (2.3).

The limit of sliding angle measurements is 90° inclination. Once test liquids do not roll off a surface even at 90° of inclination they will be referred to as “sticking” drops. No further analysis was performed on sticking drops since we were primarily interested in surfaces with low sliding angles.

4.4.2 Roll-off behavior on rough heterogeneous surfaces (“Water shedding angle”)

Figure 4.7 depicts the principle of the setup employed for the measurements of the water shedding angle (WSA) on textile samples. The setup consists of the same contact angle system used for the normal contact angle measurements as well as the custom built tilting table. Textile samples were glued onto glass cover slips with double sided adhesive tape and placed onto the tilting table at set inclination. The needle of the automated syringe was placed at 1.0±0.1cm above the sample in a way that the drops falling from the syringe would contact the sample 2cm from the bottom end of the sample. Figure 4.7 illustrates the basic principles of the setup.

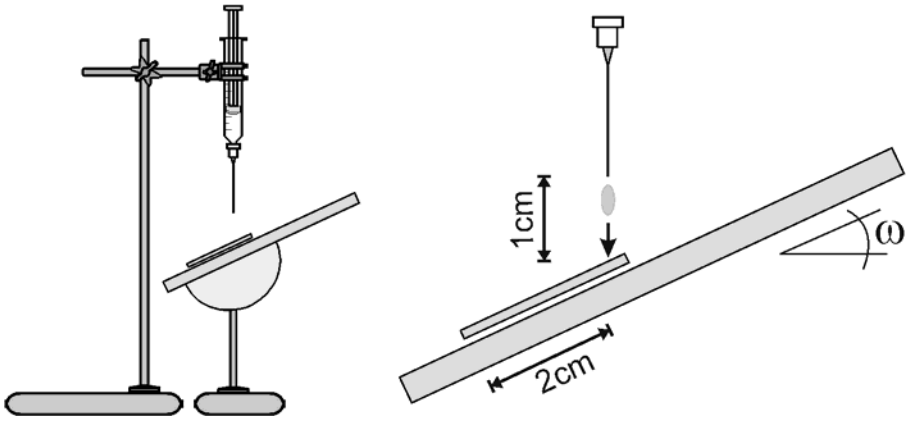

Figure 4.7. Experimental setup used for measuring the superhydrophobic character of macroscopically rough surfaces.

Two needles with inner diameters of 130µm (Hamilton #90531) and 250µm (Krüss #NE 43) were used to produce water drops of 5±0.3µl and 13±0.3µl volume respectively. To control the size of the drops released from the needle, a drop of 4.5 or 12.5 µl volume was produced at the needle tip using the automated syringe control of the contact angle system. Then the drop was successively expanded by 0.1µl until it detached from the needle.

To determine the WSA, measurements were started at an inclination angle of 85°. Drops of water were released onto the sample at a minimum of 3 different positions, each 2cm from the bottom end of the sample. If all drops completely bounced or rolled off the sample, the inclination angle was reduced by 5° and the procedure repeated until one or more of the drops would not completely roll off the surface. This could either be evident from the whole of the drop coming to rest on the surface after rolling a short distance or from parts of the drop sticking to the surface at the impact point or on the path down the incline. The lowest inclination angle at which all the drops completely rolled or bounced off the surface was noted as the WSA.

The WSA was always determined for both volume drops independently. Additionally, the WSAs were determined at a needle-substrate distance of 4cm to gage a possible effect of impact velocity on the WSA. 4cm was the greatest drop distance possible with the available setup.

4.4.3 Electron Microscopy

Electron microscopy was performed with a SUPRA 50VP (Zeiss, Germany). Unless otherwise specified, samples were coated with 5 nm of platinum and analyzed at 2 kV at a working distance of 2mm using in-lens detection.

4.4.4 UV/Vis spectroscopy

The optical transmittance of coated glass slides was measured with a Lambda 900 UV/Vis spectrometer (Perkin Elmer) against air.

4.4.5 X-Ray Photoelectron Spectroscopy (XPS)

All XPS measurements were performed by Dr. Giuseppino Fortunato of the Empa St. Gallen. XPS measurements were performed using a PHI LS 5600 instrument with standard MgKα X-ray source. The energy resolution of the spectrometer was set at 0.4 eV/step at a pass energy of 93.9 eV for survey scans and 0.125 eV/step and 29.35 eV pass energy for region scans. The X-ray beam was operated at a current of 25 mA and an acceleration voltage of 13kV. Charge effects were corrected using Carbon 1s = 285.0 eV. The concentrations of the surface species were determined using CasaXP software (peak areas were evaluated using the instrument specific relative sensitivity factors).

4.4.6 Supercritical Angle Fluorescence (SAF) biosensor

SAF measurements were performed by Michael Rabe. Details on the SAF setup can be found in various publications [79,80,82]. On the modified SNC, the retention of fluorescently labeled proteins was measured on a circular area with a diameter of roughly 60µm. The laser intensity was reduced to approximately 5µW through grey filters (New Focus, USA). A shutter across the laser beam allowed for the collection of the total fluorescence every 60s over a long period of time without risking photobleaching. All measurements were conducted in a flow cell composed of a metallic support on which a coverslip with the desired surface coating was glued. The analyte solution was pumped through the flow cell at room temperature using an Ismatec peristaltic pump (flow rate: 0.25ml/min).

5 Results and Discussion

5.1 Gas phase coating

The objective for the gas phase coating setup was to develop it in a way that enables a systematic approach to optimizing the coating process and understanding the influences of the coating parameters on the coating results. For this purpose, it was crucial to develop a coating setup and procedure that yielded reproducible coating results. With such a setup in hand, the general properties of a standard SNC were evaluated.

5.1.1 Improvements to the gas phase coating setup

The first improvement to the gas phase coating setup was the development of a new cleaning and pre treatment procedure for the standard glass substrates. Previously substrates were cleaned by ultrasonication in chloroform and a mixture of hydrochloric acid and methanol, each step followed by rinsing with deionized water [33]. Afterwards the substrates required activation either through physical (plasma treatment) or chemical ("piranha" solution) processes. The improved cleaning and activation procedure consists of only one ultrasonication step in a standard aqueous detergent solution, followed by rinsing with deionized water (4.1.1).

The second, decisive discovery was that only a single silane precursor is responsible for the formation of the SNC. Stefan Jung's work implies that a mixture of two precursors, TCMS and (3-Phenylpropyl)-trichlorosilane, is essential for the formation of the SNC. Early XPS studies conducted by Dr. Georg Artus however, already showed no contribution of (3-Phenylpropyl)-silsesquioxane to the coating composition.

The third important task was to devise a coating procedure that allowed for a better control of reaction conditions. The setup and procedure developed in the course of this work is detailed in the experimental section (4.2). Although the principle simplicity of the setup used by Stefan Jung could be preserved, several decisive improvements were introduced. Primarily, the means for a full control over the initial reaction conditions inside the reaction chamber were implemented. A system that allows for an equilibration of the reaction chamber at any desired humidity was developed, and a remote controlled opening mechanism to initiate the release of TCMS into the reaction chamber. In this way, the reaction conditions inside the chamber can be set, the system isolated and the TCMS released without the need to open the chamber and disturb the system. To avoid inconsistencies in the coating results, the coating process was furthermore formalized in

form of a protocol. In the current state the coating setup offers full control over the initial amounts of TCMS and water in the coating chamber. The temperature inside the laboratory was found to be sufficiently stable to reproduce the amount of samples needed for a meaningful evaluation of coating properties.[5]

While significantly improving the reproducibility of the coating process, the overall simplicity of the procedure was maintained. All parts of the setup consist of standard laboratory equipment or could be readily produced by the workshop and the glass blower. All chemicals are cheap and only used in small quantities. Pre-treatment of the glass substrates consist of only one cleaning step in a standard aqueous detergent solution. The whole coating process can be performed in a normal chemical laboratory under ambient conditions and, in particular, require no clean room facilities.

5.1.2 General properties of the SNC from gas phase

The coating procedure according to Protocol I (4.2.1.2) produced sufficiently reproducible coating results to be able to systematically evaluate the coatings properties. The as prepared standard coatings on glass exhibited static water contact angles of 160 ± 2° and sliding angles of 20 ± 4°. Figure 5.1 shows a drop of water on a SNC glass slide and a typical drop profile as it was recorded for CA measurements.

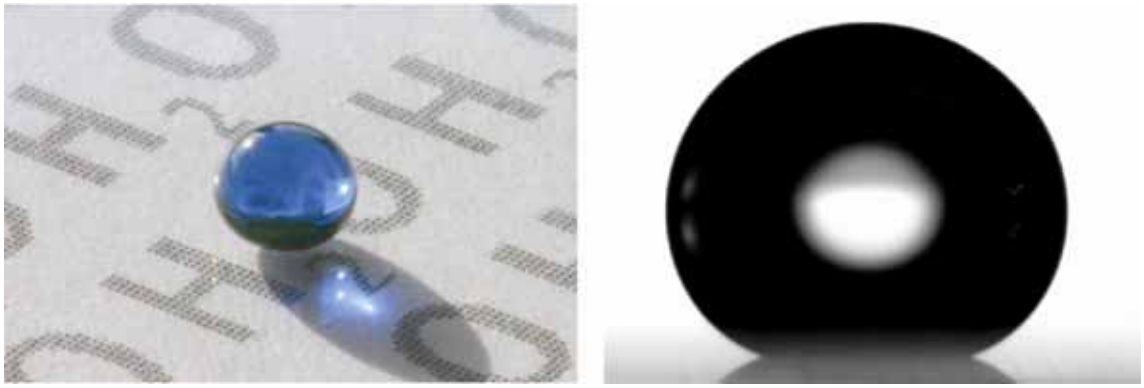

Figure 5.1. A 10µl drop of colored water on a SNC glass slide (left) and a typical drop profile recorded for CA measurements (right).

[5]Recently a temperature control unit was added to the coating setup and a full, systematic study of the influence of the individual coating parameters on the coating results is currently being conducted by Dr. Georg Artus

The standard coated glass samples showed an average increase in optical transmittance of 2.3 ± 0.6 %abs. in the visible range opposed to an uncoated glass slide (Figure 5.2).

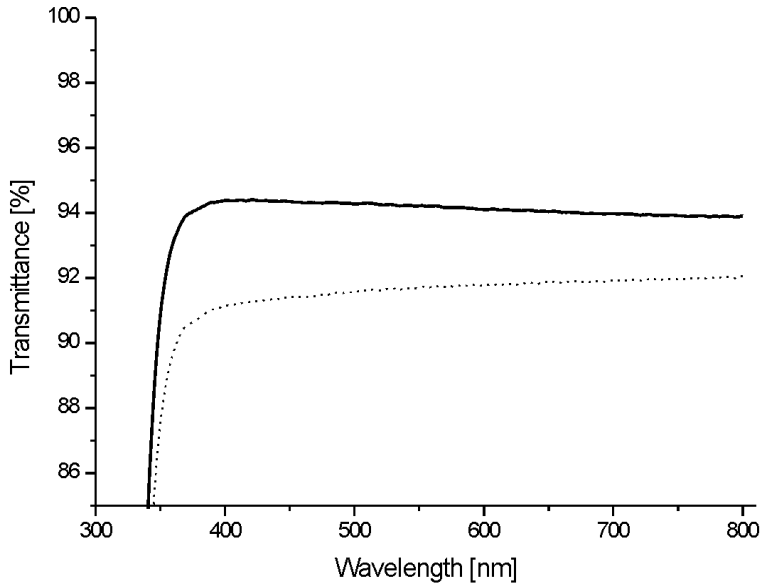

Figure 5.2. UV/vis spectrum of SNC coated glass slides according to Protocol I (solid line). Spectrum of an uncoated, freshly cleaned glass slide (dotted line).

Typical scanning electron microscopy (SEM) images of the standard coated glass slides at varying degrees of magnification are illustrated in Figure 5.3. The SEM images reveal a dense, homogeneous, carpet like growth of silicone nanofilaments on the glass surface. The filaments are roughly 10-30nm in diameter and anything from 50nm to a few micrometers in length. There is no indication of any systematic or preferred direction of growth. Filaments of varying size could be observed depending on the coating conditions, but the structure of the coatings is generally homogeneous. The inhomogeneous accumulation of large filaments that was observed on coatings produced with the old coating setup [33,70] are not observed, possibly because of the improvements to the cleaning procedure and a more rigorous coating protocol. Transmission electron microscopy performed by Dr. Artus indicate that the filaments are amorphous and solid [70].

Unfortunately a more detailed and quantitative analysis of the surface structure could not be performed due to a lack of suitable experimental procedures. Interesting parameters like surface area or surface roughness can not be determined from the 2-D SEM images. Attempts to record 3-D stereo SEM images of the coating failed due to the strong charging of the surface (despite sputtering with a conductive layer). As the filaments are flexible, surface charging during SEM imaging led to a constant change in filament arrangement. Reliable AFM measurements to

determine the surface roughness also proved difficult due to the filament flexibility and the tendency of the filaments to adhere to the scanning tip [70].

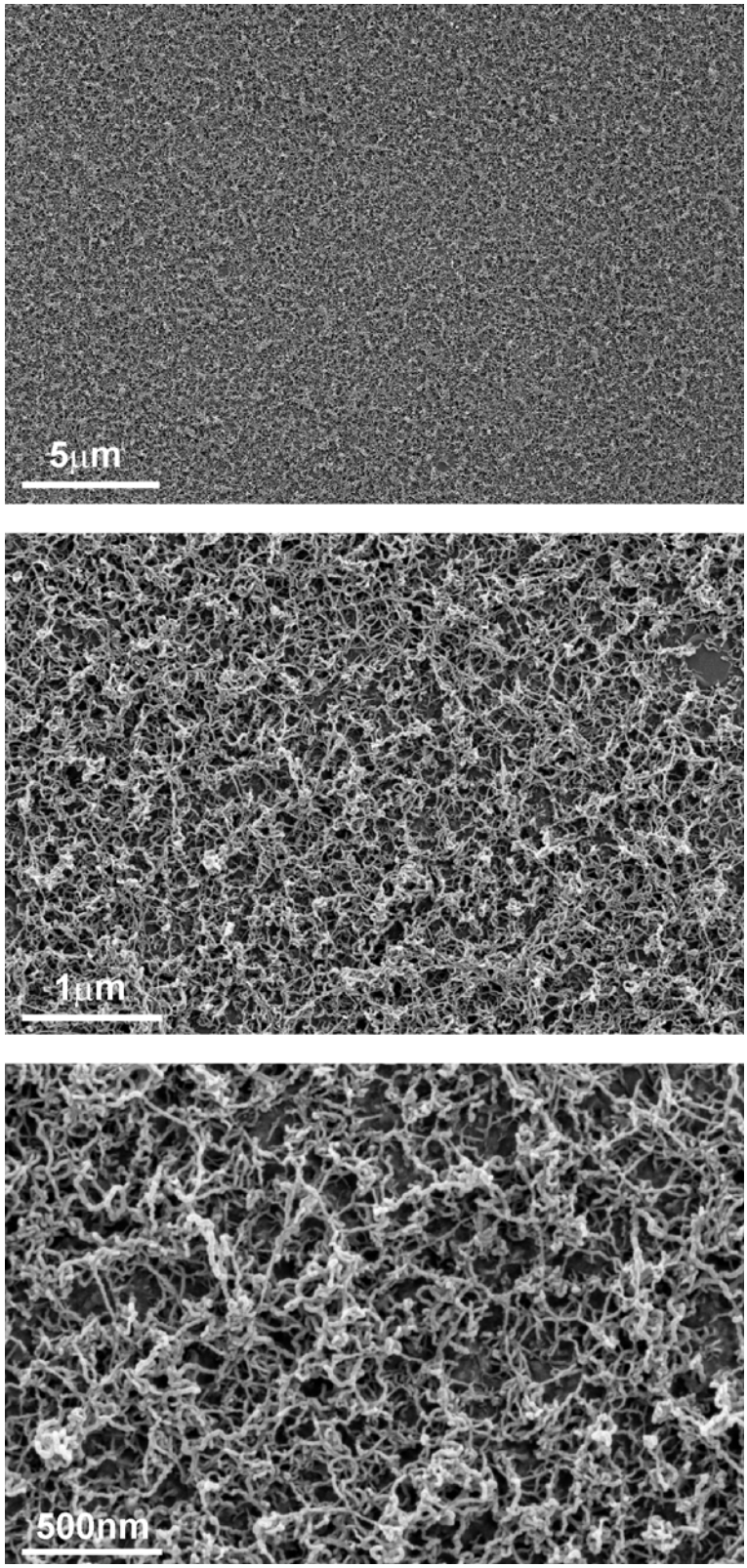

Figure 5.3. Typical SEM images of SNC glass slides at different magnifications.

Since TCMS is the only precursor molecule involved in the coating process (besides water) we can assume that the chemical composition of the filaments correspond to those of polymethylsilsesquioxane (PMSQ). XPS studies confirm this assumption and furthermore show no residual Cl-peaks, indicating that the TCMS precursors hydrolyze completely in the coating reaction or shortly afterwards upon exposure to ambient humidity. The atomic composition of the SNC on glass as determined from the XPS spectra is summarized in Table 5.1.

Table 5.1. Atomic composition and atomic ratios of the SNC as derived from its XPS spectrum.

	O	Si	C		Si/O	Si/C	C/O
AT%	41.4	29.8	28.8	AT ratio	0.72	1.03	0.72

The atomic ratios calculated from the XPS intensities correspond well with the atomic ratios expected for PMSQ (Si/O 0.67, Si/C 1, C/O 0.67).

5.1.3 Improving hydrophobicity by annealing

The hydrophobic properties of the PMSQ nanofilament coating is slightly improved by annealing. Upon annealing, the CA of the standard coatings improved from 160±2° to 164±2° while the SA decreased from 20±4° to 8±3°. The microscopic structure and the optical properties remain unchanged by the annealing process (Figure 5.4).

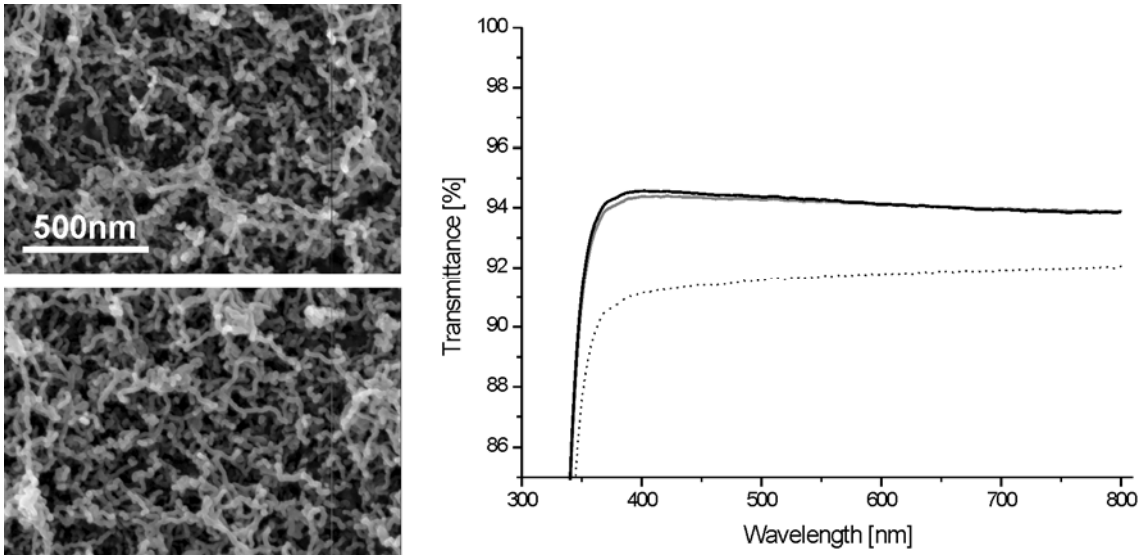

Figure 5.4. Left: high resolution SEM images of a SNC before (top) and after (bottom) annealing at 200°C for 12h. Right: Optical transmittance of the SNC before (light grey) and after annealing (black). The dotted line indicates the transmittance of a non coated glass slide.

Intrinsically PMSQ is a hydrophobic material because the solid/air interface is preferentially populated by the non polar methyl groups [40]. However, both the surface and the bulk will contain some degree of unreacted, hydrophilic silanol groups due to an incomplete polymerization [36,39,40,42]. Upon heating these will further condense and crosslink (2.1.4), increasing the hydrophobicity of the PMSQ network.

In case of the PMSQ nanofilament coating it is important to note that annealing has a stronger effect on the sliding angle than on the contact angle. Generally speaking this implies that in a Cassie state the sliding angle (or contact angle hysteresis) is more sensitive to changes in the intrinsic surface free energy of the coating material than the contact angle. This becomes clear when considering the wetting theory (2.2):

We can assume the system SNC-Water is in a Cassie-Baxter type wetting regime for the annealed as well as the non annealed samples. Both surfaces exhibit a high contact angle and a low sliding angle and show total reflectance upon immersion in water, indicating the presence of a gas/silicone nanofilament composite layer on the surface. The Cassie-Baxter equation for this system is given by equation:

$$\cos\theta_C = f_1 \cos\theta_1 + f_2 \cos\theta_2 \qquad (5.1.1)$$

where f_1 is the fraction of the liquid/air/solid interface under the drop and f_2 the solid/liquid fraction ($f_1 + f_2 = 1$). For a superhydrophobic, Cassie-Baxter type surface, the solid/liquid fraction is small. Approximating the contact angle on a flat PMSQ layer with that of PDMS (105°) and assuming that θ_1 is 180° and θ_C is 160°, this leads to an estimated solid/liquid fraction of roughly 8%, a typical value assumed for Cassie-Baxter type surfaces [55].

Assuming now, that the PMSQ filaments are largely composed of hydrophobic regions (A), with few hydrophilic defects (B), $\cos\theta_2$ can also be expressed in form of the Cassie-Baxter equation and (5.2.1) becomes:

$$\cos\theta_C = f_1 \cos\theta_1 + f_2 f_A \cos\theta_A + f_2 f_B \cos\theta_B \qquad (5.1.2)$$

with $f_A + f_B = 1$.

As before, θ_1 is 180° and assuming the hydrophilic defects to be perfectly hydrophilic (θ_B=0) the equation simplifies to:

$$\cos\theta_C = -f_1 + f_2 f_A \cos\theta_A + f_2 f_B \qquad (5.1.3)$$

From earlier considerations we know that $f_2 < f_1$ and equally $f_B < f_A$ otherwise the coating would not be intrinsically hydrophobic. Accordingly, $f_2 f_B << 1$ and is a negligible contribution to the right hand sum of Equation (5.2.3):

$$\cos\theta_C = -f_1 + f_2 f_A \cos\theta_A \qquad (5.1.4)$$

Also, the change in the hydrophobic surface fraction (f_A) due to a decrease in hydrophilic defects will be almost negligible, as the initial amount of hydrophilic defects is small. Consequently the contact angle improves only slightly with annealing.

Contact angle hysteresis on the other hand is generally considered to be caused by a pinning of the three phase contact line. The pinning of the contact line hinders an advancing or receding of the contact line by creating an energy barrier between metastable states. On a flat heterogeneous surface, surface inhomogeneities act as pinning points [83,84]. On rough surfaces, that exhibit Cassie-Baxter type wetting, contact angle hysteresis is caused by the pinning of the contact line at the surface asperities in contact with water. It has been shown to depend on the number, spacing, size and shape of pinning points [8,85,86]. How the chemical composition, or intrinsic wettability, of the surface asperities influences the contact angle hysteresis however has not been evaluated yet. In a recent work, Song *et al.* indicate that a small number of hydrophilic defects on a Cassie type surface can lead to a very high contact angle hysteresis without a significant change in contact angle [87]. If each surface asperity in contact with water acts as a pinning point, it becomes obvious that the higher the adhesion of the water to this pinning point, the larger the energy barrier for the contact line to advance or recede. Due to the larger number of hydrophilic defects, the non annealed PMSQ filaments should generally show a stronger adhesion to water than the annealed ones. The drop of water “sticks” better to the non annealed surface asperities than to the non annealed ones. Therefore the sliding angle on the non annealed samples is considerably higher than on the annealed samples. This microscopic interpretation of the influences of changes in the intrinsic wettability on the contact and sliding angle values of a Cassie-Baxter type wetting state are also supported by the results of the chemical durability tests (see Section 5.2.1).

The annealing temperature of 200°C is high enough to ensure a fast and thorough annealing but not too high as to cause a degradation of the PMSQ. Oh et al have studied the curing reaction and thermal stability of a 10’000 molecular weight PMSQ precursor under both nitrogen and air [39]. They found that the PMSQ undergoes three distinct changes upon gradual heating up to 800°C. Under nitrogen, the first step occurs between 100-425°C and is associated with the curing

reaction. In the second step, between 500-620°C, the methyl groups degrade and in the third step above 645°C the siloxane backbone degrades. Under air, the processes are the same only not as distinct. Between 100-185°C the curing reaction dominates but is already accompanied by a degradation of methyl groups. Between 213-307°C the degradation of methyl groups dominates but already a degradation of the siloxane backbone is in process. Above 307° the PMSQ backbone degrades.

To evaluate whether the annealing temperature of 200°C chosen for our experiments causes a degradation of methyl groups, the SNC coatings were annealed for a total time of 72h and the change in wettability determined by contact and sliding angle measurements (Figure 5.5).

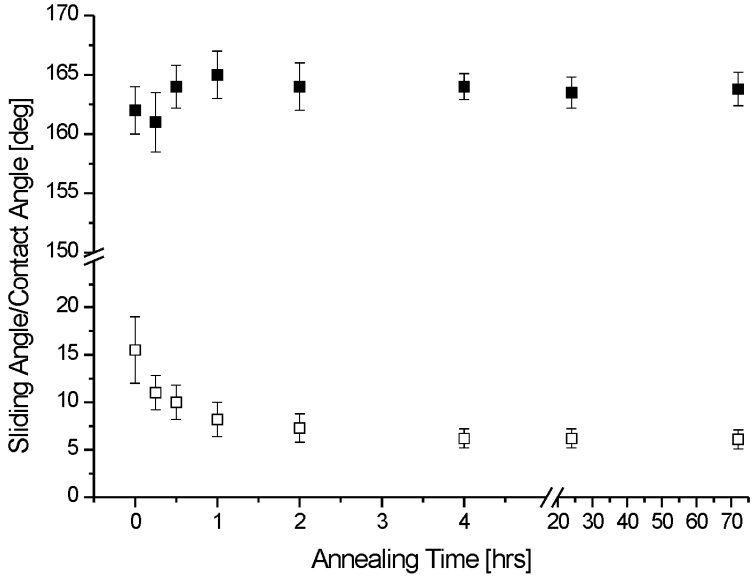

Figure 5.5. Changes in contact and sliding angles of SNC during annealing at 200°C.

The wettability data shows no indication of a degradation of the PMSQ filaments upon annealing at 200°C. A degradation of the hydrophobic methyl groups (to CO_2 and Si-O-Si) would result in a decrease of contact angle and increase of sliding angle values. The data also indicates that annealing the sample more than 4h does not further improve its hydrophobicity. We can assume that the annealing process at 200°C is completed after this time. At lower temperatures, annealing is incomplete and slower. After 72h annealing at 100°C, the contact angles of SNC remained almost constant and the sliding angles improved by only 4°.

Both the curing rate and the yield of the curing reaction of PMSQ increases with increasing temperature [40]. Annealing the PMSQ nanofilament coating at temperatures higher than 200°C would therefore possibly further improve the coating quality and reduce the curing time.

However, annealing would have to be performed under inert atmosphere to prevent the degradation of methyl groups.

An alternative method for improving the hydrophobicity of an SNC coating was applied by Gao *et al.* [88] A superhydrophobic PMSQ network coating treated with trimethylsilyl iodide which reacts with the remaining surface silanol groups. The amount of hydrophilic defects on the coating surface is thereby effectively reduced.

5.1.4 Coating with alternative precursor molecules

Methyltrimethoxysilane (MTMS) can be substituted for TCMS in the coating process leading to equivalent coating results. The advantage of this modification is that during the hydrolysis step, methanol is formed instead of HCl. This enables the coating of substrates that would otherwise be damaged by HCl. However, small amounts of TCMS or other chlorosilanes need to be included in the reaction mixture in order for the coating to be successful. Hydrolysis of the alkoxysilanes is very slow compared to that of chlorosilanes and catalytic amounts of acid or base are required to facilitate the reaction [49,89]. The additional chlorosilane in the reaction mixture provides the acid for catalysis.

Besides TCMS and MTMS, the formation of silicone nanofilaments could also be confirmed for ethyltrichlorosilane. Other precursors were not tested in the course of this work, but recently the formation of silicone nanofilaments from vinytrichlorosilane precursors was reported [90]. It can be assumed that other trifunctional silane precursors with short chain organic residues also form silicone nanofilaments. The results in Dr. Jung's thesis for instance suggest that n-propyltrichlorosilane also forms nanorough layers with superhydrophobic properties[33]. The exact structure of these layers however has not been evaluated.

5.1.5 Alternative substrate materials

The standard substrate employed in this work was glass, as it allows for a straightforward evaluation of the optical properties of the coating. However several other materials were successfully coated in both the solvent and the gas phase and the presence of silicone nanofilaments confirmed by electron microscopy. Several polymeric materials are detailed in the section on textiles (5.3). Other substrates include aluminum (plasma activation, solvent phase), silicon (plasma activation, gas or solvent phase), PDMS (plasma activation, solvent phase), Polyethylene (plasma activation, gas phase). EM images of some of these substrates including the corresponding images of a drop of water on these substrates are illustrated in Figure 5.6.

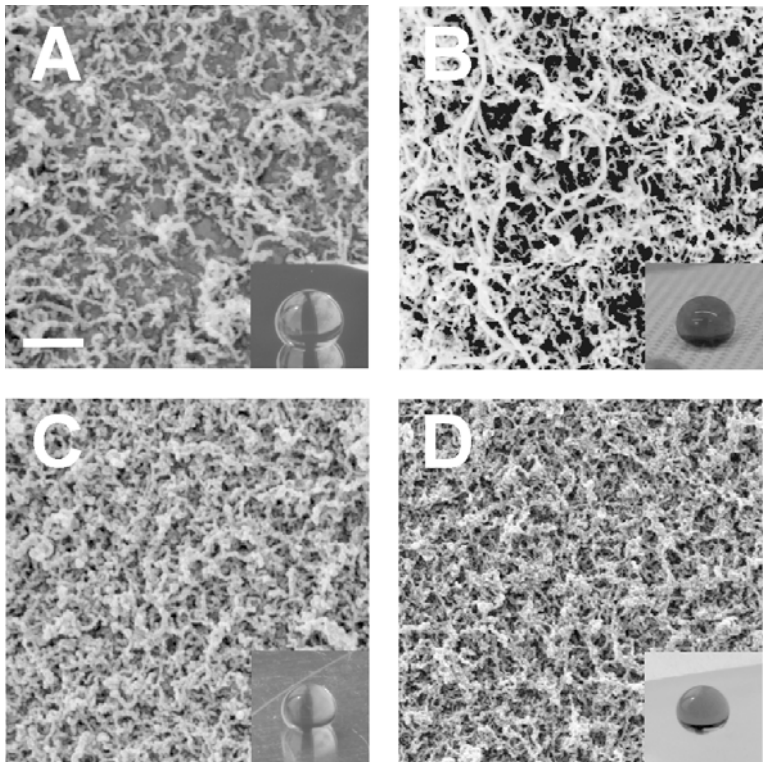

Figure 5.6. Electron microscopy images of the silicone nanofilament layers on various substrate materials, the white bar indicates 200nm. A: Silicon, B: Cotton, C: Aluminum, D: Polydimethylsiloxane (PDMS). Images in the lower right hand corners show drops of water on the respective surfaces.

5.2 Durability of the SNC

Due to the high surface roughness required for the superhydrophobic effect, superhydrophobic surfaces are generally easily damaged by scratching or abrading [11,12]. In nature, this can be balanced by regenerative processes [4], a concept that is not easily transferable to artificial surfaces. Fortunately, a number of applications can be envisioned where surfaces are not subject to strong abrasive forces, from large scale outdoor architectural applications like self cleaning facades or window panes to small scale liquid handling devices used in microfluidics. Here the usefulness of a superhydrophobic coating is determined by its chemical stability. A useful superhydrophobic surface should resist wetting even after prolonged exposure to water. The coating should withstand varying pH values, surface additives or solvents. In regards to long term outdoor applications, the coating should withstand weathering under environmental conditions.

Although a large number of fabrication techniques for (super) water repellent coatings have been published, stability data, especially in regard to long term stability, are scarcely reported. In addition to establishing the durability of their coating properties at various temperatures, Erbil *et*

al. observe that their superhydrophobic polypropylene coating did not debond in water, boiling water or heptane [91]. However, no contact angle values are reported to indicate whether the surface properties deteriorate through this treatment. Samples kept at temperatures higher than 30 °C and more than 80% relative humidity showed a decrease in the static contact angle of 10-20°. Feng *et al.* report superhydrophobic nanostructured carbon films that maintain static contact angles above 150° after 24h immersion in pure water (pH~7), acidic solution (pH~1) and basic solution (pH~14) [92]. Several groups [93-96] present superhydrophobic surfaces that are stable under ambient or high humidity conditions for weeks to months. Additional exposition of the surfaces to water overnight [94] or a week [95] are reported not to significantly change the surface properties. Guo *et al.* report "essentially" stable static water contact angles after soaking their coatings in water, acidic and basic solutions for several hours [96]. Yan *et al.* [97] report unaltered static contact angles after immersion of super water repellent poly(alkylpyrrole) films in solvents, oils, hot and cold water, without providing immersion times. Recently Wang *et al.* reported a superhydrophobic coating that retains static contact angles above 150° after a five day immersion in acetone, ethanol, toluene, water or hot water [98]. Mael *et al.* report a superhydrophobic coating with a static contact angle of 150° after more than 60 days of immersion in water [99].

In regard to the significant potential for superhydrophobic surfaces in outdoor applications, only few publications exist which evaluate a superhydrophobic coating in terms of environmental durability. Nakajima *et al.* performed experiments on the durability of superhydrophobic boehmite films for up to 75 days of outdoor exposure and 800 hours under UV irradiation [100]. Whereas static contact angles of their standard films decrease to 100° during the outdoor exposure, films doped with 2 wt% TiO_2 showed an increased durability in terms of contact angle values. This was attributed to the photocatalytic effect of TiO_2 that facilitates the removal of organic contaminants from the surface which are otherwise said to be a major factor in degradation of the surface under environmental conditions [12]. Additionally, the TiO_2 doped films exhibited contact angles above 140° after 800 hours of UV irradiation. Superhydrophobic films prepared by Sasaki *et al.* showed a decrease in contact angle from 158° to 149±5° after 40 days of outdoor exposure [101]. Thieme *et al.* performed extensive artificial weathering tests on superhydrophobic surfaces as protective coatings on aluminum, with varying outcome in regards to wetting properties and corrosion protection [102].

In regards to stability, the chemical nature of the SNC could prove advantageous. Silicones are generally known for their chemical inertness and long term durability which has led to their widespread application in nearly all areas of life [35,103]. To determine whether these properties

are also inherent in the superhydrophobic SNC, several long term stability tests were performed. The coatings resistance to chemical attack was explored in organic solvent, aqueous pH solutions and detergent solutions, the stability for outdoor applications by natural and artificial weathering experiments. All tests were performed on standard glass slides, coated in the gas phase according to Protocol I.

5.2.1 Chemical durability

5.2.1.1 Organic solvents

As would be expected from the chemical nature of the PMSQ nanofilaments, the coating and its properties are not significantly affected by organic solvents.

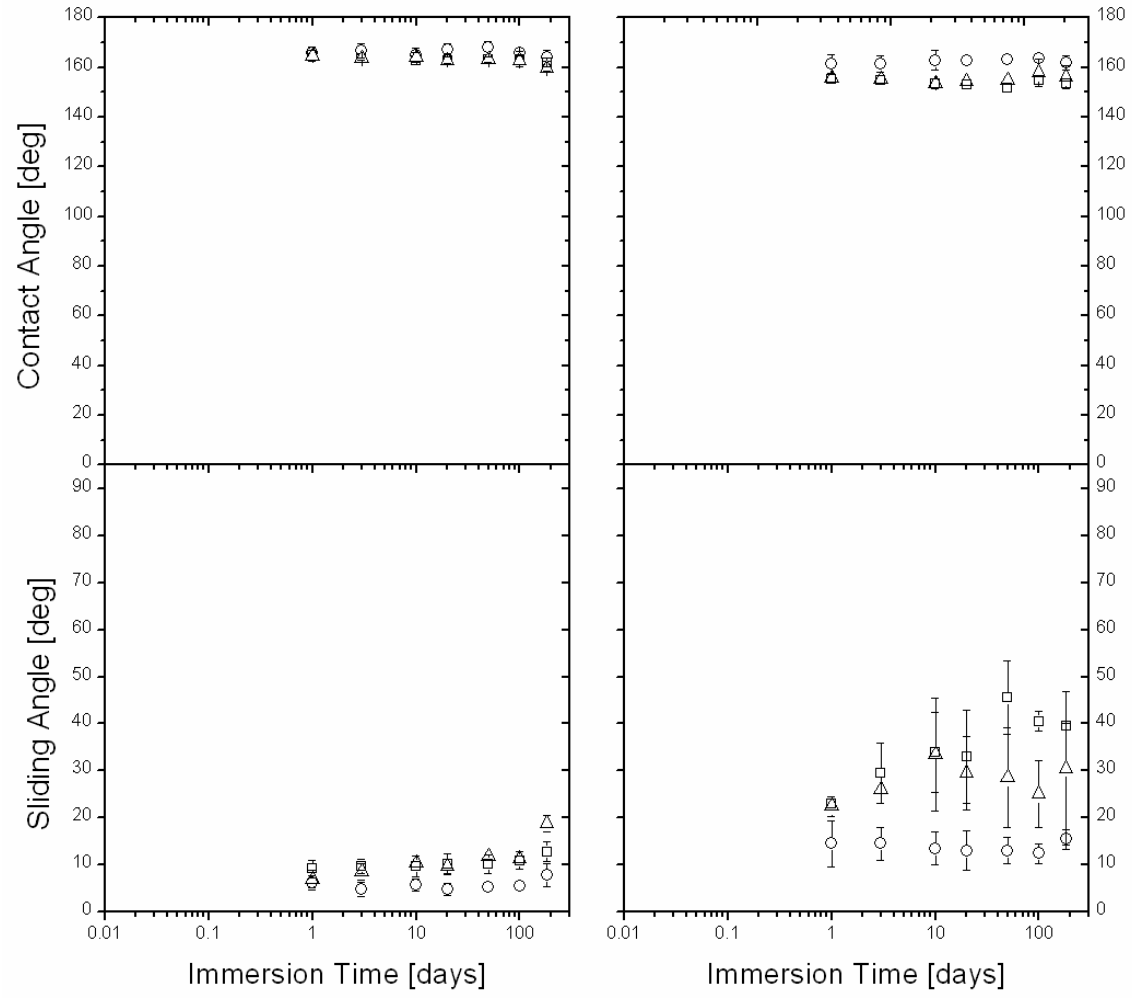

Figure 5.7. Contact and sliding angles of annealed (left) and non annealed (right) samples immersed in organic solvents (□ ethanol, △ acetone, ○ toluene). The dotted lines indicate initial values.

Figure 5.7 shows the progression of water contact and sliding angles as a function of immersion time in the polar, aprotic solvent acetone, polar, protic solvent ethanol and the non polar solvent toluene. Contact angle values remain virtually unchanged for all samples. Sliding angles show a slight increase in polar solvents and a slight decrease in toluene. The annealed samples are less affected than the non annealed samples.

Electron microscopy images of a sample before and after immersion in acetone are shown in Fig. 2, representatively for all solvents. No significant change in surface topography could be detected for any of the samples after 6 months of immersion.

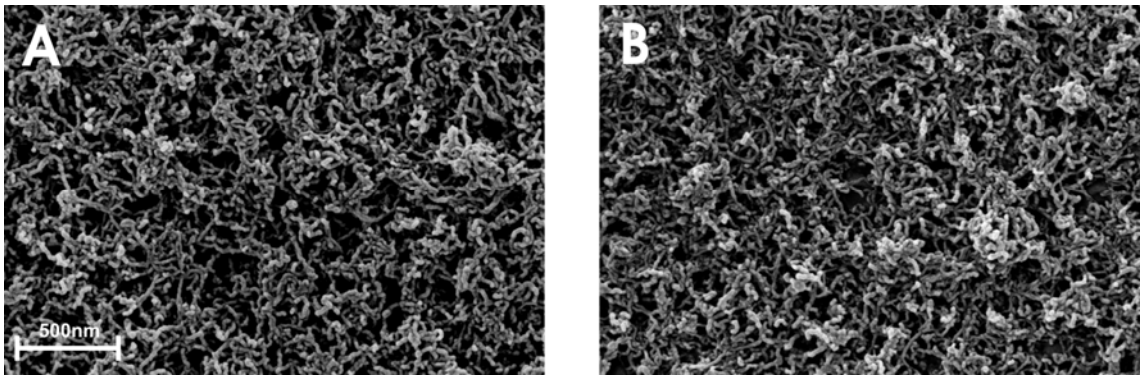

Figure 5.8. SEM images of the silicone nanofilament coating before (A) and after (B) 6 months of immersion in acetone.

The slight deterioration of contact and sliding angle values after prolonged immersion in acetone and ethanol could be attributed to hydrolysis of the silicone by residual water in the polar solvents. A gradual rearrangement of surface functional groups in response to the environment could also be a reason, the surface becoming more hydrophilic in response to the polar solvents and more hydrophobic in response to the non polar solvent [104]. Again we note that the sliding angle is much more sensitive to change than the contact angle (see also 5.1.3).

5.2.1.2 Aqueous pH solutions

In aqueous media, polysiloxanes are known to hydrolyze under strong basic and acidic conditions but are generally considered stable under mild pH conditions [34,103]. Data on the hydrolysis of polymethysilsesquioxane were not available. Various studies on the stability of the chemically related polydimethylsiloxane (PDMS) however suggest that while not affecting the bulk, mild hydrolytic conditions do have an effect on the surface properties. This is either attributed to hydrolyzation of the surface siloxane layer [105,106] or to a restructuring of the surface [83]. Bausch *et al.* measured a decrease in contact angle from 110° to 90° of PDMS after

immersion in pure water or sea water for 14 days [107]. Batich *et al.* extrapolated from experiments at higher temperatures that a PDMS surface exposed to physiological conditions would become completely hydrophilic within one month [108].

The hydrophobic properties of the SNC are superior under comparable conditions. Figure 5.9 shows the contact and sliding angles of annealed and non annealed coated glass samples as a function of immersion time in aqueous solutions of different pH values.

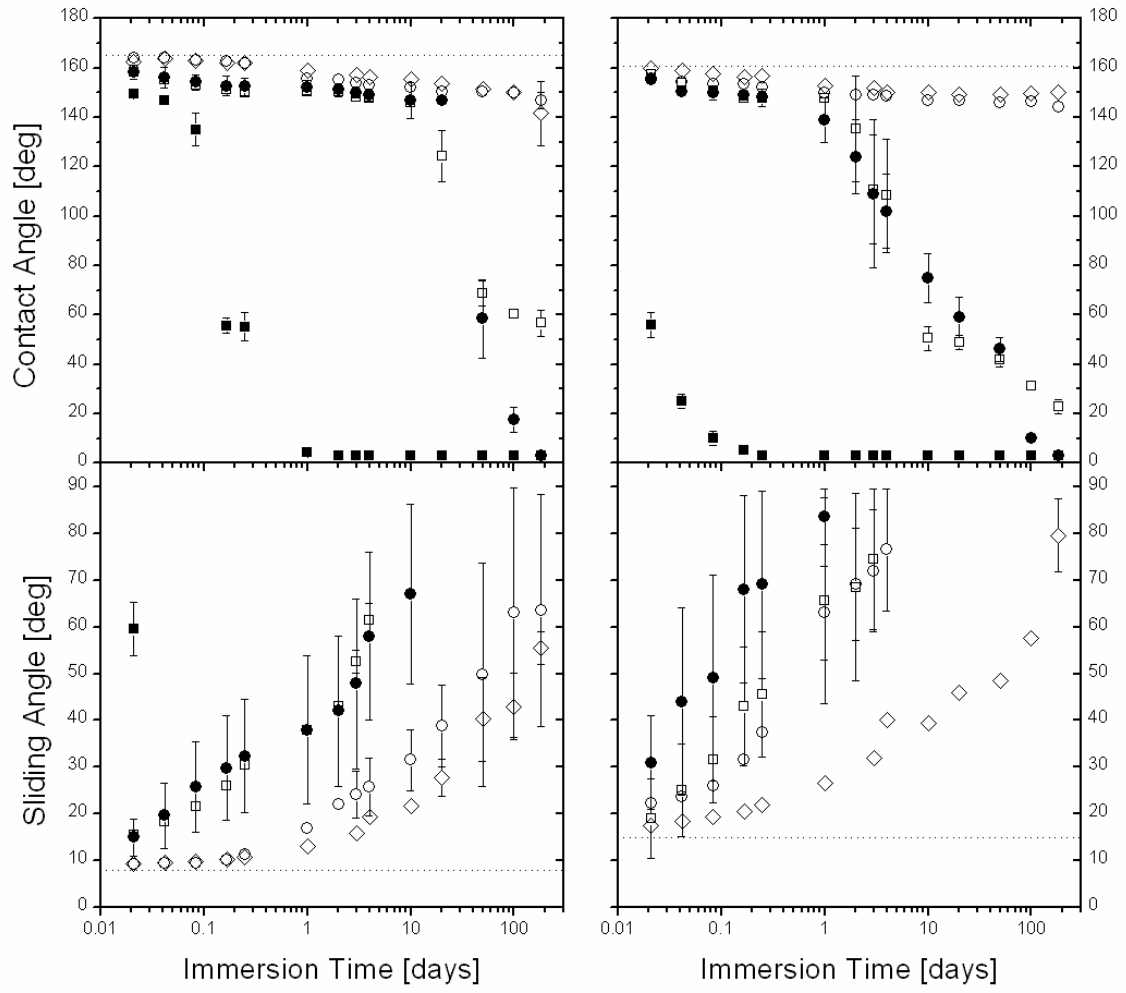

Figure 5.9. Contact and sliding angles of annealed (left) and non annealed (right) samples as a function of immersion time in aqueous pH solutions (■ pH 13, □ pH 11, ◊ pH 6.7, ○ pH 3, ● pH 0). The dotted lines indicate initial values.

In acidic or neutral media, the coating exhibits better stability than in basic media. At pH 3 and pH 6.7, the annealed coatings retain a contact angle close to 150° even after 6 months of immersion. The sliding angles are still below 90°. Under corrosive conditions at pH 0, the contact angle deteriorates significantly after 10 days and drops stay pinned on the surface even at 90° inclination. Under mildly basic conditions at pH 11 the annealed coatings deteriorate after 3

days whereas in strong alkaline solution even short immersion times suffice to eliminate the superhydrophobic effect. Overall however, the retention of the functionality of the coating is remarkable. Even the non annealed samples remain extremely hydrophobic after 6 months of immersion in water.

One reason for the good stability of the coating properties can be found when regarding the wetting process. Again a Cassie-Baxter type wetting is observed when the coated samples are immersed in aqueous media. Accordingly, only a small fraction of the surface area is wetted by the solution whereas the major part of the coating is protected from hydrolysis by a stable gas layer. This effectively retards deterioration of the coating and leads to the observed stability of the superhydrophobic properties.

As in the case of annealing, the sliding angle is again much more sensitive to change than the contact angle. Drops no longer roll off a surface although it still exhibits a contact angle of more than 150°. This can either be because the wetting state has changed from Cassie-Baxter to Wenzel due to degradation, or because the intrinsic wettability of the surface asperities in contact with the liquid changes and leads to a stronger adhesion of the three phase contact line (the reverse mechanism that reduces the sliding angle upon annealing (5.1.3)).

It is important to note in this respect, that the coating degrades in a way that would not be evident from measuring static contact angles alone. It becomes apparent from these considerations that monitoring the change in static contact angles is not sufficient when studying the durability of superhydrophobic coatings. Contact angle hysteresis or sliding angles must be examined in order to fully assess a coating's long term performance.

Figure 5.10 shows electron microscopy images of the annealed samples before and after 6 month immersion in the pH solutions. At pH 3 and pH 6.7 the surface structure responsible for the superhydrophobicity is still intact, whereas at pH 0, 11 and 13 the silicone nanofilaments are completely etched away. The transparency of the coatings was not significantly impaired by the pH solutions. Except at pH 13, where contact angles indicate that the coating has been completely etched from the surface, transmittance in the visible range remained above 92% throughout the duration of the durability tests. No hazing was observed.

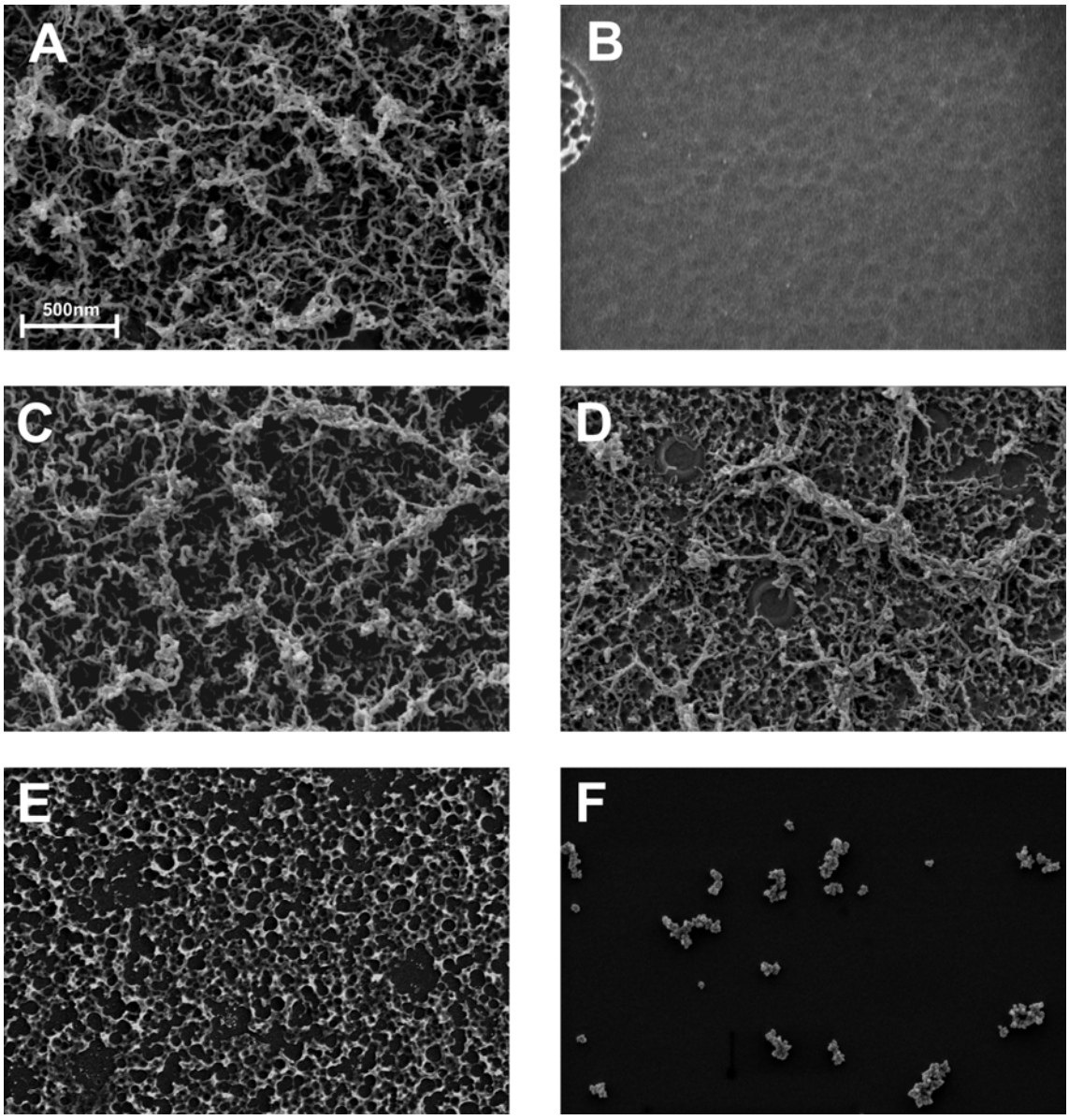

Figure 5.10. SEM images of silicone nanofilament coatings before immersion (A) and after 6 months of immersion in aqueous solution at pH 0 (B), pH 3 (C), pH 6.7 (D), pH 11 (E) and pH 13 (F).

Whereas in organic solvents the difference between the durability of the annealed and non annealed samples was slight, it is pronounced in the case of the aqueous pH solutions.

Figure 5.11 representatively shows the change in contact angle of the annealed and non annealed SNC in NH_3 solution at pH 11. Whereas for the non annealed sample the CA drops below 150° after one day of immersion, the annealed coating retains a contact angle of around 150° for 10 days. Within 9 days the contact angle of the non annealed sample drops below 60°, for the annealed coating this process takes about 90 days. Overall, the wetting properties of the non annealed sample deteriorate 10 times faster than the annealed coating. Similar relations apply to the samples exposed to the other pH values.

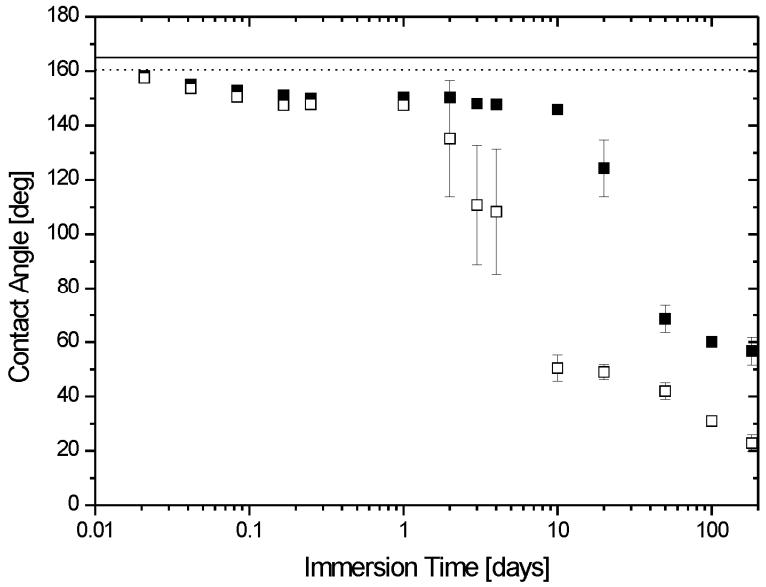

Figure 5.11. Contact angle of annealed (solid) and non annealed (open) samples in aqueous NH_3 solution (pH 11). The initial contact angles are indicated by the solid line (annealed) and dotted line (non annealed).

This is quite astonishing considering that the difference in the initial wetting properties of the annealed and non annealed coating is only marginal. Apparently the higher degree of crosslinking in the annealed sample not only improves the initial hydrophobicity but decreases the overall rate of hydrolysis leading to a significantly improved coating stability.

5.2.1.3 Detergent solutions

A process that is considered to decrease the lifetime of superhydrophobic surfaces is contamination by organic particles [12]. Oily substances that adhere to the surface will migrate into the texture and eventually fill it up, compromising the superhydrophobic effect. The SNC also suffers from this process, especially since the surface is not oleophobic (compare Section 5.4.1). A possible solution to this problem could be a cleaning step to remove contamination. Soaking the coating in organic solvents could dissolve the contaminants and regenerate the surface. Since the silicone nanofilaments are inert to organic solvents, a drop of oil for instance can be completely removed from the silicone nanofilament surface by dipping and agitating in acetone or toluene. For many applications however, and for toxicological and ecological considerations, a cleaning with aqueous surfactant solution instead of solvents is preferable.

A major function of detergents in surfactant formulations is to reduce the liquid/surface tension, thereby facilitating a complete wetting of the surface [109]. On superhydrophobic surfaces, surfactants, in sufficient concentration, will induce a transition from the Cassie-Baxter state to the Wenzel state [110]. Yet this could impair the beneficial effect of the Cassie-Baxter

state on the durability of the coating and increase the deterioration rate. In this respect the durability of the coating towards the influence of detergent solutions was tested. Among the multitude of detergents and surfactant formulations available, only one standard representative of the four surfactant families was chosen, namely an anionic, a cationic, an amphoteric and a nonionic surfactant.

Figure 5.12 shows the influence of prolonged immersion in the surfactant solutions on the contact and sliding angles of our coating. All samples were completely wetted by the detergent solutions.

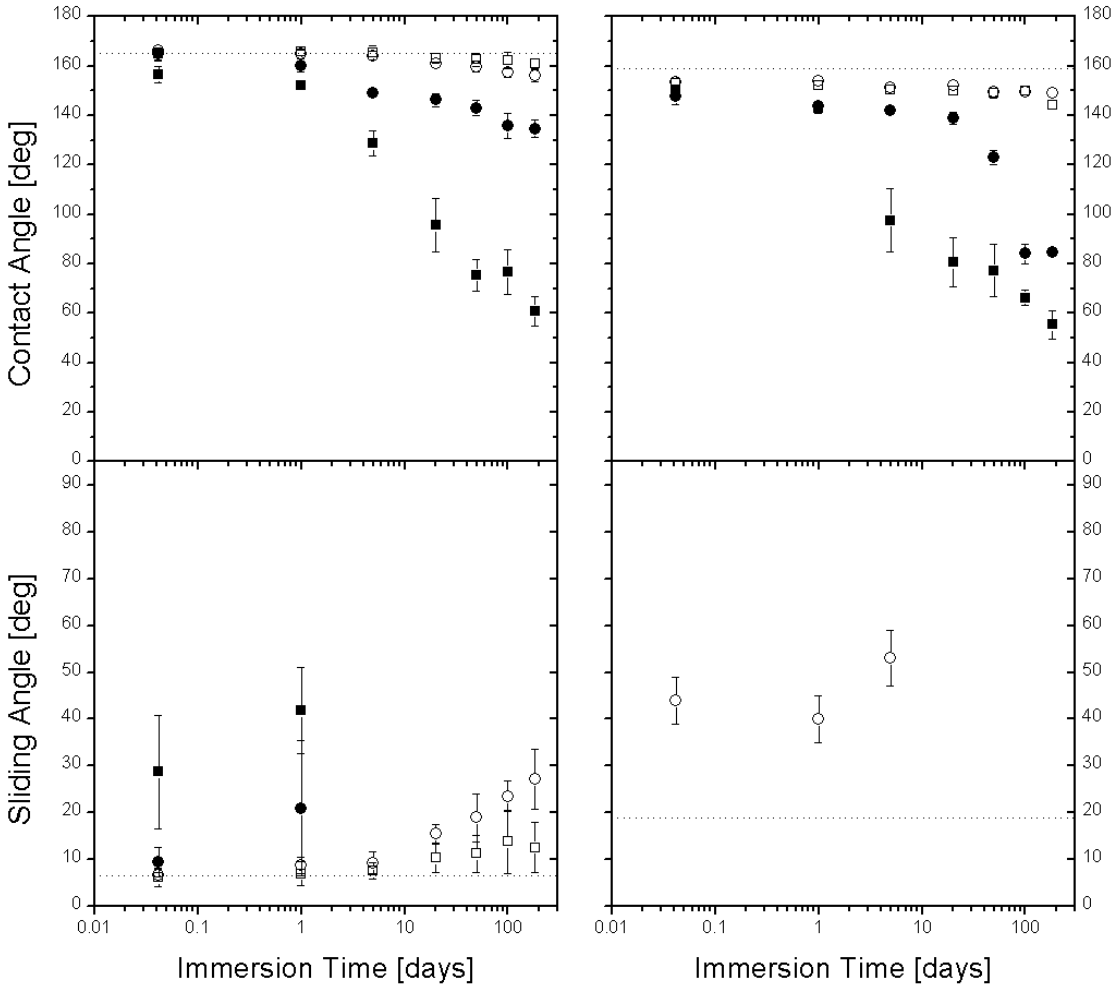

Figure 5.12. Contact and sliding angles of annealed (left) and non annealed (right) samples immersed in aqueous detergent solutions (■ Glucopon, non-ionic, pH 12, ● Dehyton, amphoteric, pH 9.5, □ Texapon, anionic, pH 4.5, ○ Dehyquart, cationic, pH 3.5). The dotted lines indicate initial values.

The strong influence of pH on the durability of the coating is also evident in the detergent solutions. Contact and sliding angles decline significantly under basic conditions but are less affected in acidic solutions. The improved durability of the annealed coatings is again evident

under these conditions. In case of the non annealed coatings, a relatively short immersion time of one hour in three of the detergent solutions already leads to a sticking of the water drops at 90° inclination. In contrast, drops still slide off the annealed coatings after 24 hours of full immersion in all of the detergent solutions. The annealed samples show an exceptional durability in the acidic detergent solutions. After 6 months of full immersion the contact angles are still well above 150° and the sliding angles below 40°.

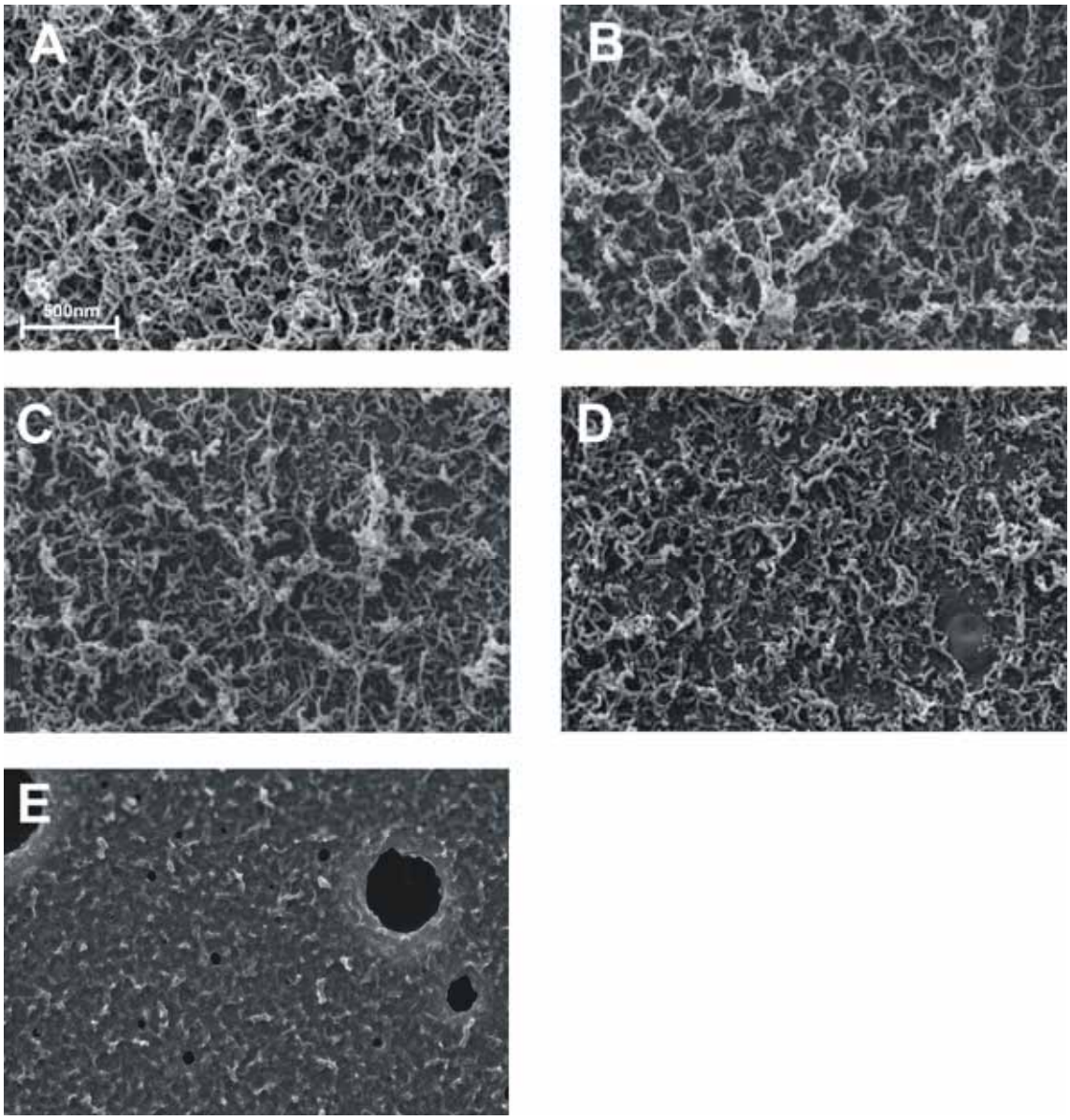

Figure 5.13. SEM images of SNCs before immersion (A) and after six months of immersion in detergent solutions: (B) Dehyquart, cationic, pH 3.5, (C) Texapon, anionic, pH 4.5, (D) Dehyton, amphoteric, pH 9.5 and (E) Glucopon, non-ionic, pH 12.

Generally the coatings are more stable in the detergent solutions than in the aqueous solutions of comparable pH which is surprising considering that through the reduced surface tension of the detergent solution, the whole surface area is wetted. Apparently however this does not lead to a faster degradation of the coating properties. A possible explanation is that the surfactant molecules assemble at the solid/liquid (hydrophobic/hydrophilic) interface forming a protective layer against the hydrolytic action of the solution. This is a well known process that is utilized in corrosion protection, for instance on metal surfaces [109,111].

The electron microscopy images in Figure 5.13 reveal no apparent change in surface structure for the coatings immersed in the acidic detergent solutions. The coatings immersed in the mildly basic solution show some degradation while the nanofilaments are completely etched from those immersed in strong basic solution.

5.2.1.4 Summary

Taking into account all the data of the chemical stability tests, the SNC coating shows a remarkable durability. In neutral and mildly acidic aqueous solution, the coating can be considered to be long term stable. The superhydrophobic properties were still intact even after 6 months of immersion in these media. Care must be taken to avoid an exposure of the coating to strong hydrolytic media, but short term exposure (< 1day) to mildly basic and strong acidic solution is possible without a loss of superhydrophobic properties. The resistance to organic solvents allows both a removal of organic contaminants from the surface as well as secondary coating using self assembled monolayer techniques (see section 4.3.5). A cleaning of the surface with mildly acidic detergent solutions can also be envisioned. Overall, the coating is superior to most other superhydrophobic coatings for which similar data is available [91-96,98,99].

Whenever possible the coating should be annealed to improve its stability towards hydrolysis. This improves both the initial hydrophobicity and, more importantly, reduces the rate of hydrolysis and degradation of the coating. A higher crosslinking density, possibly achieved by annealing the coating at higher temperatures (4.2.3), can be expected to further improve the durability of the coating. A thicker and denser layer of PMSQ filaments can also be expected to improve the coating stability, however a thicker layer will impair the optical properties of the coating (compare Section 5.5). Improving the initial hydrophobicity of the PMSQ coating by treating it with trimethylsilyliodide [88] might also have a beneficial effect on the long term durability.

The results of the stability tests clearly show that both static and dynamic wetting properties must be considered when examining the properties of superhydrophobic coatings. The static

contact angles by themselves do not adequately reflect the change in wetting properties of the surfaces in our experiment. Additionally, a long term stability towards an aqueous solution can not be attested simply by measuring the contact angle of this solution on the coating (a procedure applied in many current publications [92,96,112,113]). A high initial contact angle of an aqueous pH 13 solution, for instance, does not imply a long term stability towards this medium.

5.2.2 Environmental durability

Benefits derived from a superhydrophobic coating in outdoor applications are twofold. In a Cassie-Baxter type wetting regime, the contact area between a water and the surface is minimized. This can reduce physical defects like water stains or any physico-chemical degradation such as corrosion. The primary benefit of superhydrophobic coatings towards outdoor applications however is their ability to "self-clean". Water drops do not stick on the surface but roll off very easily. Due to the high surface roughness, dirt particles also show low adhesion and are effectively removed by the rolling drops [4,19,114]. It is therefore of primary importance to consider both the static contact angle as well as the dynamic behavior of water drops when evaluating superhydrophobic surfaces in terms of outdoor application [14,63].

5.2.2.1 Outdoor weathering

Contact and sliding angle values for the coated glass slide exposed to outdoor weathering are illustrated in Figure 5.14 as a function of time, along with the corresponding precipitation and temperature data [115]. The total precipitation of 1090mm in the course of the 12 month outdoor exposure is conforming to the 30 year average of 1086mm for the city of Zurich.

Again, the sliding angle is much more sensitive to change than the contact angle, as was already noted in the studies on the chemical durability of the coating (5.2.1). During the course of 12 months of outdoor exposure, the contact angle decreases to 148±5° and the sliding angles increase to 69±20°. A significant portion of this change occurs between day 50 and day 170. After 170 days, the contact and sliding angle values remain nearly constant.

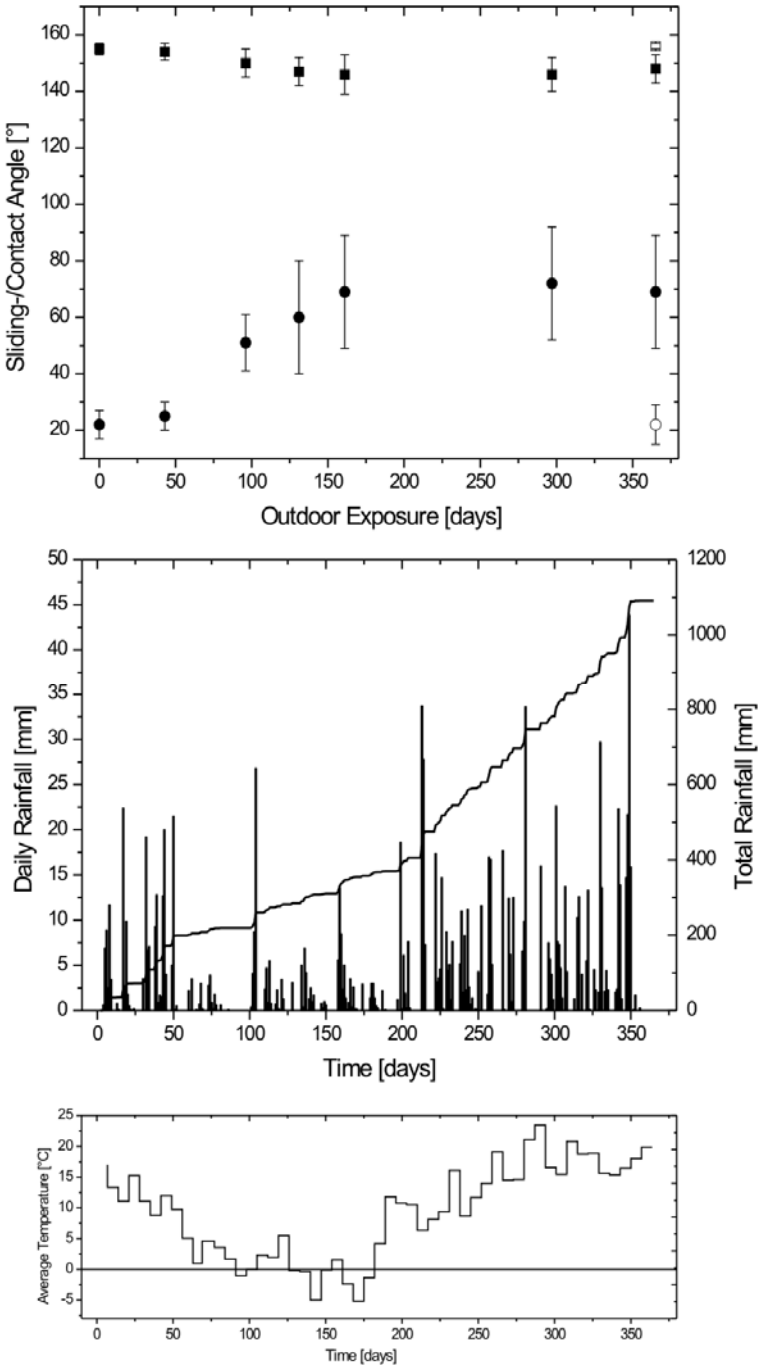

Figure 5.14. Top: Coating properties as a function of outdoor exposure time (■ contact angle, ● sliding angle, □/○ contact/sliding angle of a reference sample kept under ambient laboratory conditions). Middle: Corresponding daily precipitation (bars) and integrated precipitation (line). Day 0 corresponds to September 9th 2004. Bottom: Corresponding 7 day temperature average.

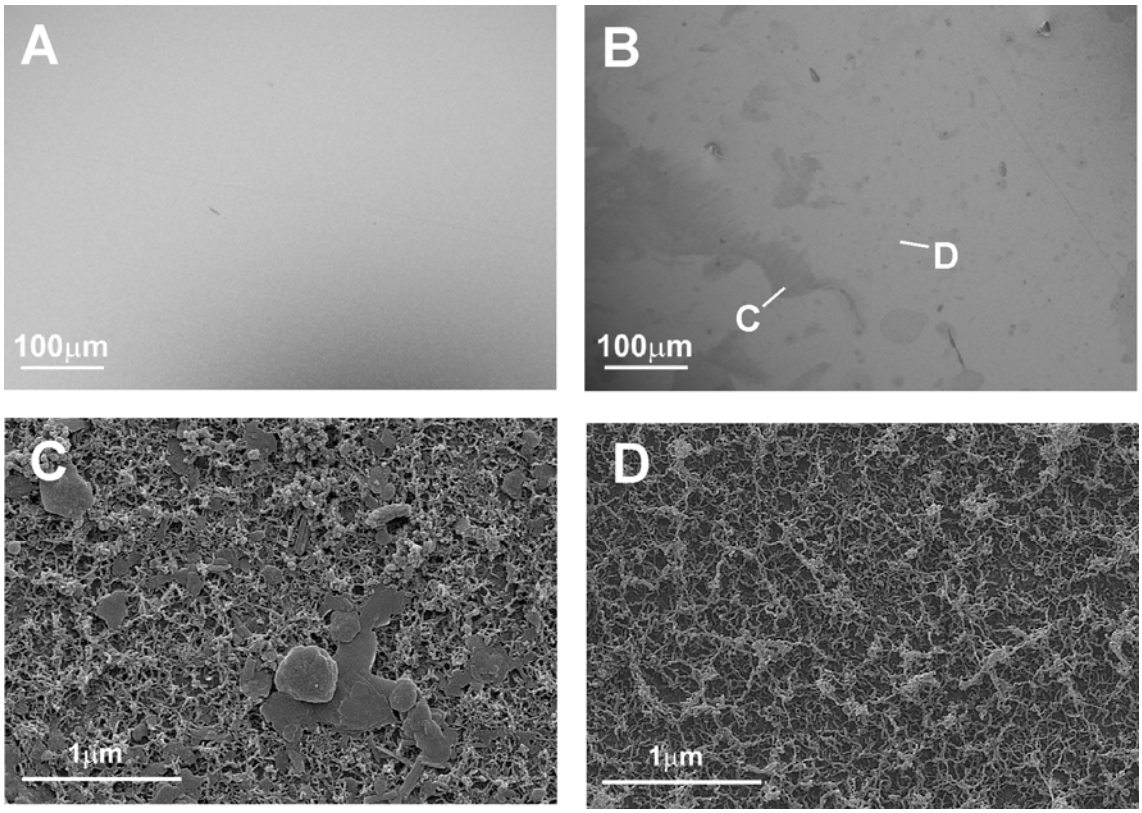

Figure 5.15. Scanning electron images of a SNC after 12 months of outdoor exposure. A: overview before exposure, B: overview after 12 months of outdoor exposure, C, D: magnification of areas indicated in B.

The scanning electron micrographs of the sample surface taken after 12 months of exposure (Figure 5.15) show a strong, inhomogeneous change in surface structure.

Compared to a freshly coated sample (Figure 5.15 A), the surface is inhomogeneously covered with spots and blotches of varying size and shape (Figure 5.15 B). Figure 5.15 C and D show magnifications of two distinct regions on the surface. A significant part of the surface is virtually unchanged by the outdoor exposure (Figure 5.15 D) whereas the blotched areas are obviously contaminated (Figure 5.15 C). This is in accordance with the general opinion, that especially organic contaminants are a major problem in degradation of superhydrophobic surfaces under environmental conditions [12,101]. Obviously the self cleaning effect is not sufficient to remove these contaminants from the surface. Since the most pronounced degradation of surface properties coincides with a time of very little precipitation (winter season), we assume that in this time span contamination accumulates on the surface to an extent which can no longer be efficiently removed during the following rain period. Additionally, most of the precipitation in this period occurred in the form of snow which does not facilitate self cleaning. At times of regular rainfall, fresh contaminants are more effectively removed from the surface and the coating properties are less affected (days 0-50, days 200-365). However, further

investigations will be necessary to evaluate the explicit effect of regular rainfall on the coating properties during outdoor exposure. Also, given the coatings good stability towards detergent solution [116], removal of contaminants and regeneration of the surface by cleaning could be envisioned.

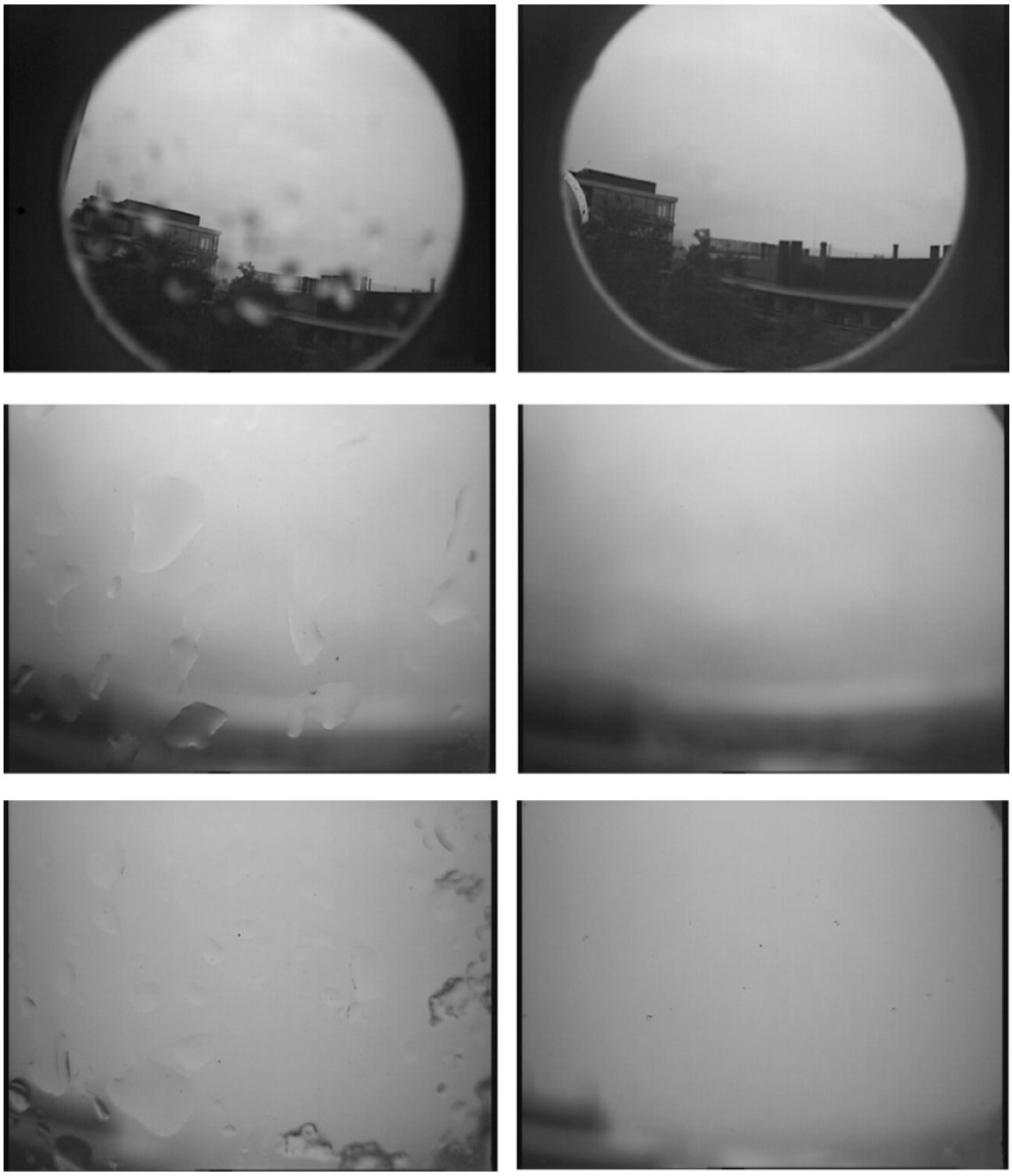

Figure 5.16. Webcam images taken through an uncoated (left column) and coated (right column) glass slide during rainfall (top, middle) and snowfall (bottom). For the topmost images the camera was focused on the horizon to illustrate the distortion of the camera image due to adhering rain. For the lower images the camera was focused on the glass slides to clearly display the adhering precipitation.

Regardless of quantitative observations, the quality of the surface in respect to its extremely low water adhesion is still sufficient, even after 12 months of outdoor exposure. Figure 5.16 shows images of the coated and uncoated glass slides taken by the webcam during rainfall at the end of the outdoor experiment (12 months).

Raindrops adhere to the uncoated glass slide whereas the coated glass slide remains perfectly clear even though the coating properties have deteriorated. Raindrops are usually larger than 10µl and possess kinetic energy when they come in contact with the surface. This explains why the coating is obviously still water repellent, although the sliding angle has increased significantly. The pinning forces between water and coating are large enough to pin a 10µl sessile drop but are insignificant compared to the energy of falling raindrops. Snow adhesion was also significantly reduced for the coated substrate. The coated slide remained clear even during heavy snowfall whereas the uncoated slide was covered with snow and ice crystals.

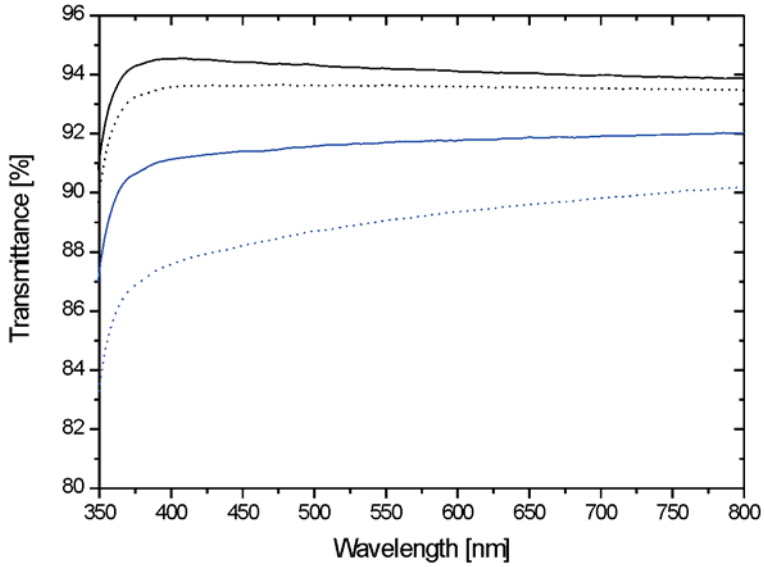

Figure 5.17. Transmittance of coated (black) and uncoated (blue) glass slides in the visible range. Solid curves indicate values before exposure, dotted curves show values after 12 months of outdoor exposure.

The anti-reflective properties observed for the SNC [70] are only slightly affected by the outdoor exposure, in contrast to a significant decrease of transparency for the uncoated glass slide (Figure 5.17). After 12 months of outdoor exposure, the coated glass slide shows an average of more than 5% higher transmittance in the visible range than the uncoated glass slide. The relative gain in optical transmittance due to the SNC obviously increases over time during the outdoor exposure. Figure 5.18 shows scanning electron microscopy images of the uncoated glass slide after 12 months of outdoor exposure.

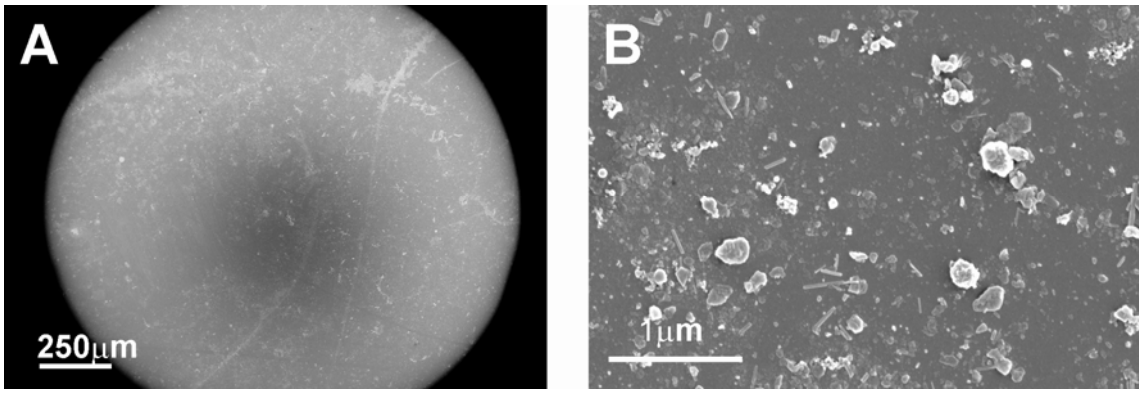

Figure 5.18. Scanning electron microscopy images of an uncoated glass slide after 12 months of outdoor exposure. A: overview, B: magnification.

In contrast to the coated glass slide (Figure 5.15) the surface of the uncoated glass slide is more thoroughly contaminated. Because water drops adhere to the uncoated glass surface, any contaminants and inorganic residues inside the drops will accumulate on the surface when the drops evaporate. This accumulated contamination is macroscopically evident by so called water stains forming on the surface and impairs the optical transmittance. On the coated glass slide, drops do not adhere to the surface and therefore contaminants do not accumulate to the same extent as on the uncoated glass slide.

5.2.2.2 Artificial weathering (ADF test)

The silicone nanofilaments are less affected by the outdoor weathering than the superhydrophobic coatings examined in related studies [12,100-102]. Naturally these comparisons are somewhat ambiguous because the coatings performance strongly depends on the environmental conditions and the setup of the outdoor experiments. For this reason additional weathering tests under controlled laboratory conditions were performed. Since to our knowledge no specific standards for the evaluation of the durability of superhydrophobic coatings under simulated environmental conditions exist, procedures were chosen, that are standards in related fields. For an assessment of UV durability ISO 9022-9 [72] was chosen, which is a standard for evaluating the influence of solar radiation on optics and optical instruments. For the assessment of the durability against the combined influence of UV irradiation, temperature and (acid) rain or fog durability, the VDI 3958 guideline (ADF test) [73] was chosen. This test has proven to be convenient to simulate the effects of aggressive environmental conditions on automotive coatings with good correlation to outdoor weathering [117]. The VDI 3958 was given precedence over the ISO 11341 [118] that was used by Thieme *et al.* [102] since it accounts for

acid precipitation and because the exact process of "moisturizing" the samples is not clearly defined in ISO 11341.

Figure 5.19 shows the development of contact and sliding angles of annealed and non annealed samples during the ADF test.

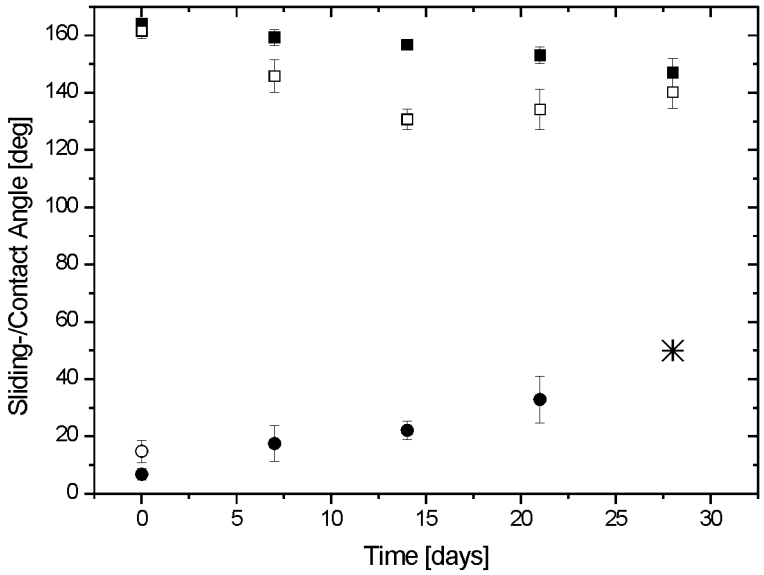

Figure 5.19. Contact and sliding angles as a function of ADF test duration. ●/■ Sliding/contact angles of annealed samples, ○/□ sliding/contact angles of non annealed samples. For * please refer to the text.

After one week of ADF test, the non annealed coatings show significant signs of deterioration. Contact angles have dropped below 150° and the 10µl drops no longer roll off the surface even at 90° inclination. Contact and sliding angles of the annealed samples indicate only a slight linear deterioration of the coating properties in the first 3 weeks of ADF testing. Contact angles drop to 153±3° and sliding angles increase to 33±8°. After four weeks the coating properties deteriorate to an extent that half of the samples show sliding angles of roughly 50° (indicated by * in Figure 5.19) and on the other half of the samples drops remain pinned at 90°. Contact angles are now in the range of 147±5°.

On the non annealed samples, defects in the surface structure are clearly evident from the scanning electron microscopy images (Figure 5.20). At low magnification a multitude of circular regions, 10-20µm in diameter, are distributed randomly on the whole surface (Figure 5.20 left). Higher magnification (Figure 5.20 right) reveals a slightly etched surface structure in these regions that is reminiscent of the changes observed during the coatings exposure to acidic solution (5.2.1).

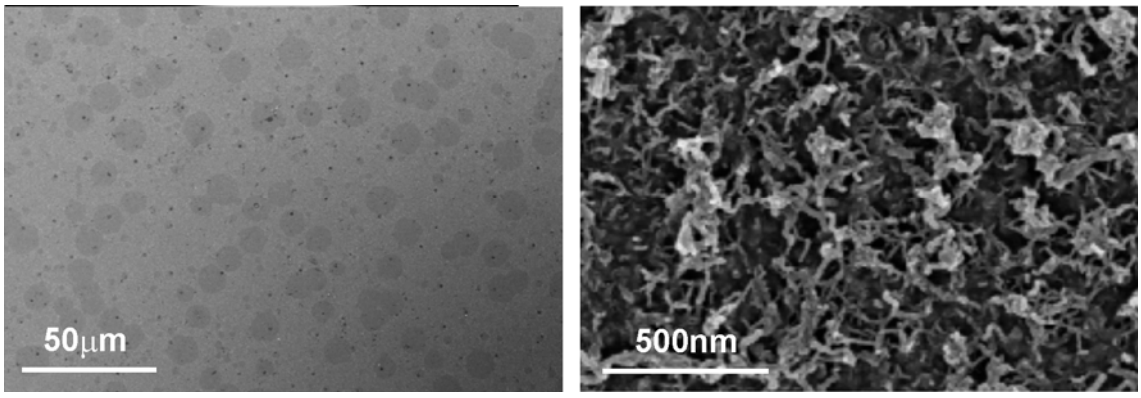

Figure 5.20. Scanning electron micrographs of a non annealed sample after one week of ADF testing. Overview (left), and magnification of a degraded area (right).

These changes in surface structure can most likely be attributed to the workings of small acid drops that adhere to the surface during spraying with the acid solution in the first step of the ADF cycle. The drop size generated with the spray pump was determined by optical microscopy to be in the range of 30-70μm. The corresponding contact diameter of the drops on the surface estimated with the spherical cap assumption and assuming a contact angle of 160° is in the range of 10-25μm which corresponds well to the size of the deteriorated regions. Similar defects could not be identified on the annealed coatings (Figure 5.21).

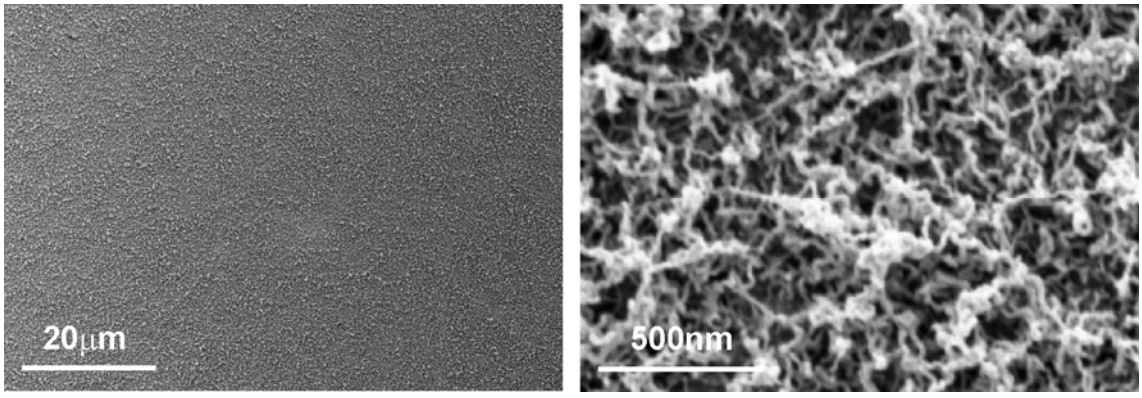

Figure 5.21. Scanning electron micrographs of an annealed coating after 4 weeks of ADF test at low (left) and high magnification (right).

Presumably this is because the annealed coating is less susceptible to hydrolysis by acids than the non annealed coating (5.2.1). Generally there is no indication of any structural damage on the coating caused by the continuous soft abrasive force of water drops acting on the surface during the rain phases of the ADF cycle.

In regard to their optical properties, all annealed coatings still show a higher transmittance in the visible range after four weeks of ADF test than freshly cleaned, uncoated glass slides. The non annealed samples develop a slight haze in the course of the ADF testing but the annealed samples stay perfectly clear. Figure 5.22 shows the optical transmittance of the coated and uncoated glass slides after 4 weeks of ADF test.

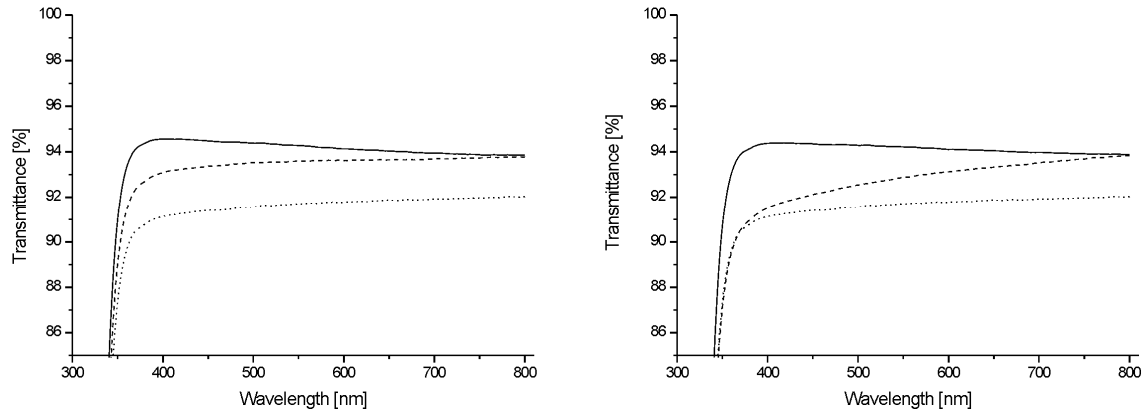

Figure 5.22. Change of transmittance of the annealed (left) and non annealed (right) SNC glass slides during ADF weathering. Solid lines indicate initial values, dashed lines the values after 4 weeks of ADF-Test and dotted lines indicate the transmittance of an uncoated, freshly cleaned glass slide.

The significantly improved resistance to artificial weathering of the annealed coating as opposed to the non annealed coating is most likely due to its improved chemical durability. Better hydrolytic stability and an increased hydrophobicity retard both the deterioration of the coating due to the acid spray as well as the artificial rain. Additionally, the improved initial superhydrophobicity of the annealed coating leads to a higher initial resistance to weathering since less acid and water drops will adhere to the annealed coating.

5.2.2.3 Global UV irradiation

The laboratory weathering test performed in the Weather-Ometer according to DIN 9022-9 showed no influence of UV irradiation on the properties of the SNC. Contact and sliding angle values remained virtually unchanged for both annealed and non annealed samples and scanning electron microscopy revealed no apparent change in surface structure. The optical properties also remained unchanged.

5.2.2.4 Summary

Principally the SNC shows a good environmental durability. It is completely inert to UV weathering and its superhydrophobic properties were sufficiently stable under outdoor exposure

to an extent that makes it useful for long term outdoor applications. Especially considering that the outdoor weathering tests were performed at a very early stage of the thesis. The initial contact angle of the tested coating was about 8° less than the standard coatings employed in the other stability tests and the sliding angle was more than 10° higher. Accordingly the current "standard" coatings can be expected to perform even better in the outdoor experiments.

Contamination contributes to the degradation of the SNC during outdoor weathering. However it is not as pronounced as could be expected in view of the strong oleophilicity of the coating (see 5.4.1). This could either be because the experiment was performed at a location with low immission of organic contaminants or because a significant part of these contaminants was removed due to the self cleaning effect of the coating. In respect to further reducing the number of organic contaminants adhering to the surface it would be interesting to see how an additional oleophobic functionality added to the SNC (5.4.1) will affect the coatings performance in outdoor weathering experiments.

In terms of artificial weathering there is no scientific data available to compare the results of the SNC to those of other superhydrophobic coatings. The ADF test however has proven to be a useful tool in judging the durability of a superhydrophobic coating towards rain and acid precipitation. In this regard the results of the ADF test show a strong correlation to the chemical durability tests. Although only able to simulate two of the possible degradation pathways, the ADF test is a sensible alternative to time consuming outdoor experiments for the initial optimization of a superhydrophobic coating.

5.2.3 Mechanical stability

Superhydrophobic coatings generally face the problem of a low mechanical stability because of the delicate micro- and nanostructure that is required for the superhydrophobic effect [11,12]. This is also the case for the SNC. Even lightly rubbing an SNC glass slide with a duster or with a finger leads to an immediate loss of superhydrophobic properties.

Improving the mechanical properties of the individual fibers might improve the coatings stability to some extent, but it is highly questionable if such strategies will lead to a coating that is mechanically stable enough for even mildly abrasive applications, since in essence the fragile nanofilament structure will be (and needs to be) retained. A better approach is therefore one that focuses not on the stability of the individual fibers but on the retention of the overall superhydrophobic properties of the coating. The lotus leaf surface for instance shows a hierarchical structure of microscopic "bumps" and nanoscopic wax crystals [4]. The microstructure effectively shields the nanostructure from abrasion, i.e. the nanostructure is only

destroyed on the tops of the bumps. Under mild abrasion the superhydrophobic effect is therefore retained. Additionally the Lotus leaf, as a biological system, has a repair mechanism that is able to regenerate the destroyed structures to some extent. Such a self healing mechanism is of course difficult to implement into an artificial coating. But towards an improved short to intermediate term mechanical robustness of the superhydrophobic effect a two tier roughness would likely suffice, as is indicated by the results of the abrasion tests on SNC coated textile samples (5.3).

5.3 Application of SNC to textiles

A commercially interesting application of the superhydrophobic effect is undoubtedly the waterproofing of textiles. Superhydrophobically coated textiles could find applications as water resistant apparel and would generally be useful for any kind of application where textiles are exposed to the environment (parasols, umbrellas, etc.). Other benefits include the self cleaning and anti fouling properties that are associated with the superhydrophobic effect. Additional oleophobic properties could confer anti soiling and stain resistant properties to the textile. Despite the fact that the original work of Cassie and Baxter [2], cited in almost every publication regarding superhydrophobicity, is concerned with the wettability of woven fibers, and despite the fact that most publications in the field of superhydrophobicity ascribe a significant potential of superhydrophobicity for textile applications, few reports exist that actually apply a superhydrophobic coating to textiles. Zhang *et al.* report a superhydrophobic plasma coated cotton fabric and characterize the coated fabric in a series of standard test such as softness, color, weight loss and friction upon abrasion, water retention, etc. [119]. However apart from the initial contact angle, no information on the retention of the water repellent properties upon the various treatments such as abrasion is supplied. Daoud *et al.* report a sol gel based superhydrophobic silica nanocomposite coating on cotton and characterize it in terms of physical properties, contact angle and water uptake upon washing [120]. However the initial contact angles of the coated fabrics was only reported to be in the range of 140°. Gao *et al.* produced a superhydrophobic textile by coating a PET microfiber fabric with a silicone coating procedure patented in 1945. This method however relies on the microtexture of the fabric itself to induce superhydrophobicity. A conventional fabric coated in the same manner was not superhydrophobic. Apart from contact angle data, no additional information on the properties of the coated fabrics was reported. Yu *et al.* also report a sol gel procedure involving a perfluorooctylated quaternary ammonium silane coupling agent to produce superhydrophobic cotton fabrics [121]. However, the maximum water contact angles are reported to be 145°. The oleophobicity of the fluorine based coating is reported to result in an oil repellency grade of 4 to

5. Again no additional information on the properties of the coated fabric are reported. Michielsen *et al.* mechanically and chemically modified a nylon 6,6 woven fabric to create a superhydrophobic textile with contact angles as high as 168° and performed experiments to confirm the Cassie-Baxter equation [122]. Wang *et al.* report a "simple and inexpensive" method of creating superhydrophobic fabrics from commercial cloths by modifying the fabrics with gold micro- and nanostructures and applying a layer of n-dodecanthiol [123]. Contact angles "close to 180°" are reported but no further characterization of the coated fabrics or the stability of the superhydrophobic effect was performed.

Early experiments performed by Stefan Jung already indicated that a large variety of material surfaces can be coated with a layer of silicone nanofilaments and rendered superhydrophobic via the gas phase coating technique [33,70,124]. In the following section the potential of the SNC towards textile applications is explored. Aside from evaluating the wetting properties of various textile materials coated with PMSQ nanofilaments, coated PET samples were characterized in terms of wetting properties, long term water resistance, tensile strength, abrasion resistance, durability towards washing and the possibility to add oleophobic functionality to the coating in a series of experiments conducted in collaboration with the AdvancedFibers group of the Empa St. Gallen.

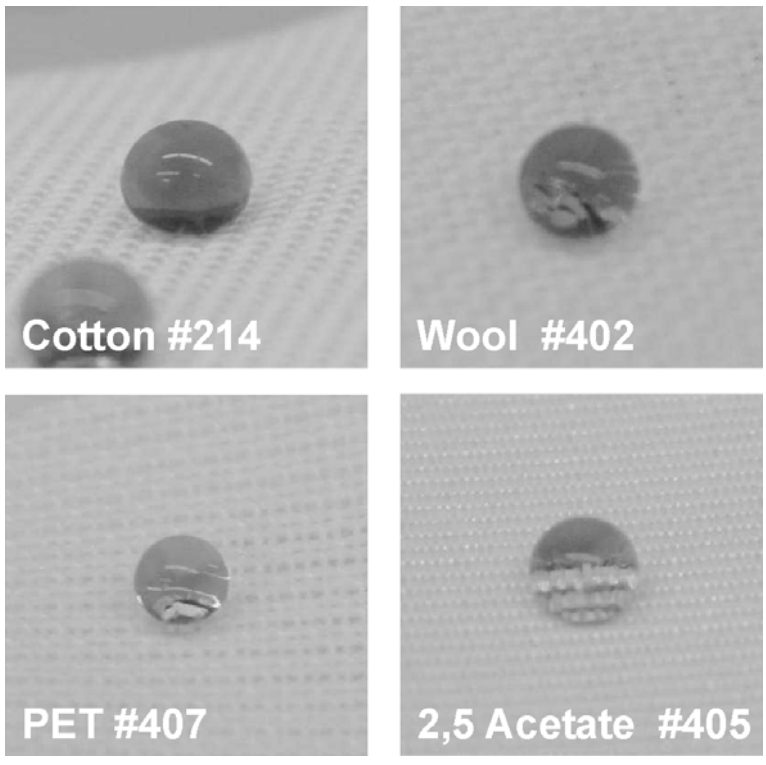

Figure 5.23. Drops of water on four different textile samples coated with PMSQ nanofilaments.

5.3.1 Evaluating textile samples coated with PMSQ nanofilaments

Eleven textile samples made from natural and artificial fibers were supplied by the Empa St. Gallen and coated with the gas phase setup according to Protocol I. On all samples, drops of water show a high contact angle after coating and drops roll off the surface without leaving a trace. Figure 5.23 exemplarily shows drops of water on four of the coated textile samples.

Upon trying to evaluate the quality of the coated textiles in terms of wetting properties it was found that on such macroscopically rough surfaces contact and sliding angle measurements are unsuited. Classical contact angle measurements fail because the roughness of the substrate makes it impossible to determine the three phase contact line or the substrate base line (see Figure 5.24). Sliding angle measurements are ambiguous because the macroscopic roughness results in a relatively large scattering of sliding angle values.

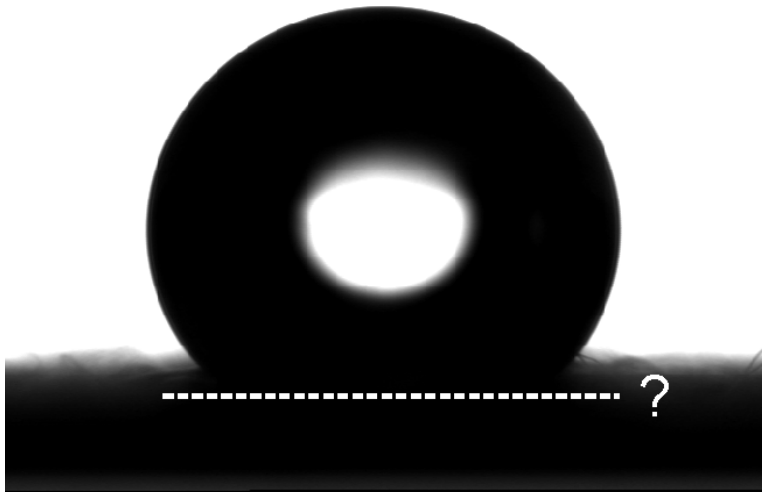

Figure 5.24. Typical profile of a sessile drop on a superhydrophobic textile.

To overcome these difficulties, a new procedure to evaluate the superhydrophobicity of textile samples was developed. The procedure is adapted from a method described in the literature by which the self cleaning effect of superhydrophobic surfaces was evaluated [125]. A water drop of defined size is released onto an inclined substrate from a defined height and the minimum angle of inclination ("water shedding angle", WSA, ω) at which this drop completely rolls off the surface is determined (see 4.4.2).

Table 5.2 summarizes the WSA of various natural and synthetic textile fibers coated with silicone nanofilaments according to Protocol I. WSA for two different drop sizes (5 and 13µl)

and two different heights (10 and 40mm) were determined to assess the influence of impact velocity and drop weight on the WSA.

Table 5.2. Water shedding angles of various textile samples coated with silicone nanofilaments.

Drop height	Sample #	211	213	214	402	403	404	405	407	408	413	414
10mm	ω_{13}	35	10	35	15	5	25	55	2	10	25	40
	ω_5	70	20	45	20	10	25	-	5	20	35	65
40mm	ω_{13}	45	10	40	40	15	40	70	3	35	50	45
	ω_5	75	15	50	30	15	35	-	3	30	50	70

The results reflect the qualitative differences in the superhydrophobic character of the individual coated textiles and are, with few exceptions, independent of drop height and drop volume. Naturally, the chemical nature of the textile as well as its structure and weave will influence the quality of the coating and the superhydrophobic effect in terms of the WSA. A loose knit of textile fibers for instance will result in a more flexible, less dense substrate into which the water drops can penetrate to some extent. This will cushion the fall of the water drops and absorb some of their kinetic energy, increasing the WSA. Also the drop might get stuck inside the depressions and not roll off the surface. A detailed evaluation of all chemical and structural parameters that influence the hydrophobicity of textile samples is however not subject of this work. At this point it is only noteworthy that all coated textile samples exhibit superhydrophobic properties which is remarkable considering that all samples were coated under the same coating conditions, without any processing (cleaning or activating) prior to coating and without specifically optimizing the coating procedure.

5.3.2 Evaluation of a superhydrophobic PET fabric

In terms of superhydrophobicity, the PET fabric showed the best results in the water shedding experiments. WSA of 2-5° depending on the drop size and drop height were measured. In relation, the sliding angle for a 10µl drop of water was in the region of 15° on these samples. Figure 5.25 illustrates the extreme non wetting properties of the coated PET textile samples. Small drops of water appear to float on the textile surface and a jet of water bounces off the surface.

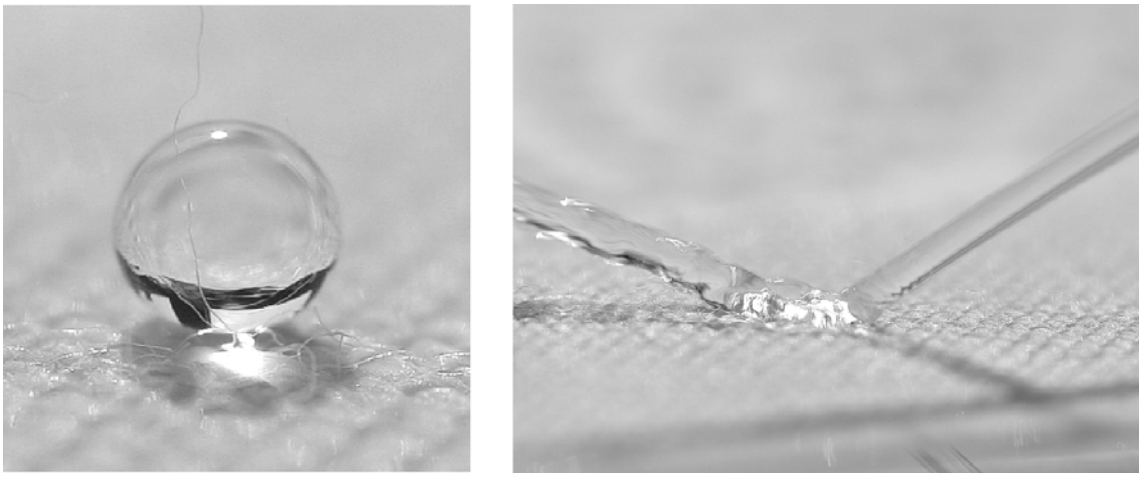

Figure 5.25. Water wetting properties of an SNC PET textile. Left: 5µl drop of water on the coated PET sample. Right: a jet of water bounces off the coated PET sample.

Upon immersion in water, a thin layer of gas is trapped on the coated PET surface. This so called plastron layer gives the textile a silver sheen due to a total reflectance of light at the liquid/gas interface. As with the coated glass samples the plastron layer was found to be stable over weeks [70]. Figure 5.26 shows pictures of a coated PET sample immersed in water over the course of 2 months.

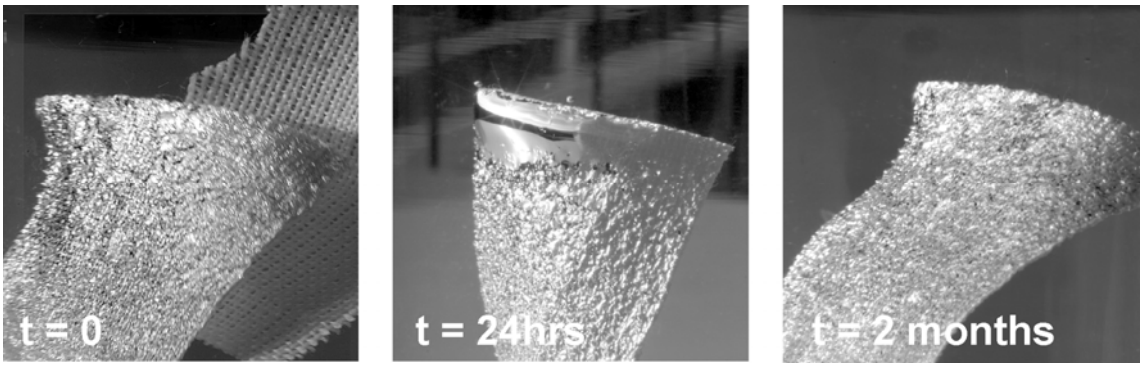

Figure 5.26. A superhydrophobic coated SNC PET textile immersed in water. As a reference the left image also shows an uncoated PET sample immersed in water.

So far there are few reports of stable plastron layers on artificial superhydrophobic surfaces [16,126]. Plastron layers are utilized in nature by some water dwelling species such as the water spider to capture and trap air for breathing under water [16,127]. They can even act as gas exchange barriers for oxygen and CO_2 exchange in water and enable insects like the water bug (Aphelocheiridae) to remain indefinitely submerged underwater (plastron respiration). That this

effect can be mimicked with artificial, superhydrophobic surfaces has recently been shown by Shirtcliffe *et al.* [16].

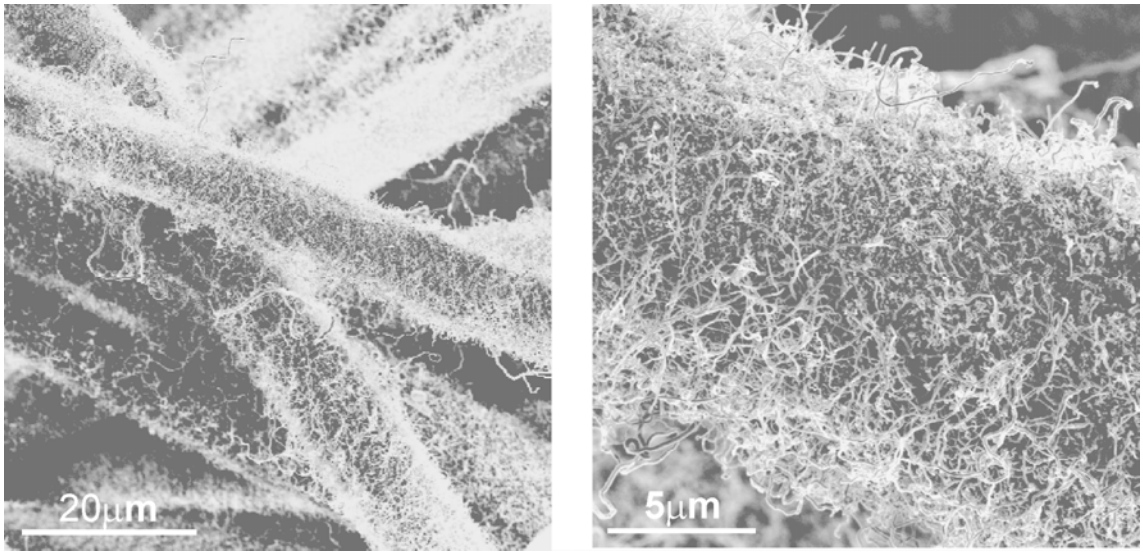

Figure 5.27. SEM images of a PET textile sample coated with silicone nanofilaments.

Electron microscopy images of the coated samples reveal that the individual PET fibers are covered by a dense layer of PMSQ nanofilaments (Figure 5.27). Even the deeper layers of the fabric show this structure, indicating that the mobility of the reactive precursors in the gas phase is sufficient to penetrate into and react on the whole fabric. Similar coating results were observed on all other coated fabrics but they typically showed a less dense PMSQ nanofilament growth (data not shown).

Table 5.3. Tensile strength measurements on SNC cotton (#413) and PET (#407) textile samples.

Sample	Coating type	Elongation at break [%]	Tensile strength∅ [N/cm]
Cotton #413	uncoated	33.3 ± 1.3	83 ± 5
Cotton #413	I	5.9 ± 0.9	1.4 ± 0.4
Cotton #413	II	21.0 ± 0.5	11.3 ± 0.6
PET #407	uncoated	39.0 ± 1.0	128 ± 3
PET #407	I	37.6 ± 1.0	120 ± 7

Since PET is among the most frequent materials employed in textile applications, efforts were made to further evaluate the properties of the PET samples in terms of relevant parameters like tensile strength, abrasion resistance, durability upon washing and oil repellence.

In Table 5.3 the results of tensile strength tests performed according to ISO 13934-1:1999 on coated and uncoated cotton (#413) and PET (#407) samples are summarized. The results of the cotton samples clearly show that the fabric is damaged by the coating process. If TCMS is replaced by MTMS in the coating reaction according to Protocol II, the tensile strength of the coated cotton fabric improves. Obviously the hydrochloric acid generated in the coating reaction damages the cotton fibers. Since a small amount of TCMS is also added in Protocol II to catalyze the condensation reaction, the cotton is still damaged but not as severely. PET on the other hand generally shows a better resistance to acid attack which is reflected in the tensile strength measurements. Both the elongation at break and tensile strength decrease by less than 10% after coating with PMSQ nanofilaments, a value considered acceptable for textile coatings.

One of the greatest problems facing the application of superhydrophobic coatings is their generally low mechanical stability. Abrasive forces will destroy the delicate nanostructures on the surface and result in a loss of superhydrophobicity. The SNC is faced with the same problem (5.2.3).

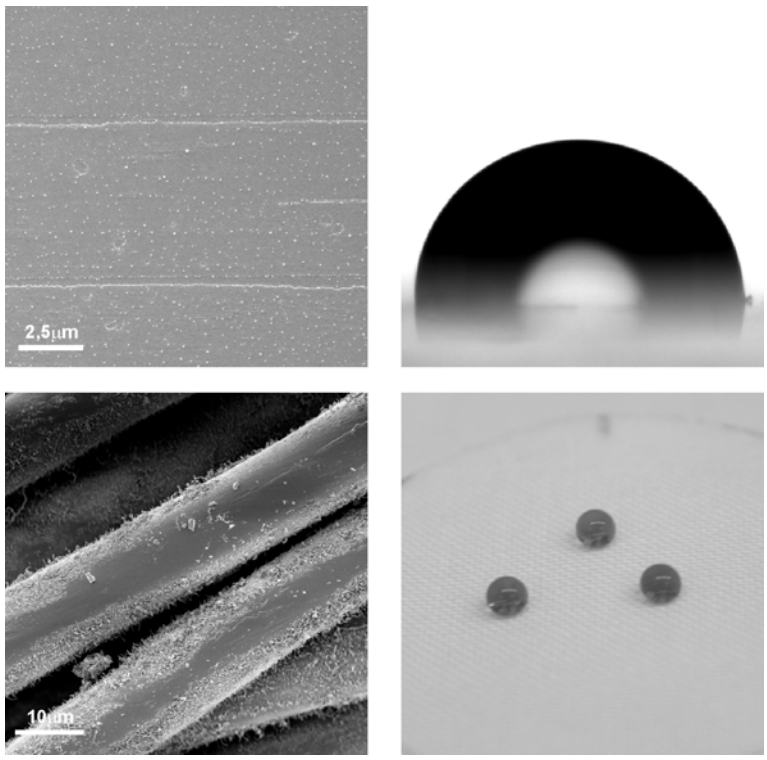

Figure 5.28. SEM images and wetting properties of a coated glass sample (top) and coated PET sample (bottom) after the abrasion test.

Nature has developed strategies to counter or circumvent the problem of low abrasion resistance. The lotus leaf surface for instance protects its nanoscopic epicuticular wax crystals by an underlying, microscopically rough papillose arrangement of epidermal cells [4,66]. Upon mild abrasion, only wax crystals from the tops of the papillae are removed and the superhydrophobicity is maintained.

The SNC on textile fabrics mimics the two tier roughness structure of the lotus leaf, and leads to a significant improvement of the stability of the superhydrophobic effect generated by the PMSQ nanofilaments. Figure 5.28 shows SEM images and wetting properties of a coated, flat glass sample and a coated PET sample after 1450 abrasion cycles against a skin simulating friction partner on a Textile Friction Analyzer (TFA).

While on the flat substrate the structure of the coating is completely destroyed, it is only damaged on the most exposed parts of the textile fibers. The major part of the PMSQ filaments is protected by the 3-D microstructure of the woven textile. Consequently the superhydrophobic character of the coated PET fabric is maintained.

Table 5.4 summarizes the wetting properties of the glass and PET sample before and after the abrasion test. As observed earlier, the simple handling or touching of a flat SNC surface already leads to an immediate loss of superhydrophobic properties. In contrast, the coated textile samples could be freely handled and touched without loosing their superhydrophobic character.

Table 5.4. Wetting properties of a coated glass and PET sample before and after the abrasion test.

Substrate		Before abrasion	After abrasion
Glass	θ	162°	90°
	α	16°	-
	ω_{13}	1°	-
	ω_5	2°	-
PET # 407*	ω_{13}	2°	25°
	ω_5	5°	35°

*The values are identical for samples rubbed along the weft and warp direction.

The situation changes when the abrasive forces act throughout the textile. In a washing machine for instance, textiles are mangled to facilitate the cleaning process. Additionally, basic cleaning

agents chemically affect the SNC (5.2.1). To assess the damage to the SNC caused by even mild washing in a washing machine, a standard washing cycle according to ISO 6330:2000 was performed. The effect of this procedure on the coating is visualized in Figure 5.29.

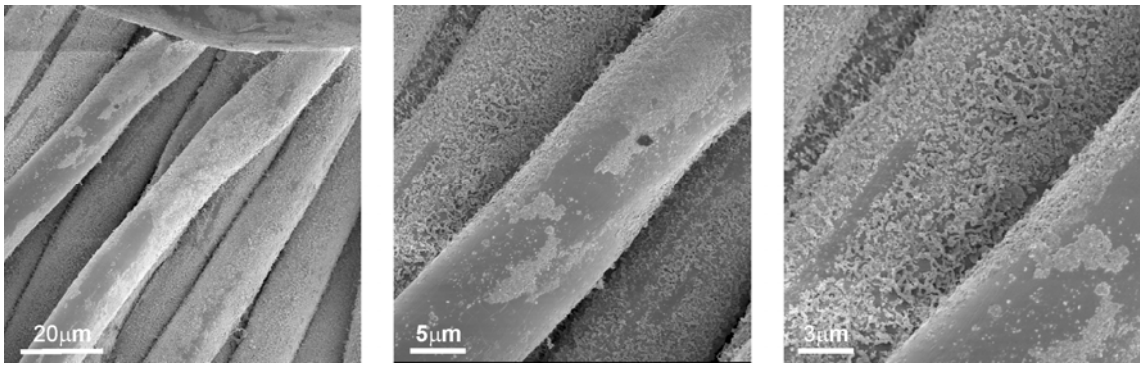

Figure 5.29. SEM images of a coated PET sample after washing at 30°C according to ISO 6330:2000.

Opposed to the samples of the abrasion test, the SNC is destroyed more thoroughly on all areas of the textile fibers and signs of a chemical degradation are also evident in the SEM pictures.

In terms of wetting properties, the coated textile samples show a delayed wetting behavior after washing. Initially, drops of water do not wet the washed samples and the water shedding angles of 20° for a 13µl drop and 25° for a 5µl drop were even superior to those after the abrasion test. However, when a drop of water was suspended on the samples it only maintained a high contact angle for the first 15-20s and then seeped into the fabric within less than a second. A similar observation was made by Lau *et al.* on surfaces covered with unmodified carbon nanotubes [128]. Possibly the drop is initially suspended on enough hydrophobic patches to support a metastable superhydrophobic state. But with time the contact line moves further into the fabric and encounters the degraded, hydrophilic patches at which point the drop is completely drawn into the fabric due to capillary forces.

To add oil repellent properties to the superhydrophobic textile, the SNC was modified with a fluorinated silane (4.3.5, 5.4.1). PET samples coated with silicone nanofilaments and modified with PFOTS showed a pronounced resistance to wetting by organic liquids. Oil resistance tests according to ISO 14419:1998 resulted in an oil repellency grade of 6 (on a scale from 1-8). Even decane ($\sigma_{disperse}$~24 mNm^{-1}) formed stable contact angles of more than 120° on the coated fabric (Figure 5.30). Octane ($\sigma_{disperse}$~21 mNm^{-1}), on the other hand was immediately absorbed.

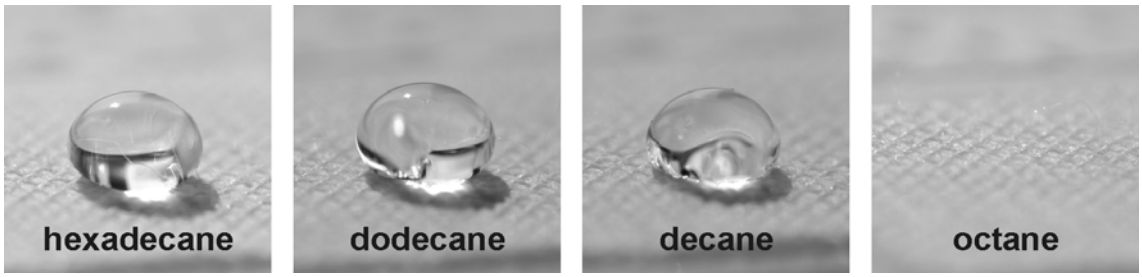

Figure 5.30. Oil repellency test on a SNC and fluorinated PET textile sample according to ISO 14419:1998.

Surprisingly, drops of hexadecane did not stick to the modified SNC textile. Hexadecane showed a SA of roughly 20° (10µl drop) and a WSA of 35° (13µl drop) on this surface. Compared to the same coating on flat glass substrates (5.4.1), this constitutes a significant increase in oil repellence. Apparently, the additional micro and macrostructure of the textile further reduces the contact area of the hexadecane drop on the surface and decreases its adhesion.

The stable oleophobicity of the coated and fluorinated PET fabric even towards organic liquids with low surface tensions such as decane is quite surprising. On Teflon for instance decane is reported to exhibit contact angles of only 32-40° [56]. That the same liquid exhibits a contact angle of more than 90° on the rough, coated textile substrate is therefore contradictory to the Wenzel equation. Similar observations were made with non polar liquids on fluorinated SNC on glass (see next section).

5.4 Chemically modified silicone nanofilaments

In the following sections, results showing the potential of the PMSQ filaments for other applications besides superhydrophobic coatings are presented. The filaments were chemically modified to create coatings that exhibited superwetting and antiwetting properties towards polar and non polar liquids. Ion exchanger residues were attached to the surface to produce high surface area coatings with specific protein adsorption properties. The coating was patterned with regions of varying (super)functionality or continuously degraded to produce full wettability gradients.

5.4.1 Superwetting/-nonwetting coatings

A recently published review summarizes the advances in fabricating surfaces with extreme wetting properties for a variety of applications such as water and/or oil repellence, water/oil separation strategies, antisoiling, antifouling or antifogging applications [129]. Underlying principle for all the presented surfaces is a high surface roughness which amplifies the wetting properties given by the surface chemistry. Typically any of the presented surfaces realizes only

one type of wettability and often involves complicated procedures. The fundamental idea for the work in this section is that the SNC essentially represents a nanorough surface with a chemical composition easily accessible for modification. Consequently any possible type of superwetting or –nonwetting surface can be created from a silicone nanofilament template.

Tailoring the functionality of silicon and silicone surfaces is a well established process and has found a multitude of applications [52,130]. In a first step, reactive sites (OH-groups) are generated on the surface either by chemical (etching) or physical (plasma) processes. In the case of silicone, the surface Si-CH_3 bonds that form the outer layer of the silicone are oxidized and reactive Si-OH groups are formed [131]. In a second step these sites can react with functionalized silanes (usually trichlorosilanes) in gas or solvent phase, leading to mono- or multilayer formation on the surface (see 2.1.5). The same process was applied to the superhydrophobic SNC (4.1.2 and 4.3.5).

Table 5.5 summarizes the wetting properties of various test liquids on SNCs modified by plasma treatment and subsequent coating with OTS or PFOTS. As a reference, contact angle values of OTS and PFOTS SAM (or related SAM) on flat surfaces found in the literature are given.

Table 5.5. Contact and sliding angles on functionalized SNCs and on planar SAM. "–" indicates that drops stick to the surface and do not roll off.

	Silicone nanofilaments (SN)	Plasma activated SN	OTS modified SN	PFOTS modified SN	Planar OTS SAM	Planar PFOTS SAM
θ_{H_2O}	165° ± 2°	<2°	167° ± 2°	168° ± 2°	~110°[132-134]	~115°[53,133]
α_{H_2O}	5° ± 3°	-	4° ± 2°	8° ± 2°	-	-
$\theta_{C_{16}H_{34}}$	~2°	<2°	<2°	140° ± 5°	~40°[132-134]	~70°[133,135]
$\theta_{CH_2I_2}$	115° ± 4°	<2°	50° ± 4°	165° ± 2°	~72°[134]	~98°[135]
$\alpha_{CH_2I_2}$	-	-	-	6° ± 2°	-	-

Water, hexadecane and diiodomethane are common test liquids applied in surface tension measurements to probe the polar and disperse parts of solid surface tensions. Whereas water possesses one of the highest polar surface tensions ($\sigma_{polar} \sim 50 mNm^{-1}$) plus a smaller contribution of disperse surface tension ($\sigma_{disperse} \sim 20 mNm^{-1}$), CH_2I_2 possesses one of the highest known

disperse liquid surface tensions ($\sigma_{disperse} \sim 51 mNm^{-1}$) with no polar contribution. Consequently, water is often used to probe the polar, CH_2I_2 to probe the disperse part of a solid surface tension in wettability studies. Hexadecane also has only a non polar surface tension ($\sigma_{disperse} \sim 27 mNm^{-1}$) but one that is considerably lower than that of CH_2I_2.

Figure 5.31 shows the wetting behavior of water and hexadecane on the individual modified coatings as well as corresponding SEM images. The SEM images indicate that the surface structure of the coating is not significantly altered by the plasma activation or subsequent functionalization steps.

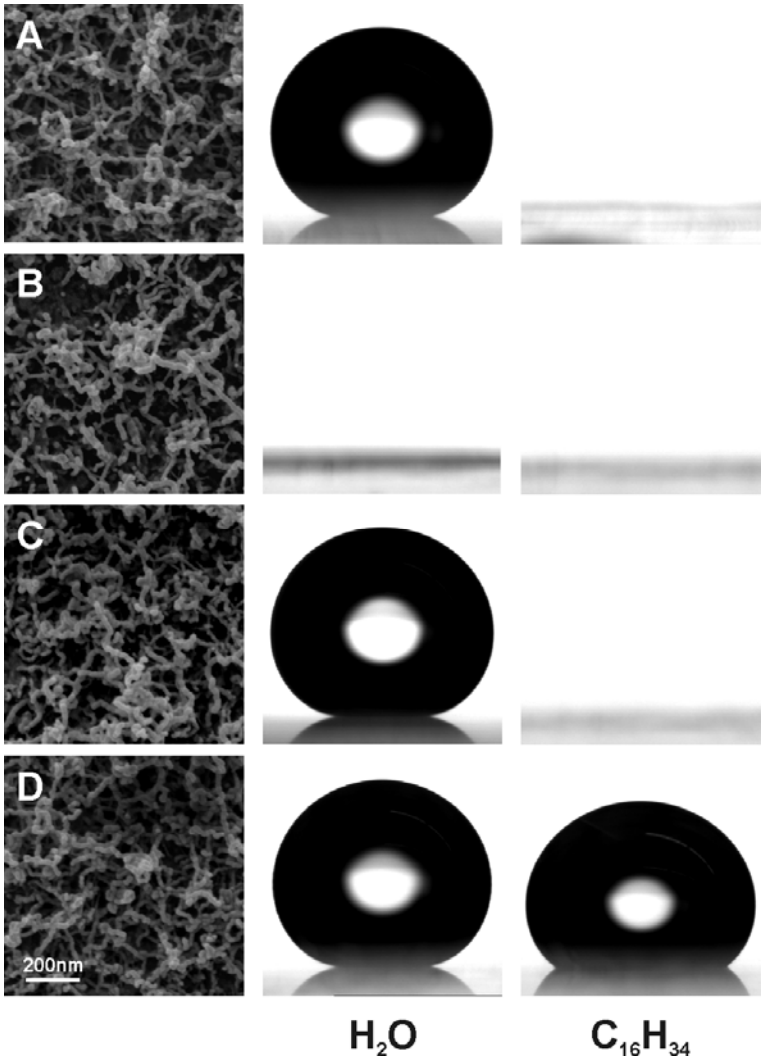

Figure 5.31. Electron microscopy images of an as prepared SNC (A), after plasma modification (B), after OTS modification (C) and after PFOTS modification (D). Middle and right columns show 10µl drops of water and hexadecane on the individual coatings respectively.

Whereas the as prepared SNC is ideally non-wetting for water, it is almost completely wet by hexadecane. CH_2I_2, on the other hand, exhibits a relatively high macroscopic contact angle due to its much higher surface tension. Plasma treatment of the surface results in a complete wetting of the surface by all test liquids, it becomes superamphiphilic. The OTS treatment slightly improves the original hydrophobicity of the silicone nanofilaments and noticeably increases the oleophilicity. This becomes clear considering that by the plasma treatment and subsequent OTS coating CH_3 groups are essentially replaced by $C_{18}H_{37}$ groups on the surface, resulting in stronger hydrophobic interactions between the surface and the test liquid. This is in accordance with the results of Fadeev *et al.* who found that for SAM of alkylsilanes on silicon wafers, the hexadecane and CH_2I_2 contact angles decrease with increasing chain length [47]. When PFOTS is applied in the refunctionalization step, the coating becomes non-wetting for both polar and non polar liquids (superamphiphobic).

Figure 5.32 again shows a drop of water and hexadecane on a PFOTS modified silicone nanofilament surface.

Figure 5.32. 10µl drop of colored hexadecane (yellow) and colored water (blue) on a PFOTS modified SNC on glass.

A stable hexadecane contact angle of more than 140° on the PFOTS modified coating is surprising, considering that hexadecane exhibits a contact angle of less than 90° on flat fluorinated surfaces. According to the Wenzel equation the contact angle should decrease on the rough, PFOTS modified coating. Although there are a few reports of fluorinated superoleophobic surfaces with hexadecane contact angles above 90°, this apparent contradiction has not been discussed in the literature. A possible explanation for the apparent contradiction to the Wenzel

equation could be that a drop of hexadecane deposited on the surface is not in equilibrium and therefore exhibits an unnaturally high contact angle. However the performed wettability studies showed that the drop shape was stable for many minutes without any apparent change in contact angle. That hexadecane wets the PFOTS modified coating in a Wenzel type wetting regime, and not in a Cassie-Baxter type, can be confirmed by dipping the coating in hexadecane. The substrate emerges completely wet when withdrawn from the fluid, indicating that hexadecane completely penetrates into the surface structure.

As opposed to the PFOTS modified textile samples (5.3.2) drops of hexadecane do not roll off the PFOTS modified SNC glass surface but stay pinned even at 90° inclination, again an indication of a Wenzel type wetting. Obviously the combination of surface energy and surface structure in this case is not suited so support a Cassie-Baxter state. That drops of non polar liquids remain pinned to the surface and do not roll off is a typical observation for superoleophobic surfaces [136-138]. To my knowledge, only one superoleophobic surface has ever been reported from which drops of a non polar liquid roll off [21,22]. In this sense, the PFOTS modified PET fabric introduced in Section (5.3.2) shows very unique properties in terms of superoleophobicity.

If the surface tension of the non polar liquid is high enough, the PFOTS modified SNC on glass also shows these unique properties. Drops of CH_2I_2 for instance roll off the surface even at slight inclination and the contact angle of CH_2I_2 reaches a value almost as high as the water contact angle (see Table 5.5). To my knowledge this is the highest contact angle ever reported for a non polar liquid on a solid surface. Apparently a stable Cassie-Baxter type wetting state is supported for CH_2I_2 due to its relatively high liquid surface tension.

When comparing the roll off behavior of water and CH_2I_2 on the PFOTS modified coating, another anomaly is observed. Drops of water do not accelerate when rolling off the PFOTS modified surface but move with a constant velocity. In contrast, drops of CH_2I_2 accelerate normally when rolling off the PFOTS modified SNC. To my knowledge this unusual behavior of water drops on a superhydrophobic surface has never been reported before and is even contradictory to the common observation that water drops accelerate when rolling off superhydrophobic surfaces [139,140]. Currently the difference in sliding behavior of water drops on flat hydrophobic surfaces is being studied to some small extent [141,142] but the conclusions cannot be transferred to the case of rough surfaces. A possible explanation for the effect could be the strong polarization of the C-F bonds. This can lead to a static charging of the surface [139,142-144] which would only influence polar liquids such as water but leave non polar liquids like CH_2I_2 unaffected.

To further confirm the functionalization of the silicone nanofilaments XPS measurements were performed. Table 5.6 summarizes the chemical composition of the as prepared and modified SNC as determined from XPS measurements.

Table 5.6. Atomic composition of the bare and modified SNC as determined by XPS.

	Silicone nanofilaments	OTS modified SN	PFOTS modified SN
O [At%]	41	40	30
C [At%]	29	38	18
Si [At%]	30	22	16
F [At%]	-	-	36

The carbon content on the surface increases after OTS modification and the fluorine content increases after the PFOTS modification. Unfortunately at this point a more quantitative interpretation of the XPS data is not possible. Due to the high surface roughness and unique composition of the coating, the individual contributions of the top coating, bulk silicone nanofilament and underlying glass substrate to the XPS signal can not be distinguished. Information on the actual coverage of the silicone nanofilaments by OTS or PFOTS molecules could therefore not be gained and whether the nanofilaments are covered with a full monolayer, a multilayer or if the OTS and PFOTS molecules only punctually attach to the filaments remains unknown. Further experiments will be necessary to gain some insight on the exact composition of the modified coatings and to devise strategies on how a potentially incomplete coverage can be improved.

Nevertheless, the performed wetting experiments show that the SNC and the simple modification techniques already constitute a versatile toolbox to create and explore surfaces with extreme wetting properties towards both polar and non polar liquids. In terms of actual application of the modified coatings, for instance as anti soiling coatings, further studies need to be performed, especially in terms of the long term stability of the functionalization.

5.4.2 Patterning

The above section has shown that the SNC can be readily functionalized to exhibit extreme wetting or extreme non wetting properties towards polar or non polar liquids. If the functionalization is selectively performed on different areas of the same substrate, patterned

surfaces with an extreme wetting contrast between for instance superhydrophobic and superhydrophilic domains can be created. Such surfaces are of considerable interest to liquid handling, biochip and water harvesting applications to name a few. Furthermore, these surfaces show great potential in the development of open geometry microfluidics devices for lab-on-a-chip applications [25]. Surprisingly, scientific publications that actually involve superhydrophobic/superhydrophilic patterns are rare and usually involve complicated procedures [145,146]. Recently however, Zhai *et al.* introduced a relatively simple procedure to create hydrophilic patterns on a superhydrophobic surface via the selective deposition of polyelectrolyte monolayers and have demonstrated some of their potential [24]. Still in order to create superhydrophilic regions on a superhydrophobic background as many as 14 bilayers of poly(allylamine hydrochloride) and silica nanoparticles had to be applied selectively on the previously hydrophilized areas.

The SNC enables an even simpler approach to creating surfaces with spatially well defined wettability patterns. To create surface patterns of varying functionality on a single substrate, areas of the substrate are masked during the activation step (4.3.6). Since no reactive sites are created on the masked areas, the subsequent functionalization is limited to the activated areas, even if the full substrate is immersed in the coating solution. Through this simple strategy coatings can be created that have a constant surface structure (i.e. roughness, surface area) but designated areas of contrasting wetting properties. An example of a coating that combines all possible superwetting/antiwetting combinations on a single substrate is shown in Figure 5.33.

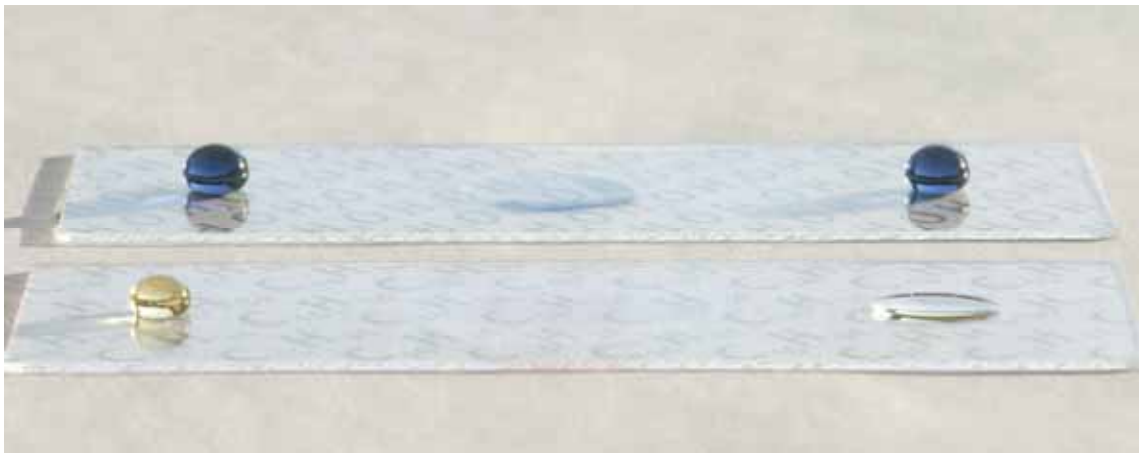

Figure 5.33. Drops of water (back) and hexadecane (front) on identical samples with three distinct regions of functionality: superamphiphobic (left), superamphiphilic (middle), superhydrophobic/superoleophilic (right). Note that hexadecane spreads almost completely on the middle region of the front sample, making the drop almost invisible.

The two samples in Figure 5.33 are completely identical only that drops of colored water were placed on the top and drops of colored hexadecane on the bottom sample. The samples are superamphiphobic on the left, superamphiphilic in the middle and super-hydrophobic/superoleophilic on the right. The combination superhydrophilic/superoleophobic is not possible because an oleophobic surface is always hydrophobic. Changing the shape, size and location of the functionalized areas on the sample is only a question of choosing an appropriate mask and coating sequence.

Figure 5.34 illustrates that with simple techniques even sub mm structures can be created on the silicone nanofilament template. It shows a superhydrophilic stripe on a superhydrophobic background, visualized by fluorescence microscopy. The aqueous fluorescent dye solution applied to the surface spreads only on the hydrophilic region and does not penetrate the hydrophobic background.[6]

The two examples in Figure 5.33 and Figure 5.34 show that in principle wetting contrasts of arbitrary size and shape can be realized on a single substrate. The masking techniques applied in our experiments were very crude and consisted of covering parts of the surface by glass slides during plasma activation. In this sense the presented examples only constitute a proof of principle.

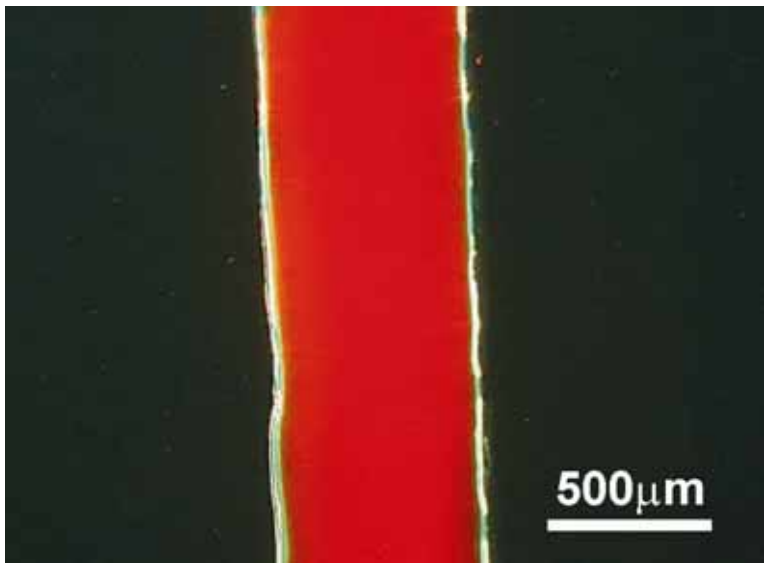

Figure 5.34. Fluorescent dye inside a superhydrophilic canal on a superhydrophobic background.

[6] In total the stripe runs the entire breadth of the coated glass slide (2.5cm) although admittedly not always as smooth as implied in the figure. This is however only due to the very crude fabrication method applied for these experiments.

Using state of the art masking techniques like PDMS stencils [147] will enable the creation of much cleaner and more diverse functional macro- and micropatterns on the PMSQ filament surface. Naturally other patterning techniques such as microcontact printing, etching, mechanical abrasion or photolithography could also be suited to create patterns on the SNC. Preliminary experiments have shown that it is possible to pattern the growth of the SNC by masking the substrate during the initial coating step. However all of these techniques are either more complicated or will result in patterns that are contrasting in both chemistry and surface structure. The unique feature of the presented method is that the surface structure is not changed by the functionalization process. Surface area and surface roughness remain constant over the whole substrate area and the wetting contrast is realized solely by a change in surface chemistry.

5.4.3 Protein adsorption

Apart from modifying the wettability of the SNC, other interfacial properties like protein adsorption characteristics can be altered by applying (bio)chemical functionalities to the SNC. For instance by applying the same methods that were used to alter the wetting properties of the coating, the SNC were modified with aminopropytriethoxysilane (APTES) and 2-(carbomethoxy)-ethyltrichlorosilane (CETS) to mimic high surface area coatings with specific protein adsorption/retention characteristics. Through the APTES modification, a basic amino functionality is added to the PMSQ nanofilaments. The CETS modification (and post treatment in basic buffer solution) adds an acidic carboxyl functionality (Figure 5.35).

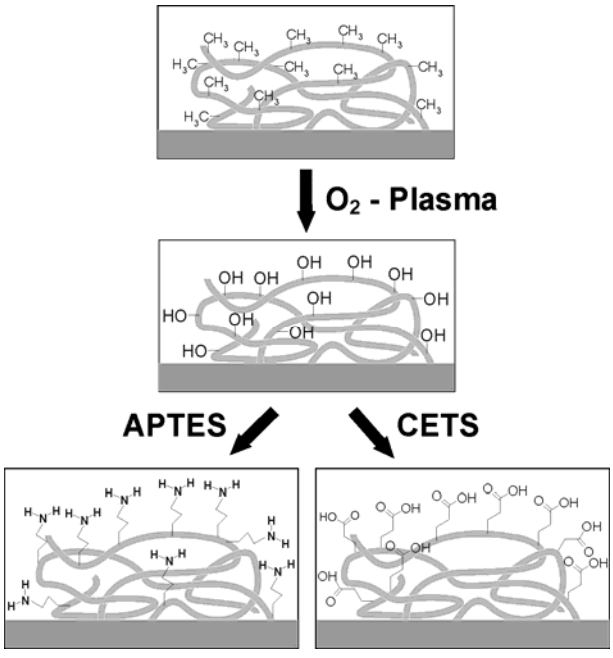

Figure 5.35. Schematic representation of the modification of silicone nanofilaments with APTES and CETS.

As before, the functionalization process does not noticeably change the structure of the coating (Figure 5.36).

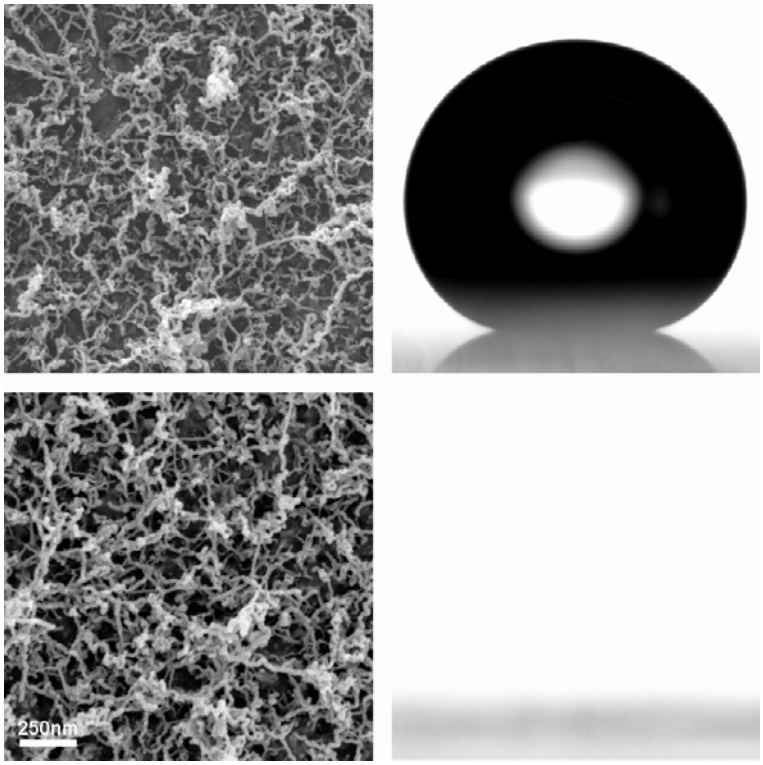

Figure 5.36. Electron microscopy image and water wetting behavior of the SNC before (top) and after modification with APTES (bottom). The coating after CETS modification behaves analogous to the APTES modified coating (not shown).

The coatings remain superhydrophilic after the APTES and CETS coating because of the hydrophilicity of the amino and carboxyl groups introduced to the surface (Figure 5.36, right). Therefore the functionalization cannot be confirmed by contact angle measurements as in the previous section. The protein adsorption experiments performed on these coatings however unambiguously confirm their successful functionalization.

Figure 5.38 shows the binding kinetics of fluorescently labeled β-Lactoglobulin (β-Lg) on the plasma activated and the amino- and carboxyl- functionalized surface monitored at pH 3 and pH 6 (citrate buffer, 50mM) in a continuous flow cell setup using the SAF biosensor. The SAF biosensor selectively detects the emission of fluorophores located in the near vicinity (<200nm) of an interface. When monitoring the adsorption of fluorescently labeled proteins, the fluorescence count rate measured with the SAF biosensor accurately reflects the density of surface adsorbed proteins and is therefore a direct measure of the retention efficiency.

β-Lg has an isoelectric point (pI) of 5.2 and is net negatively charged at pH 6 and net positively charged at pH 3. Accordingly at pH 6 it shows a high affinity to the positively charged APTES surface and a low affinity to the negatively charged CETS surface. At pH 3 the inverse behavior is observed: low affinity to the APTES and high affinity to the CETS modified surface.

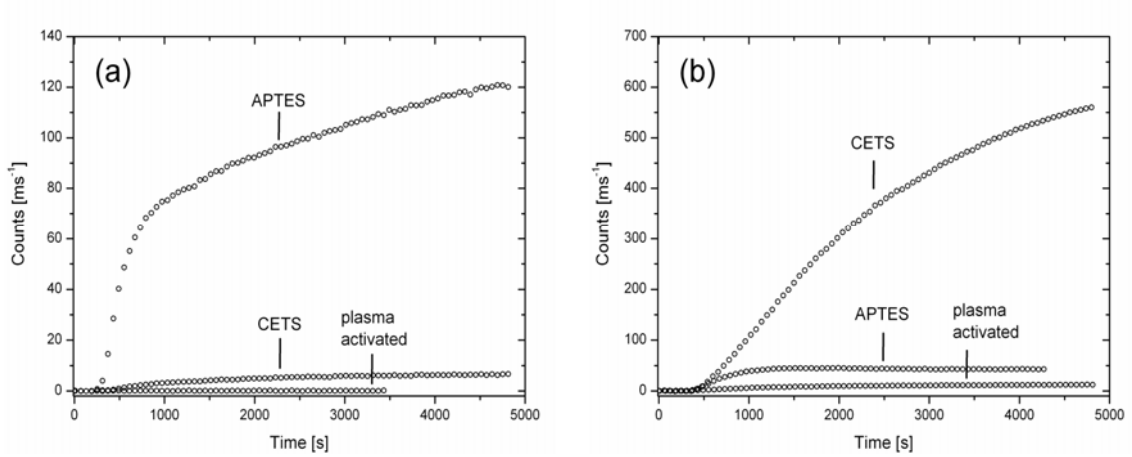

Figure 5.37. Binding kinetics of fluorescent dye labeled β-Lactoglobulin on plasma activated and CETS or APTES modified SNCs at pH 6 (a) and pH 3 (b).

As highlighted in Figure 5.38 the relatively modest pH change of three units causes a threefold increase of equilibrium protein retention on the APTES surface. On the CETS surface the increase in protein retention is even in the range of two orders of magnitude. Clearly the APTES and CETS modified SNCs act as high surface area cationic and anionic exchange resins towards charged proteins.

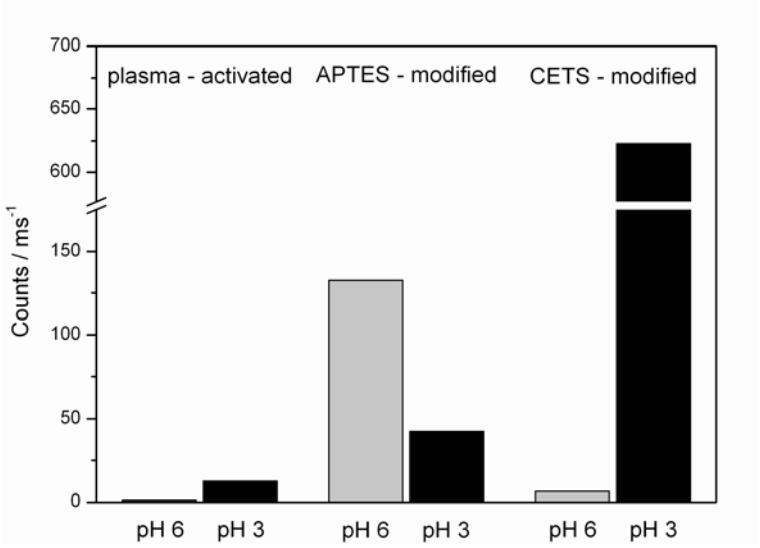

Figure 5.38. Equilibrium coverage intensities of fluorescent dye labeled β-Lactoglobulin adsorbed on modified SNCs at different pH levels.

Under both pH conditions, adsorption of β-Lg is extremely low on the plasma activated coating. Adsorption is suppressed by 2-3 orders of magnitude under high affinity conditions and a factor of 5-10 at low affinity conditions (see Figure 5.37). Hydrophilic surfaces are generally known to enhance protein resistance [148-150]. On polydimethylsiloxane (PDMS), chemically related to the silicone nanofilaments, protein adsorption can be reduced by oxidizing the surface with plasma or corona discharge methods, however not to the extent observed in our experiments [151]. Typically PDMS also suffers from "hydrophobic recovery" and reverts to its initial state after a short time due to a diffusion of uncondensed monomers and small chain oligomers to the surface [151,152]. Similar effects could not be observed on the activated SNC. The coatings remain superhydrophilic for an indefinite time when stored under ambient laboratory conditions and exhibit the same low protein affinity even after prolonged storage in air or buffer solution. This indicates that the PMSQ filaments indeed represent a thoroughly crosslinked matrix with no free monomers or short chain oligomers.

An essential requirement for protein enrichment systems is a full and reproducible reversibility. Figure 5.39 exemplarily shows the adsorption kinetics of β-Lactoglobulin on the CETS modified surface. When the protein solution of pH 3 is replaced by a protein-free buffer of pH 6 practically all surface bound molecules are released within a few minutes. Upon switching back to protein solution of pH 3, β-Lactoglobulin can be re-adsorbed, following the same kinetics as before. As many as five adsorption-retention cycles were run on a single substrate in the course of several days without any loss of performance.

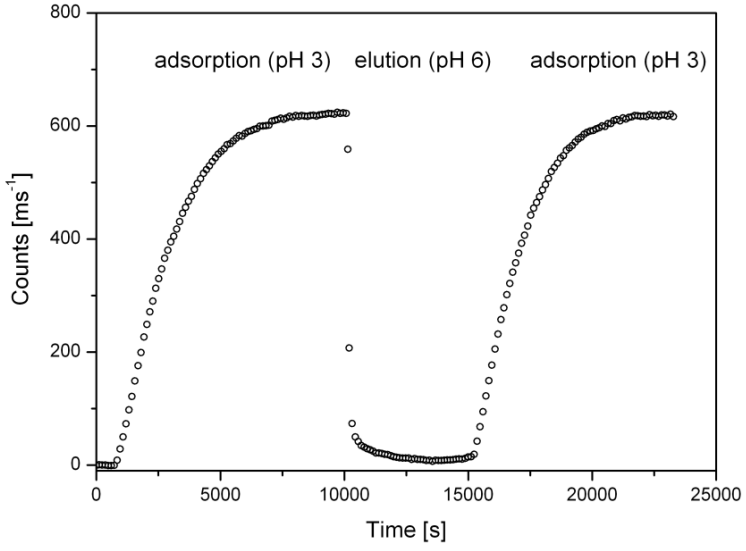

Figure 5.39. Adsorption and desorption curves of β-Lactoglobulin on a CETS modified surface.

Irreversible retention caused by strong protein-surface interactions that would possibly alter the binding capacity of the nanofilament surface was not noticed during the experiments. Further, the reproducible adsorption kinetics presented in Figure 5.39 underline that the coating itself is not irreversibly altered or damaged by the exposure to the different pH levels.

For proteins of different pI, adsorption on the modified SNCs becomes selective. Figure 5.40 shows the adsorption of β-Lactoglobulin (pI 5.2), α-Chymotrypsin (pI 8.1), and Lysozyme (pI 11.5) on the APTES and CETS modified silicone nanofilament surface at a constant pH level of 6. All three proteins are globular with dimensions of roughly 5 nm in diameter which is about one order of magnitude smaller than the estimated average pore size between the nanofilaments.

On the positively charged APTES modified surface at pH 6, the negatively charged β-Lactoglobulin shows a 4 – 7 fold increase of adsorption as opposed to the positively charged proteins α-Chymotrypsin and Lysozyme. On the negatively charged CETS surface the positively charged proteins α-Chymotrypsin and Lysozyme are enriched by a factor of 8 – 15 over the negatively charged β-Lactoglobulin.

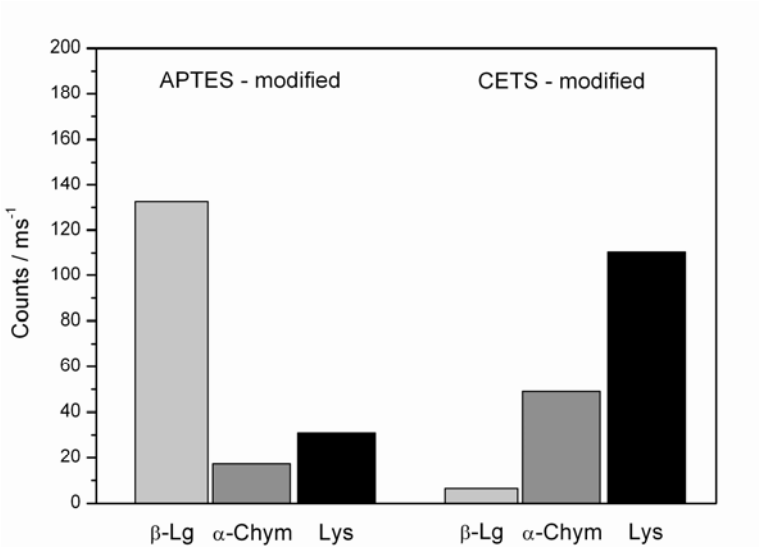

Figure 5.40. Equilibrium coverage intensities of fluorescent dye labeled β-Lactoglobulin, α-Chymotrypsin and Lysozyme on APTES and CETS modified silicone nanofilaments at pH 6.

The high roughness of the SNC and the resulting higher surface area and density of functional groups appears to enhance its selectivity towards biomolecular interactions. The observed enrichment factors are up to 7 times higher than those typically found on flat functionalized surfaces [148,153,154]. Possibly the 3-D charge distribution on the nanofilament coating plus the flexibility of the filaments contributes to a better shielding of the (repelling) charges of the

adsorbing protein, allowing for a higher loading of proteins in the adsorptive state than on a 2-D surface.

Overall the CETS modified coating exhibits better characteristics in terms of protein retention and selectivity than the APTES modified coating. However, both the SNC as well as the functionalization leave room for improvements. Increasing the layer thickness and filament density by adjusting the coating parameter for instance (5.5) should further enhance the protein retention characteristics. Optimizing the functionalization step could result in a higher density of functional groups. These first results however indicate that the studied modified SNCs represent a new approach to efficient and flexible surface bound ionic exchange resins with high selectivity and reusability. There are no apparent constrains that hinder the immobilization of other functional groups or active molecules on the surface which opens the opportunity to create enzyme or receptor based biosensors [28,155].

5.4.4 Wettability gradients

The data of the chemical stability studies (4.3.1) show that the wettability of the SNC changes upon immersion in hydrolytic media. The change in wettability can be attributed to a change in surface chemistry (generation of OH-groups on the surface) and a change in surface structure (etching of the silicone filaments), both caused by hydrolysis (4.3.1). In principle this degradation process can be utilized to tune the water wettability of the SNC in the entire range from almost completely non wetting ($\theta>160°$) to almost complete wetting ($\theta<3°$).

By selectively exposing areas of the coating to hydrolytic media for a controlled amount of time, the wetting properties of this region can be set to any desired value. In fact, if a SNC glass slide is gradually immersed in hydrolytic media, the gradual change in wettability can be transferred onto the vertical axis of the sample, creating a wettability gradient. In principle this gradient can be achieved over the full range of wettability from superhydrophobic to superhydrophilic, which has been rarely achieved so far [156,157]. Figure 5.41 depicts two SNC glass slides gradually immersed in 2M NaOH at two different immersion speeds.

Sample A has been immersed at 5µm/sec for a total time of 180min and sample B at an immersion speed of 15µm/sec for a total time of 60min. The resulting wettability gradient reaches from <3° to 70° on a length of 4.5cm on sample A and from 60° to 160° over a distance of 5.5cm on sample B. The lower image in Figure 5.41 is a montage of pictures of 5µl drops of water placed along the gradient axis of both surfaces.

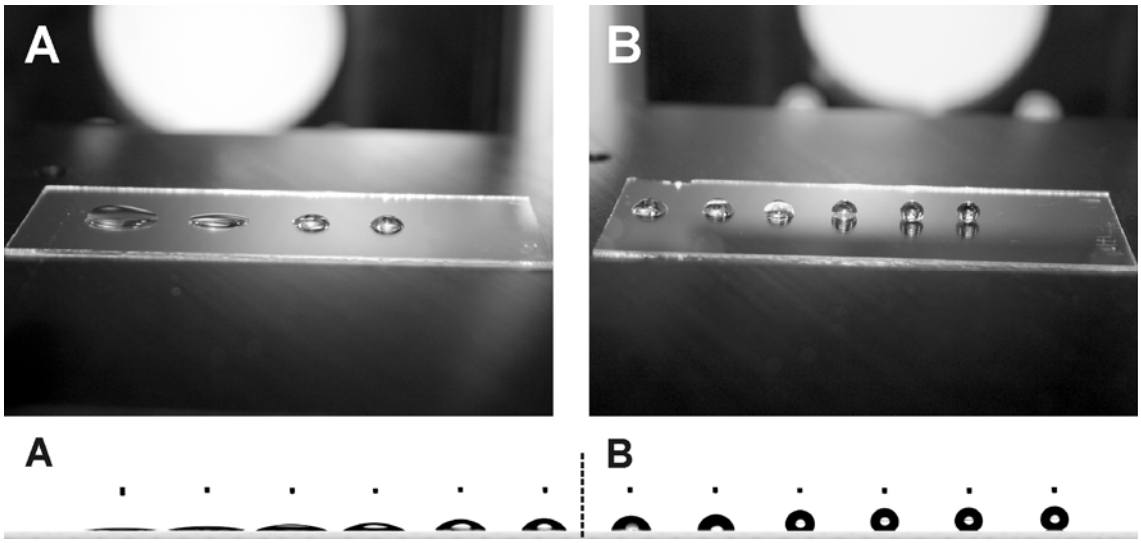

Figure 5.41. Top: SNC glass slides gradually immersed in a 2M NaOH solution at 5µm/sec (A) and 15µm/sec (B). Bottom: combined image of 5µl drops of water placed on the two surfaces at regular intervals along the gradient (see text).

The two experiments illustrate that, depending on the immersion speed, different regions within the wettability range can be transferred onto the SNC. Alternately (as the chemical durability studies indicate), the pH of the immersion solution can be adjusted to vary steepness and wettability range of the gradient. The montage indicates that by varying the immersion speed during immersion it should in principle be possible to create a full, linear wettability gradient on an SNC. Attempts to realize such a gradient however failed except in individual cases due to many experimental difficulties. As is evident from the data of the chemical degradation of the SNC, the degradation process and the resulting change in contact angle is not a linear process. The immersion process must therefore be strictly controlled to produce a linear gradient. However it was found that minute changes in pH, the initial wetting properties of the substrate and temperature influence the degradation speed making it difficult to establish a fixed immersion protocol for a given gradient length. None the less, the described technique is able to produce full wettability gradients from almost 0 to more than 160° on a single substrate which could be useful to study wettability and surface structure dependant phenomena like crystallization, protein adsorption or droplet motion. The fact that the chemical etching of the surface gradually changes the surface structure could be exploited to fabricate surfaces with a gradually changing surface roughness but constant surface chemistry (by activating and functionalizing the complete gradient). These could for instance be useful to analyze the effect of surface roughness/filament density on the protein adsorption of the CETS or APTES modified coatings (4.3.7).

5.5 Solvent phase coating

Preliminary experiments performed by Stefan Jung indicated, that the coating process can be transferred from the gas phase to the solvent phase. Mixing 100ml anhydrous toluene and 100µl TCMS under ambient conditions and immersing an activated substrate in this solution overnight result in a superhydrophobic coating. As with the gas phase coating, a sufficient amount of water in the reaction mixture is required for a successful coating. This is supplied by the water uptake of the anhydrous toluene during preparation of the reaction mixture under ambient conditions, as anhydrous toluene is extremely hygroscopic.

As with the gas phase setup, this initially very simple procedure required adaptation for a better control of reaction conditions and to ensure reproducibility. The detailed coating setup and protocol can be found in the experimental section (4.2.2). With the developed setup, the initial water content of the solvent as well as the total amount of silane in the reaction chamber can be selectively adjusted. Both are required to achieve reproducible coating results. Additionally a temperature control unit was implemented. To perform a rough characterization of the coating parameters with this setup, coating was performed under varying silane and water contents, coating times and temperatures. Although the results are by no means comprehensive they survey the field for future work and offer some insights into the coating mechanism.

The first general observation was that stirring the coating solution significantly reduces the coating time. Without stirring, coating times of 10 hours and more were necessary to form a superhydrophobic SNC coating. Under stirring, coating times of 30min and less could be achieved, indicating that the coating reaction and formation of the nanofilaments is a diffusion controlled process.

5.5.1 TCMS amount

Coating was performed at 23°C with an absolute water content of 1.9 ± 0.2mmol at a coating time of 4 hours. 5, 10, 50, 100 and 200µl TCMS were added to the reaction mixture respectively, corresponding to 0.04, 0.09, 0.42, 0.85 and 1.7mmol of TCMS. Only the last composition does not contain the stoichiometric amount of water needed for a full hydrolyzation and condensation of the silane precursors.

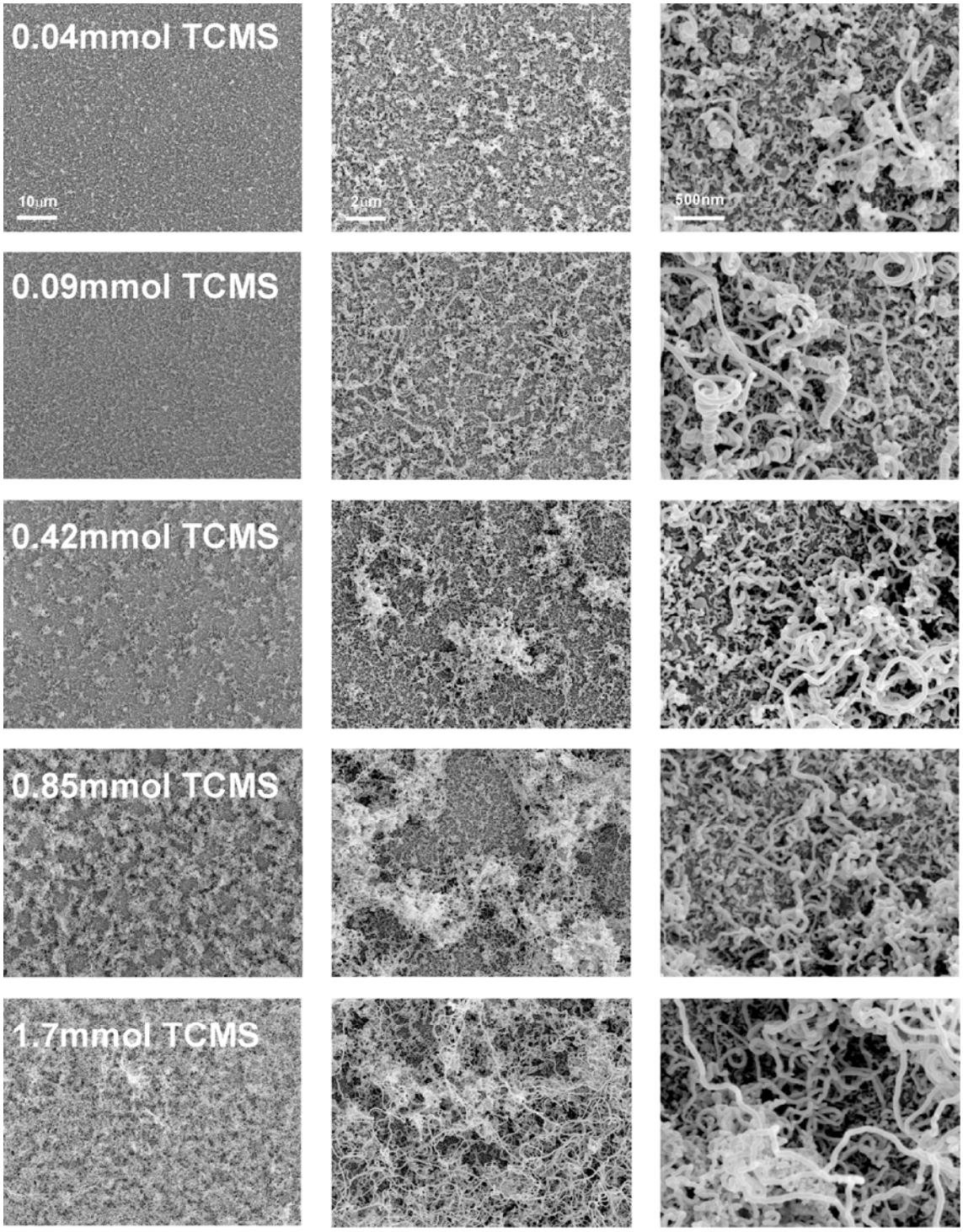

Figure 5.42. Electron microscopy images of glass slides coated at constant coating temperature, time and water content and at varying TCMS contents.

Figure 5.42 shows SEM images of the resulting coatings at three different magnifications. Under all conditions, even at extremely low TCMS concentrations (< 200μmolL^{-1}), the characteristic filament growth is observed. All coatings appear to consist of a dense base layer of short (few 100nm long) and fine (roughly 10-20nm in diameter) filaments. From this base layer, individual filaments protrude that are both thicker (40-60nm in diameter) and longer (several μm). At very low TCMS content, these filaments are more or less randomly distributed on the surface and often take on peculiar spiral forms. At higher TCMS concentration, the growth of the long filaments is no longer homogeneous. Conglomerates form on the base layer, which grow and build up with increasing TCMS content. This second layer appears to add a microtopography to the coating surface as becomes especially evident in the images of intermediate magnification. Ultimately the whole surface is again covered completely by a dense layer of these thicker filaments. At very high TCMS content, individual filaments of more than 10μm in length extend through this layer. All coatings are superhydrophobic, independent of TCMS content, with contact angles above 150° and sliding angles below 30°.

Figure 5.43 shows the contact and sliding angles of the individual coatings before and after annealing.

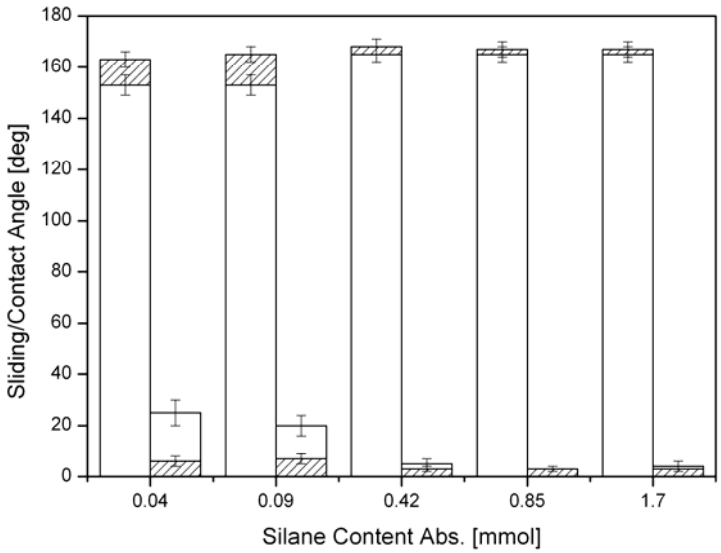

Figure 5.43. Contact and sliding angles of SNC coated at constant temperature, time and water content and at varying TCMS contents. White bars indicate values before, hatched bars values after annealing.

With increasing TCMS content, the coating properties improve in terms of superhydrophobicity. Also the beneficial effect that annealing has on the wetting properties diminishes for higher

TCMS content. The sliding angles on the substrates coated at high TCMS content are significantly better than the sliding angles typically obtained in the gas phase coating.

The optical properties of the coatings develop contrary to the wetting properties. As can be seen in Figure 5.44, the transmittance of SNC glass slides decrease with increasing TCMS concentration. Even the slides coated at very low TCMS concentration show a slight hazing. The generally low transmission in these coating could be due to a relatively high water content in the reaction mixture (5.5.2).

At very high TCMS content (>1mmol), the coatings removed from the reaction chamber and dried without rinsing with toluene and ethanol tended to show an increasing number of macroscopic, white, brittle residues distributed on the surface. Under SEM investigation these turned out to be large clusters of polymerized TMCS that nevertheless also showed a filament structure. These clusters could be partially removed from the surface by rinsing under a strong jet of water, by a strong nitrogen stream or by short (30s) ultrasonication of the substrates in an organic solvent.

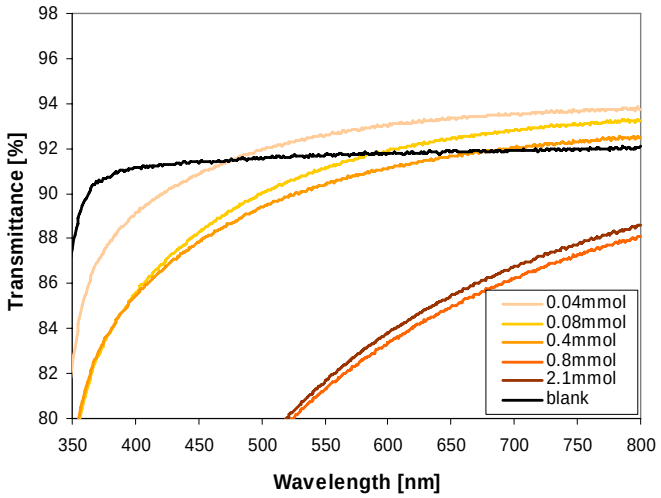

Figure 5.44. UV/Vis spectra of SNC glass slides coated at constant temperature, time and water content and at varying TCMS contents.

5.5.2 Water content

Coating was performed at 23°C with an absolute TCMS content of 0.21±0.03mmol at a coating time of 4 hours. The water content in the reaction chamber was adjusted to 28, 45, 60, 80 and 107ppm respectively which correspond to absolute water contents of 0.32, 0.51, 0.71, 0.95 and 1.25mmol. All but the first composition contain more than the stoichiometric amount of water needed for a full hydrolyzation and condensation of the silane precursors.

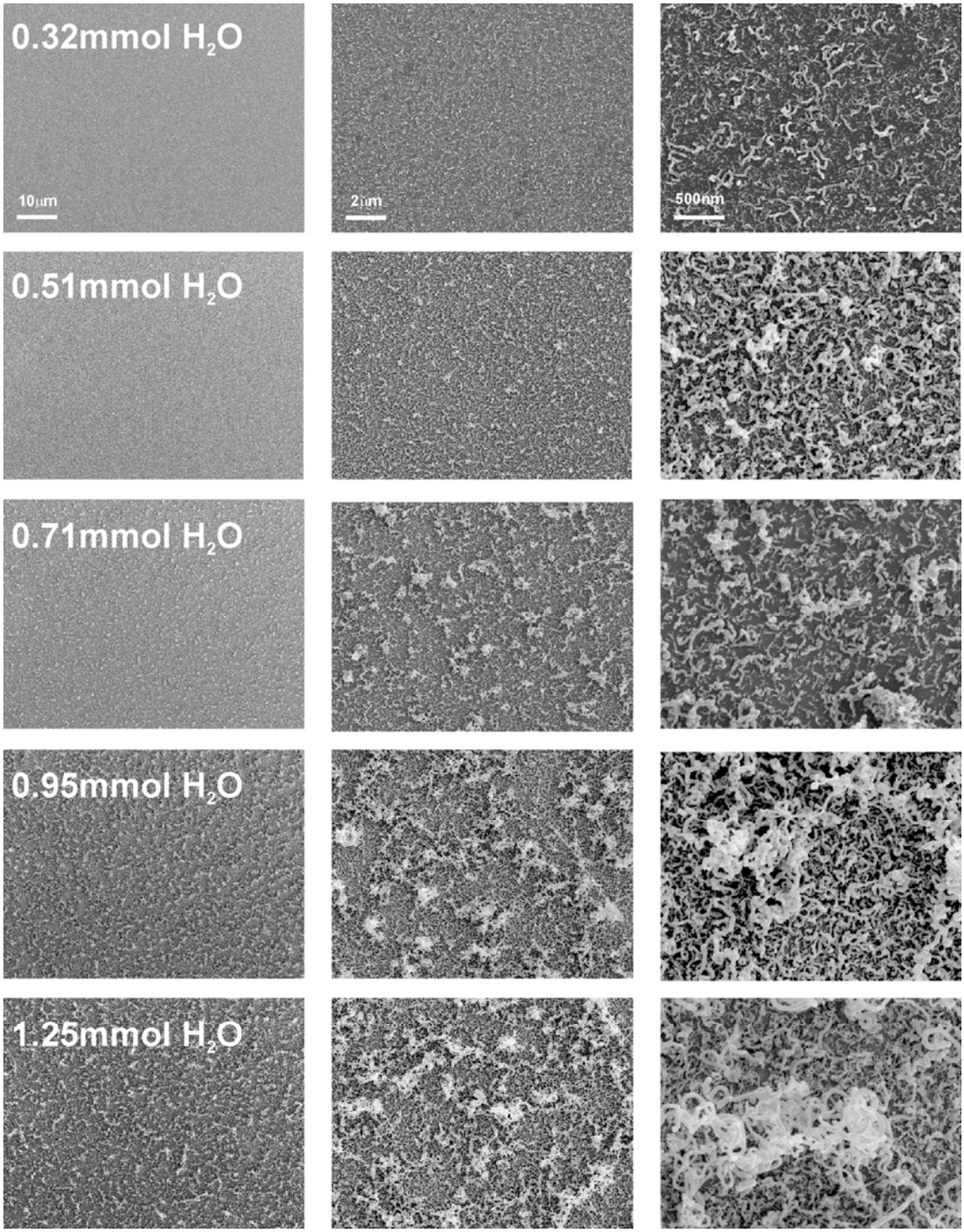

Figure 5.45 Electron microscopy images of glass slides coated at constant coating temperature, time and TCMS content and at varying water contents.

Figure 5.42 shows SEM images of the resulting coatings at three different magnifications. Although all systems contain enough water for a full hydrolyzation of the TCMS, the silicone nanofilament growth progresses with increasing water content. Again we observe a base layer of short and fine filaments from which thicker and longer filaments protrude. As before the thicker filaments appear as conglomerates randomly distributed on the surface.

The coating properties improve in terms of superhydrophobicity with increasing water content. Figure 5.46 shows the contact and sliding angles of the individual coatings before and after annealing.

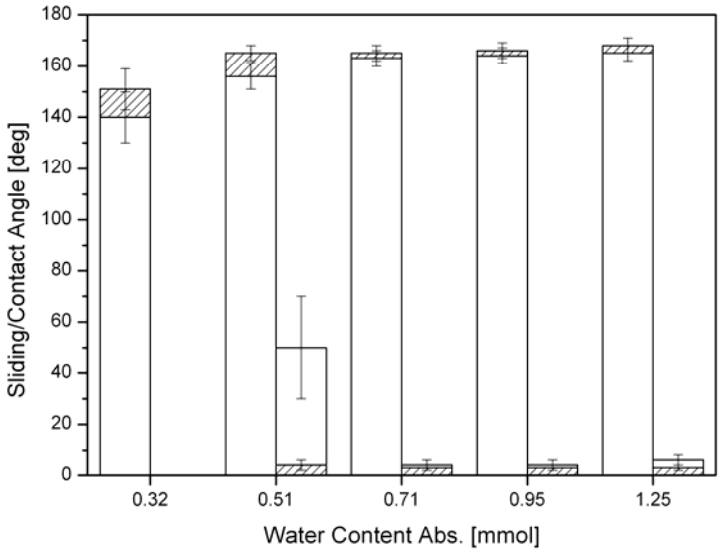

Figure 5.46. Contact and sliding angles of SNC coated at constant temperature, time and TCMS content and at varying water contents. White bars indicate values before, hatched bars values after annealing.

Even though the coating at 0.32mmol water content exhibits the typical nanostructure, it is not superhydrophobic in the sense that 10µl drops of water do not roll off the surface even though the contact angle is in the range 150° after annealing,. At higher water content the coating becomes superhydrophobic with contact angles well above 150°, even before annealing, and sliding angles below 60° before and well below 10° after annealing. At high water contents the wetting properties are not significantly improved by annealing.

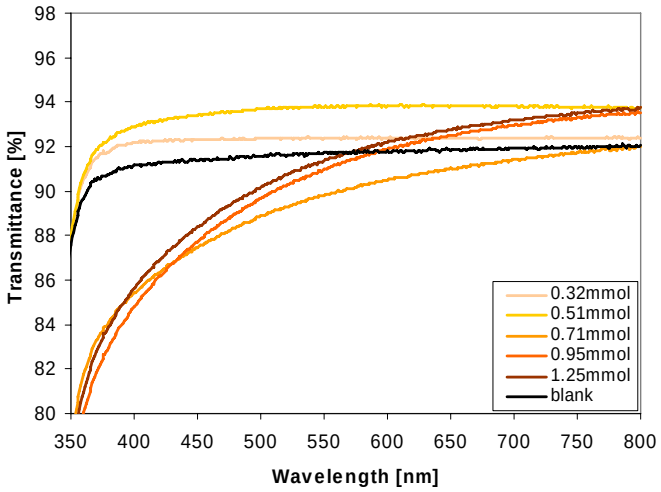

Figure 5.47. UV/Vis spectra of SNC glass slides coated at constant temperature, time and TCMS content and at varying water contents.

The UV/Vis spectra of the coatings are illustrated in Figure 5.47. At 0.32 and 0.51mmol water content the coating is not hazed and the transmittance is above that of an uncoated glass slide. The transmittance is even improved by more than 1%abs. over almost the whole visible range for the slightly higher water content. At 0.72mmol and above the coated slides show hazing and their optical transmittance is reduced, especially towards shorter wavelengths.

5.5.3 Coating time

Coating was performed at 20°C with an absolute water content of 1.40±0.06mmol and an absolute TCMS content of 0.21±0.03mmol. Coating was performed for 1, 2, 3, 4 and 14 hours of coating time. Figure 5.48 shows SEM images of the resulting coatings at three different magnifications. The characteristic coating formation is also observed in the time dependent coating experiments. Generally the coatings obtained under these coating conditions appear to be denser than those in the previous experiments.

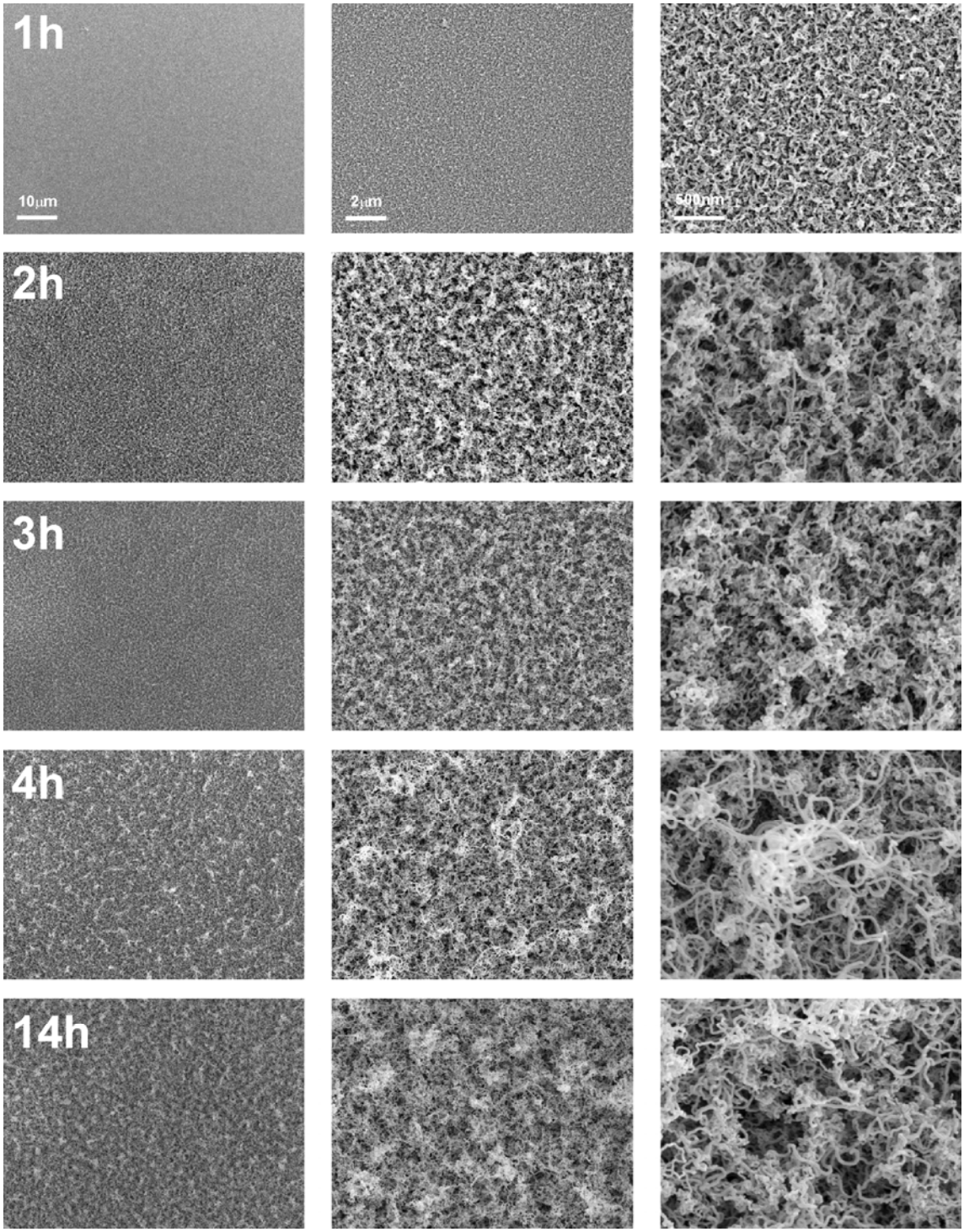

Figure 5.48. Electron microscopy images of glass slides coated at constant coating temperature, TCMS and water content and at varying coating times.

The wettability data is shown in Figure 5.49.

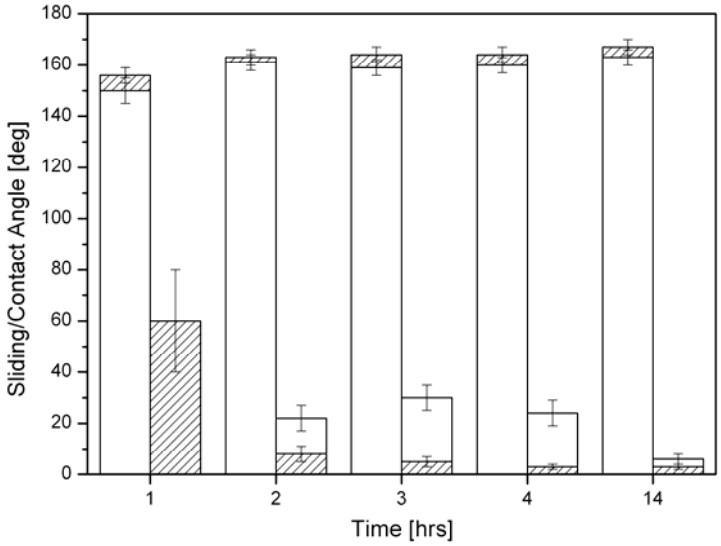

Figure 5.49. Contact and sliding angles of SNC coated at constant temperature, water and TCMS content at varying coating times. White bars indicate values before, hatched bars values after annealing.

After 1 hour the coating is not superhydrophobic in the sense that drops of water stick to the surface and do not roll off. Annealing however results in measurable sliding angles even on this coating. The coating improves with coating time, but the difference in terms of wettability is not significant between 2 and 4 hours coating time. All coatings up to 4 hours coating time are noticeably improved by annealing, especially in terms of sliding angle values. After 14 hours coating time the coating is only slightly improved by annealing.

Again the optical properties of the coating decrease with increasing coating thickness. The thin, dense and very homogeneous PMSQ filament layer that has formed after one hour coating time exhibits the best optical properties of all coatings so far. The transmittance of this coating is 4-7% higher than that of an uncoated glass slide. After three hours the coatings begin to show slight hazing and the optical properties deteriorate as can be seen in the UV/Vis spectra shown in Figure 5.50.

The last experiments clearly indicate that the formation of a first, dense layer of silicone nanofilaments is relatively fast. One hour coating time is sufficient to produce a coating that is superhydrophobic after annealing. Single experiments performed at very high TCMS and water contents even suggest that even less time is required to produce a superhydrophobic SNC in the solvent phase setup (5.5.4).

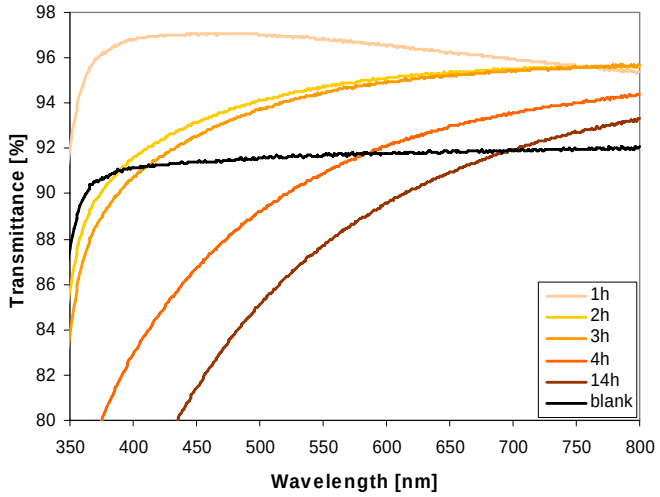

Figure 5.50. UV/Vis spectra of SNC glass slides coated at constant temperature, water and TCMS content and at varying coating times.

5.5.4 Temperature

Although the coating setup allows for a control of the coating temperature, it needs to be further improved to be able to evaluate the influence of temperature on the coating results. The current reaction chamber has a volume of 700ml but only 250ml solvent (enough to cover the substrates) was used in the coating process. To adjust the water content of the solvent, the remaining free volume was flushed with nitrogen (see 4.2.2). Because of their vapor pressures, a fraction of the reactants (water and TCMS) will migrate into the gas phase. In the current coating procedure the water content of the solvent is controlled (though coulometric titration 4.2.2) and the total amount of TCMS introduced into the reaction chamber. The distribution of reactants between the gas and solvent phase cannot be analyzed. Depending on the temperature inside the reaction chamber however, the equilibrium concentrations of water and TCMS in the liquid and gas phase will vary. The temperature variable can therefore not be isolated from the TCMS and water content with the current coating setup and procedure. To improve the setup towards evaluating the influence of coating temperature on the coating results the perturbing gas layer could be removed either by decreasing the size of the coating chamber or by filling the whole chamber with solvent. This would either limit the size of the substrates or require the use of large quantities of solvents. Additionally new strategies to adjust the water content of the solvent would need to be devised as the gas layer is required to flush the chamber with nitrogen.

Despite these problems, a few preliminary experiments were performed at varying temperatures between 10 and 50°C. For all temperatures tested in this range conditions could be

found that resulted in a superhydrophobic coating. The preferential condensation of TCMS into filament like nanostructures was observed in all cases. Two examples are illustrated in Figure 5.51.

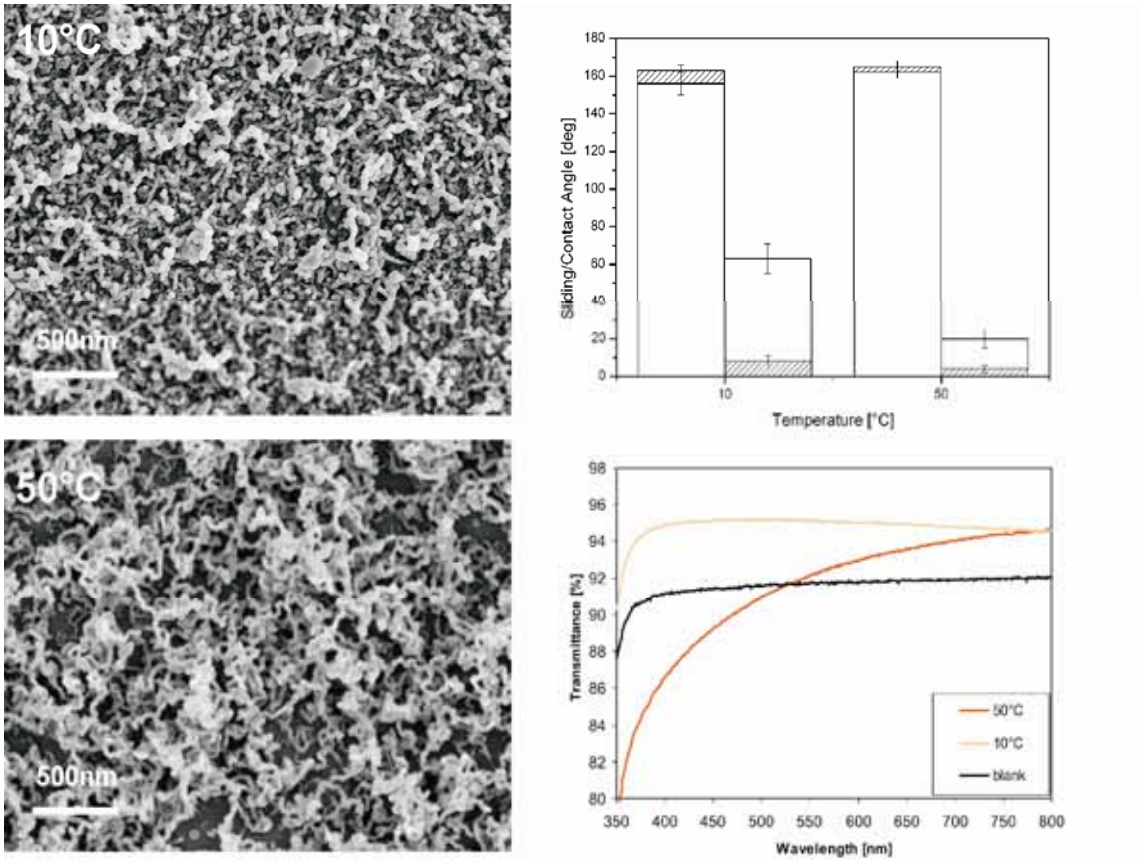

Figure 5.51. Electron microscopy images, wettability data and UV/vis spectra of two coatings prepared under a water content of 1.5mmol and a TCMS content of 1.3mmol at 10°C and 50°C. Coating time was 30min in both cases.

Although the nominal amounts of water and TCMS in the system were the same in both examples, we can assume that the actual concentration of TCMS in the solvent phase is higher at 10°C than at 50°C due to the difference in vapor pressure. The coating at 10°C is fully transparent, the coating at 50°C noticeably hazed. Both coatings are superhydrophobic with almost identical wetting properties after annealing. Before annealing the coating at 50°C is superior to that produced at 10°C.

5.5.5 Summary

Under all coating conditions applied in the solvent phase coating experiments, a filament type growth was observed. With increasing reactant concentration, layer thickness/filament density of filaments increases. Together with the observation that a stirring of the coating solution significantly shortens the coating time, this indicates that the filament growth is diffusion limited. Accordingly, a further increase in reactant concentration and reaction temperature should further reduce the coating time.

A second general observation is that with increasing reactant concentration and increasing coating time the effect a subsequent annealing has on the wetting properties of the coating diminishes. Even in case of the highly sensitive sliding angle. This indicates that under these conditions the condensation reaction is more complete or that the surface chemistry of the individual filament surfaces is more uniform. A high initial water content facilitates the hydrolysis of silane precursors and increases the rate of surface condensation. A high initial silane content has the same effect, the number of silane molecules available for surface condensation is increased. Thereby hydrophilic groups that remain on the surface of the individual filaments are more thoroughly reacted and "quenched" by the available silane moieties. A long coating time essentially has the same effect as reactive moieties are given the time to diffuse to the surface and react with the remaining hydrophilic defects.

Overall the performed coating experiments indicate, that slight adjustments of coating parameters allow a tuning of the SNC in terms of size, shape, density of filaments, wetting and optical properties. A dense layer of short, thin filaments is beneficial towards optical transmittance, whereas a thicker layer benefits the wetting properties. Once a certain layer structure is reached however, the wetting properties become independent of layer thickness. How the layer thickness and filament density influences the mechanical, chemical and environmental stability of the SNC remains to be evaluated, but the preliminary experiments indicate that the chemical stability of the superhydrophobic effect increases with increasing layer thickness.

Toluene was the solvent of choice for all solvent phase coating experiments, primarily due to the fact that the coating reaction was initially successful in this solvent. Although it has been shown on the formation of OTS monolayers on glass that toluene is best suited for a controlled hydrolyzation and polymerization of chlorosilane precursors on siliceous substrates, silanization of surfaces has also been successfully performed in other solvents such as benzene, hexadecane or carbon tetrachloride [158]. For environmental and processing considerations however it would be beneficial if the coating could be transferred to a less problematic solvent. Considering that

many commercial silanes are applied from ethanol solution (for instance in silane coupling agent chemistry) it would be interesting to see if conditions can be found that allow for the formation of silicone nanofilaments from ethanol solution.

6 Summary and Outlook

Surfaces with extreme wetting properties are currently receiving considerable attention in regards to their potential for application. Superhydrophobic surfaces show potential as non wetting, antifouling and self cleaning coatings or for applications where low friction flows are desired. Superhydrophilic surfaces are equally interesting for self cleaning or anti fogging applications. In contrast, superoleophobic surfaces could find application as antisoiling and stain resistant coatings. Patterned surfaces with areas of contrasting wetting properties show potential in microfluidic or biosensor applications. In view of this diverse field of potential uses, various strategies have been developed to create surfaces with either of the above properties. However, usefulness of the individual coating strategies seldom exceed a single type of application and often involve experimentally and commercially challenging procedures.

In the course of this work, a novel type of surface coating has been explored, that is not only remarkably simple and inexpensive in its fabrication but can be easily modified to express any of the above mentioned functionalities. Besides developing and characterizing the fabrication process, the initially superhydrophobic coating was evaluated in terms of wetting and optical properties, surface structure and chemical as well as environmental stability. Additionally, a first evaluation for a commercially relevant application, as a waterproofing coating for textiles, was performed. In a series of subsequent proof of principle experiments the initial coating was chemically functionalized to yield coatings with arbitrary (super)wetting properties as well as coatings that exhibited specific biochemical properties. Equally it could be shown that a patterning of the surface with contrasting physicochemical properties down to the sub millimetre range can be realized by simple techniques.

With the initial coating procedure, dense layers of one dimensional, filament like nanostructures of polymethylsilsesquioxane can be grown on a substrate either in a gas or solvent phase reaction. The unique surface structure and chemical nature of the coating result in exceptional superhydrophobic properties with contact angles in excess of 160° and sliding angles below 10°. In the course of this work, the initial gas phase coating procedure has been improved in terms of pre processing, reproducibility of coating results and post processing. Furthermore, a completely new procedure was developed that allows for the reproducible coating of substrates under controlled reaction conditions in solvent phase. The cleaning and activation procedure for the standard substrate glass was reduced to a single, combined cleaning and activation step in a

commercial detergent solution forgoing the need of organic solvents or harsh chemicals. Both coating setups now allow a precise control of reaction conditions. An optional post processing step, annealing at elevated temperatures, was introduced in order to further increase the hydrophobicity of the coating and significantly improve its chemical and environmental stability. Both setups enabled the fabrication of a large number of standard samples towards a meaningful evaluation of coating properties.

These studies revealed that the SNC offers many of the benefits looked for in a superhydrophobic coating. In contrast to most other contemporary coating strategies, both the high surface roughness and low surface energy required for the superhydrophobic effect are intrinsic properties of the coating. No pre or post processing like etching or chemical passivation is necessary. Furthermore, the coating can be applied in a gas or solvent phase process which allows for a coating of arbitrary surface geometries. It can be readily prepared under ambient conditions without the need of expensive equipment, chemicals or even clean room facilities. It can be fabricated to be transparent or even anti reflective and supports a stable plastron layer upon immersion in water. Finally, a variety of substrates materials such as glass, silicon, aluminium, PDMS and other natural and artificial polymeric materials were successfully coated with minimal requirements towards a pre treatment of the substrates. Future work should include a comprehensive evaluation of the individual coating parameters for both the gas and solvent phase setup. Understanding their influence on the microscopic appearance and the coating properties will enable a tailoring of coating towards specific applications.

Extensive long term durability tests, performed on standardized coatings on glass, revealed that the coating is superior to other superhydrophobic coatings on which similar studies have been performed and published, both in terms of chemical and environmental durability. The annealed coating proved to be inert towards the organic solvents toluene, acetone and chloroform. Under aqueous pH conditions, the annealed coating maintained its superhydrophobic properties (CA ~ 150°, SA < 90°) for at least 6 months at pH 3 and 7, at least 10 days at pH 0 and more than 3 days at pH 11. In strong hydrolytic media such as 2M NaOH (pH 13), the coating degraded within a few minutes. The non annealed samples were significantly less stable in all media, however at neutral pH the coating was still superhydrophobic after 6 months of immersion and only slight changes in the SA were observed upon immersion in organic solvents. Long term outdoor weathering experiments showed that the coating retained its superhydrophobic properties for more than a year and the gain in optical transmittance in respect to an uncoated glass slide increased from roughly 2 to 5%abs. Under accelerated ageing in a laboratory environment, the coating proved to be inert towards global UV

irradiation according to ISO 9022-9:2000-09 and remained superhydrophobic during artificial weathering according to VDI 3958 Part 12 (Acid Dew and Fog Test) for three of four weeks. Collectively, the performed experiments have set a benchmark towards a future improvement of the coating in terms of chemical and environmental durability. The dip tests have shown that long term immersion and a monitoring of both the static and dynamic wetting properties is necessary to assess the chemical stability of a superhydrophobic coating. Short term immersion or the simple determination of the contact angle a hydrolytic liquid forms on a superhydrophobic surface, as it is employed in many contemporary publications, is not sufficient to assess a coatings potential for long term application. The accelerated ageing experiments have proven to be a useful tool towards determining the SNC's potential for outdoor applications. In this sense, future work on improving the durability of the coating could facilitate a combination of dip tests in strong hydrolytic media and ADF test for a rapid evaluation of the coatings chemical and environmental durability. A maximization of the coating thickness (in consideration of the desired optical properties) combined with annealing at higher temperatures under inert atmosphere should produce coatings with superior properties.

At this time, application of the coating is limited to a mechanically non abrasive environment when applied to planar substrates, a general problem facing most nanostructured surfaces. On micro or macroscopically rough substrates like textiles however, the superhydrophobic effect was shown to be stabilized towards abrasion, as the nanofilament layer is sheltered in the grooves of the surface structure. The evaluation of coated PET textile samples has shown that the SNC can be utilized to produce highly water repellent, long term stable and abrasion resistant fabrics without compromising the fabric strength. Although washing of the coated fabrics in a washing machine requires a higher chemical and mechanical stability, the as prepared coating already shows potential for textile applications which require no washing, like umbrellas, parasols or other outdoor textile applications.

In terms of adapting the SNC for applications besides superhydrophobicity it was shown that its surface chemistry can be readily modified by simple silane chemistry without changing its surface structure. By plasma activation and subsequent coating with a fluorosilane, the wetting properties of the coating were selectively tuned to yield superhydrophobic, superhydrophilic, superoleophobic or superoleophilic coatings. Further chemical functionalities like amino and carboxyl groups were introduced onto the surface to yield coatings with highly specific protein retention characteristics. Proof of principle experiments showed that the surface functionalization can be selectively performed with sub millimeter accuracy which should enable the creation of 2-D surface patterns with defined wettability and (bio-)chemical functionality towards biosensor,

bioassay or open channel microfluidics devices. There are no apparent constrains that hinder the immobilization of other functional groups or active molecules on the surface which opens the opportunity to create enzyme or receptor based biosensors. Finally the chemical properties of the silicone nanofilaments can be utilized to create full wetting gradients from almost zero degrees of contact angle to above 160° which could for instance be utilized to study wettability and surface structure dependant phenomena like crystallization, protein adsorption or droplet motion. In this respect the SNC has proven to be a versatile template material to readily fabricate a number of interfaces with very unique physico-chemical properties whose full potential is yet to be explored.

Finally, as the scope of this thesis focuses mainly on the fabrication and properties of the SNC, the mechanism of filament formation, that appears to be a fundamental aspect of the condensation reaction of short chain trifunctional silane precursors under the studied conditions, remains to be explored. Understanding this mechanism may reveal new possibilities to selectively alter the shape, size and distribution of filaments and increase the control of coating morphology or even allow a generation of specific filament types for nanoengineering purposes.

In conclusion, the silicone nanofilament coating in its current form already proves to be a useful addition to the toolbox of surface scientists and chemical engineers. The ease of fabrication, the optical transparency and the exceptional long term stability of coating set it apart from contemporary superhydrophobic coating solutions and make it an interesting candidate for numerous applications for which superhydrophobicity is ascribed potential; from low friction flows in microfluidics to self cleaning and antireflective panels for solar cell applications. With the vast amount of knowledge on the chemical modification of planar siliceous surfaces available today, numerous options to alter the high surface area SNC expand the potential uses of the coating and provide an interesting field for future research.

References

[1] Wenzel, R. N. *Ind. Eng. Chem.* 28, 988 (1936).
[2] Cassie, A. B. D.; Baxter, S. *Trans. Faraday Soc.* 40, 546 (1944).
[3] Johnson, R. E.; Dettre, R. H. *Adv. Chem. Ser.* 43, 112 (1964).
[4] Barthlott, W.; Neinhuis, C. *Planta* 202, 1 (1997).
[5] He, B.; Patankar, N. A.; Lee, J. *Langmuir* 19, 4999 (2003).
[6] Patankar, N. A. *Langmuir* 19, 1249 (2003).
[7] Patankar, N. A. *Langmuir* 20, 8209 (2004).
[8] Öner, D.; McCarthy, T. J. *Langmuir* 16, 7777 (2000).
[9] Yoshimitsu, Z.; Nakajima, A.; Watanabe, T.; Hashimoto, K. *Langmuir* 18, 5818 (2002).
[10] Marmur, A. *Langmuir* 20, 3517 (2004).
[11] Blossey, R. *Nat. Mater.* 2, 301 (2003).
[12] Callies, M.; Quéré, D. *Soft Matter* 1, 55 (2005).
[13] Feng, L.; Li, S. H.; Li, Y. S.; Li, H. J.; Zhang, L. J.; Zhai, J.; Song, Y. L.; Liu, B. Q.; Jiang, L.; Zhu, D. B. *Adv. Mater.* 14, 1857 (2002).
[14] Nakajima, A.; Hashimoto, K.; Watanabe, T. *Monatsh. Chem.* 132, 31 (2001).
[15] Sun, T. L.; Feng, L.; Gao, X. F.; Jiang, L. *Acc. Chem. Res.* 38, 644 (2005).
[16] Shirtcliffe, N. J.; McHale, G.; Newton, M. I.; Perry, C. C.; Pyatt, F. B. *Appl. Phys. Lett.* 89, 104106 (2006).
[17] Feng, X. J.; Jiang, L. *Adv. Mater.* 18, 3063 (2006).
[18] Lee, D.; Rubner, M. F.; Cohen, R. E. *Nano Lett.* 6, 2305 (2006).
[19] Parkin, I. P.; Palgrave, R. G. *J. Mater. Chem.* 15, 1689 (2005).
[20] Cebeci, F. C.; Wu, Z.; Zhai, L.; Cohen, R. E.; Rubner, M. F. *Langmuir* 22, 2856 (2006).
[21] Tsujii, K.; Yamamoto, T.; Onda, T.; Shibuichi, S. *Angew. Chem. Int. Edit.* 36, 1011 (1997).
[22] Shibuichi, S.; Yamamoto, T.; Onda, T.; Tsujii, K. *J. Colloid Interface Sci.* 208, 287 (1998).
[23] Feng, L.; Zhang, Z. Y.; Mai, Z. H.; Ma, Y. M.; Liu, B. Q.; Jiang, L.; Zhu, D. B. *Angew. Chem. Int. Edit.* 43, 2012 (2004).
[24] Zhai, L.; Berg, M. C.; Cebeci, F. C.; Kim, Y.; Milwid, J. M.; Rubner, M. F.; Cohen, R. E. *Nano Lett.* 6, 1213 (2006).
[25] Gau, H.; Herminghaus, S.; Lenz, P.; Lipowsky, R. *Science* 283, 46 (1999).
[26] Lion, N.; Rohner, T. C.; Dayon, L.; Arnaud, I. L.; Damoc, E.; Youhnovski, N.; Wu, Z. Y.; Roussel, C.; Josserand, J.; Jensen, H.; Rossier, J. S.; Przybylski, M.; Girault, H. H. *Electrophoresis* 24, 3533 (2003).
[27] Sotiropoulou, S.; Chaniotakis, N. A. *Anal. Bioanal. Chem.* 375, 103 (2003).
[28] Vamvakaki, V.; Tsagaraki, K.; Chaniotakis, N. *Anal. Chem.* 78, 5538 (2006).
[29] Kim, P.; Kim, D. H.; Kim, B.; Choi, S. K.; Lee, S. H.; Khademhosseini, A.; Langer, R.; Suh, K. Y. *Nanotechnology* 16, 2420 (2005).
[30] Rechendorff, K.; Hovgaard, M. B.; Foss, M.; Zhdanov, V. P.; Besenbacher, F. *Langmuir* 22, 10885 (2006).

[31] Tserepi, A. D.; Vlachopoulou, M. E.; Gogolides, E. *Nanotechnology* 17, 3977 (2006).
[32] Galli, C.; Collaud Coen, M.; Hauert, R.; Katanaev, V. L.; Gröning, P.; Schlapbach, L. *Colloids Surf. B* 26, 255 (2002).
[33] Jung, S. *Silanbeschichtung zur DNA-Fragmentlängenbeschichtung und zur Herstellung superhydrophober Schichten aus neuartigen Nanofilamenten*. Dissertation, Universität Zürich, Zürich (2003).
[34] Rochow, E. G. *Silicon and Silicones*. Springer: Berlin (1987).
[35] Arkles, B. *Chemtech* 13, 542 (1983).
[36] Baney, R. H.; Itoh, M.; Sakakibara, A.; Suzuki, T. *Chem. Rev.* 95, 1409 (1995).
[37] Rao, A. V.; Kulkarni, M. M.; Amalnerkar, D. P.; Seth, T. *J. Non-Cryst. Solids* 330, 187 (2003).
[38] Shirtcliffe, N. J.; McHale, G.; Newton, M. I.; Perry, C. C. *Langmuir* 19, 5626 (2003).
[39] Oh, W.; Shin, T. J.; Ree, M.; Jin, M. Y.; Char, K. *Macromol. Chem. Physic.* 203, 801 (2002).
[40] Oh, W.; Ree, M. *Langmuir* 20, 6932 (2004).
[41] Dong, H. J.; Brook, M. A.; Brennan, J. D. *Chem. Mater.* 17, 2807 (2005).
[42] Maciel, G. E.; Sullivan, M. J.; Sindorf, D. W. *Macromolecules* 14, 1607 (1981).
[43] Netzer, L.; Sagiv, J. *J. Am. Chem. Soc.* 105, 674 (1983).
[44] Sagiv, J. *J. Am. Chem. Soc.* 102, 92 (1980).
[45] Wasserman, S. R.; Whitesides, G. M.; Tidswell, I. M.; Ocko, B. M.; Pershan, P. S.; Axe, J. D. *J. Am. Chem. Soc.* 111, 5852 (1989).
[46] Tripp, C. P.; Hair, M. L. *Langmuir* 11, 149 (1995).
[47] Fadeev, A. Y.; McCarthy, T. J. *Langmuir* 16, 7268 (2000).
[48] Fadeev, A. Y.; McCarthy, T. J. *Langmuir* 15, 3759 (1999).
[49] Arkles, B. *Chemtech* 7, 766 (1977).
[50] Maoz, R.; Sagiv, J. *J. Colloid Interface Sci.* 100, 465 (1984).
[51] Waddell, T. G.; Leyden, D. E.; Debello, M. T. *J. Am. Chem. Soc.* 103, 5303 (1981).
[52] Onclin, S.; Ravoo, B. J.; Reinhoudt, D. N. *Angew. Chem. Int. Edit.* 44, 6282 (2005).
[53] Chaudhury, M. K. *Biosens. Bioelectron.* 10, 785 (1995).
[54] Young, T. *Phil. Trans. Roy. Soc. London* 95, 65 (1805).
[55] Quéré, D. *Physica A* 313, 32 (2002).
[56] Butt, H.-J.; Graf, K.; Kappl, M. *Physics and Chemistry of Interfaces*. Wiley-VCH: Weinheim (2003).
[57] Owens, D. K.; Wendt, R. C. *J. Appl. Polym. Sci.* 13, 1741 (1969).
[58] Good, R. J.; Girifalco, L. A. *J. Phys. Chem.* 64, 561 (1960).
[59] Fowkes, F. M. *Ind. Eng. Chem.* 56, 40 (1964).
[60] van Oss, C. J.; Good, R. J.; Chaudhury, M. K. *J. Colloid Interface Sci.* 376, 111 (1986).
[61] McHale, G. *Langmuir* 23, 8200 (2007).
[62] Lafuma, A.; Quéré, D. *Nat. Mater.* 2, 457 (2003).
[63] Chen, W.; Fadeev, A. Y.; Hsieh, M. C.; Öner, D.; Youngblood, J.; McCarthy, T. J. *Langmuir* 15, 3395 (1999).
[64] Furmidge, C. G. *J. Colloid Sci.* 17, 309 (1962).
[65] Wolfram, E.; Faust, R. *Wetting, Spreading, and Adhesion*, p. 213. Academic Press: London (1978).
[66] Neinhuis, C.; Barthlott, W. *Ann. Bot.-London* 79, 667 (1997).
[67] Lam, A. N. C.; Lu, J. J.; Neumann, A. W. Measuring Contact Angle. In *Applied Surface and Colloid Chemistry,* Vol. 2, pp 251, Holmberg, K., Ed. John Wiley & Sons Ltd: Chichester, (2002).
[68] Singh, S.; Houston, J.; van Swol, F.; Brinker, C. J. *Nature* 442, 526 (2006).
[69] Dorrer, C.; Rühe, J. *Langmuir* 22, 7652 (2006).

[70] Artus, G. R. J.; Jung, S.; Zimmermann, J.; Gautschi, H.-P.; Marquardt, K.; Seeger, S. *Adv. Mater.* 18, 2758 (2006).
[71] Birch, W. R. *Coatings: An introduction to the cleaning procedures*, http://www.solgel.com/articles/June00/Birch/cleaning.htm (2000).
[72] ISO 9022-9:1994-07-15: *Optics and optical instruments - Environmental test methods - Part 9: Solar radiation*. International Organization for Standardization: Geneva (1994).
[73] VDI 3858 Part 12: *Environmental simulation - Effects of acidic precipitation on polymers - Test methods*. VDI Verein Deutscher Ingenieure: Düsseldorf (2004).
[74] ISO 13934-1:1999: *Textiles -- Tensile properties of fabrics -- Part 1: Determination of maximum force and elongation at maximum force using the strip method*. ISO International Organization for Standardization: Geneva (1999).
[75] Gerhardt, L.-C.; Mattle, N.; Schrade, G. U.; Spencer, N. D.; Derler, S. *Skin Re. Tech.* 14, 77 (2008).
[76] ISO 6330:2000: *Textiles -- Domestic washing and drying procedures for textile testing*. ISO International Organization for Standardization: Geneva (2000).
[77] ISO 14419:1998: *Textiles - Oil repellency - Hydrocarbon resistance test*. ISO International Organization for Standardization: Geneva (1998).
[78] Flink, S.; Veggel, F. C. J. M. v.; Reinhoudt, D. N. *J. Phys. Org. Chem.* 14, 407 (2001).
[79] Ruckstuhl, T.; Enderlein, J.; Jung, S.; Seeger, S. *Anal. Chem.* 72, 2117 (2000).
[80] Ruckstuhl, T.; Rankl, M.; Seeger, S. *Biosens. Bioelectron.* 18, 1193 (2003).
[81] Rabe, M.; Verdes, D.; Rankl, M.; Artus, G. R. J.; Seeger, S. *ChemPhysChem* 8, 862 (2007).
[82] Enderlein, J.; Ruckstuhl, T.; Seeger, S. *Appl. Opt.* 38, 724 (1999).
[83] Kennan, J. J.; Peters, Y. A.; Swarthout, D. E.; Owen, M. J.; Namkanisorn, A.; Chaudhury, M. K. *J. Biomed. Mater. Res.* 36, 487 (1997).
[84] Holmberg, K. *Applied Surface and Colloid Chemistry*, Vol. 2. John Wiley & Sons Ltd: Chichester (2002).
[85] Ramos, S. M. M.; Charlaix, E.; Benyagoub, A. *Surf. Sci.* 540, 355 (2003).
[86] Ramos, S. M. M.; Charlaix, E.; Benyagoub, A.; Toulemonde, M. *Phys. Rev. E* 67, (2003).
[87] Song, X. Y.; Zhai, J.; Wang, Y. L.; Jiang, L. *J. Phys. Chem. B* 109, 4048 (2005).
[88] Gao, L.; McCarthy, T. J. *J. Am. Chem. Soc.* 128, 9052 (2006).
[89] Jones, R. G.; Ando, W.; Chojnowski, J. *Silicone-Containing Polymers*. Kluwer Academic Publishers: Dordrecht (2000).
[90] Rollings, D.-A. E.; Tsoi, S.; Sit, J. C.; Veinot, J. G. C. *Langmuir* 23, 5275 (2007).
[91] Erbil, H. Y.; Demirel, A. L.; Avci, Y.; Mert, O. *Science* 299, 1377 (2003).
[92] Feng, L.; Yang, Z. L.; Zhai, J.; Song, Y. L.; Lin, B. Q.; Ma, Y. M.; Yang, Z. Z.; Jiang, L.; Zhu, D. B. *Angew. Chem. Int. Edit.* 42, 4217 (2003).
[93] Han, J. T.; Zheng, Y.; Cho, J. H.; Xu, X.; Cho, K. *J. Phys. Chem. B* 109, 20773 (2005).
[94] Ming, W.; Wu, D.; van Benthem, R.; de With, G. *Nano Lett.* 5, 2298 (2005).
[95] Zhai, L.; Cebeci, F. C.; Cohen, R. E.; Rubner, M. F. *Nano Lett.* 4, 1349 (2004).
[96] Guo, Z. G.; Zhou, F.; Hao, J. C.; Liu, W. M. *J. Am. Chem. Soc.* 127, 15670 (2005).
[97] Yan, H.; Kurogi, K.; Mayama, H.; Tsujii, K. *Angew. Chem. Int. Edit.* 44, 3453 (2005).
[98] Wang, S.; Feng, L.; Jiang, L. *Adv. Mater.* 18, 767 (2006).
[99] Nicolas, M.; Guittard, F.; Géribaldi, S. *Angew. Chem. Int. Edit.* 45, 2251 (2006).
[100] Nakajima, A.; Hashimoto, K.; Watanabe, T.; Takai, K.; Yamauchi, G.; Fujishima, A. *Langmuir* 16, 7044 (2000).
[101] Sasaki, M.; Kieda, N.; Katayama, K.; Takeda, K.; Nakajima, A. *J. Mater. Sci.* 39, 3717 (2004).
[102] Thieme, M.; Frenzel, R.; Hein, V.; Worch, H. *Journal of Corrosion Science and Engineering* 6, C113 (2003).

[103] Voronkov, M. G.; Mileshkevich, V. P.; Yuzheleskii, Y. A. *The Siloxane Bond*. Consultants Bureau: New York (1978).
[104] Nevell, T. G.; Edwards, D. P.; Davis, A. J.; Pullin, R. A. *Biofouling* 10, 199 (1996).
[105] Batich, C.; DePalma, D.; Marotta, J.; Latorre, G.; Hardt, N. S. *Curr. Top. Microbiol. Immunol.* 210, 13 (1996).
[106] West, J. K. *J. Biomed. Mater. Res.* 35, 505 (1997).
[107] Bausch, G. G.; Stasser, J. L.; Tonge, J. S.; Owne, M. J. *Plasmas and Polymers* 3, 23 (1998).
[108] Christopher Batich, D. D. *J. Long. Term Eff. Med. Implants* 1, 255 (1992).
[109] Holmberg, K. *Applied Surface and Colloid Chemistry*, Vol. 1. John Wiley & Sons Ltd: Chichester (2002).
[110] Ferrari, M.; Ravera, F.; Rao, S.; Liggieri, L. *Appl. Phys. Lett.* 89, (2006).
[111] Zhao, T.; Mu, G. *Corros. Sci.* 41, 1937 (1999).
[112] Qu, M.; Zhang, B.; Song, S.; Chen, L.; Zhang, J.; Cao, X. *Adv. Funct. Mat.* 17, 593 (2007).
[113] Guo, Z.-G.; Fang, J.; Hao, J.-c.; Liang, Y.-m.; Liu, W.-m. *ChemPhysChem* 7, 1674 (2006).
[114] Fürstner, R.; Barthlott, W.; Neinhuis, C.; Walzel, P. *Langmuir* 21, 956 (2005).
[115] *Data supplied by MeteoSchweiz*.
[116] Zimmermann, J.; Artus, G. R. J.; Seeger, S. *Appl. Surf. Sci.* 253, 5972 (2007).
[117] Schulz, U. *Gefahrstoffe- Reinhaltung der Luft* 1, 61 (2004).
[118] ISO 11341:2004: *Paints and varnishes- Artificial weathering and exposure to artificial radiation - Exposure to filtered xenon-arc radiation*. International Organization for Standardization: Geneva (2004).
[119] Zhang, J.; France, P.; Radomyselskiy, A.; Datta, S.; Zhao, J.; van Ooij, W. *J. Appl. Polym. Sci.* 88, 1473 (2003).
[120] Daoud, W. A.; Xin, J. H.; Tao, X. M. *J. Am. Ceram. Soc.* 87, 1782 (2004).
[121] Yu, M.; Gu, G. T.; Meng, W. D.; Qing, F. L. *Appl. Surf. Sci.* 253, 3669 (2007).
[122] Michielsen, S.; Lee, H. J. *Langmuir* 23, 6004 (2007).
[123] Wang, T.; Hu, X. G.; Dong, S. J. *Chem Commun* 1849 (2007).
[124] Zimmermann, J.; Seeger, S.; Artus, G. R. J.; Jung, S. *Superhydrophobic Coating*. WO2004113456, (2004).
[125] Wagner, P.; Fürstner, R.; Barthlott, W.; Neinhuis, C. *J. Exp. Bot.* 54, 1295 (2003).
[126] Larmour, I. A.; Bell, S. E. J.; Saunders, G. C. *Angew. Chem. Int. Edit.* 46, 1710 (2007).
[127] Shirtcliffe, N. J.; Pyatt, F. B.; Newton, M. I.; McHale, G. *J. Plant Physiol.* 163, 1193 (2006).
[128] Lau, K. K. S.; Bico, J.; Teo, K. B. K.; Chhowalla, M.; Amaratunga, G. A. J.; Milne, W. I.; McKinley, G. H.; Gleason, K. K. *Nano Lett.* 3, 1701 (2003).
[129] X. J. Feng, L. J. *Advanced Materials* 18, 3063 (2006).
[130] Vansant, E. F.; Voort, P. V. D.; Vrancken, K. C. *Characterization and chemical modification of the silica surface*. Elsevier: Amsterdam (1995).
[131] Duffy, D. C.; McDonald, J. C.; Schueller, O. J. A.; Whitesides, G. M. *Anal. Chem.* 70, 4974 (1998).
[132] Ashurst, W. R.; Yau, C.; Carraro, C.; Maboudian, R.; Dugger, M. T. *J. Microelectromech. S.* 10, 41 (2001).
[133] Srinivasan, U.; Houston, M. R.; Howe, R. T.; Maboudian, R. *Transducers* (1997).
[134] Kessel, C. R.; Granick, S. *Langmuir* 7, 532 (1991).
[135] Chaudhury, M. K.; Whitesides, G. M. *Science* 255, 1230 (1992).
[136] Xie, Q.; Xu, J.; Feng, L.; Jiang, L.; Tang, W.; Luo, X.; Han, C. C. *Adv. Mater.* 16, 302 (2004).

[137] Li, H.; Wang, X.; Song, Y.; Liu, Y.; Li, Q.; Jiang, L.; Zhu, D. *Angew. Chem. Int. Edit.* 40, 1743 (2001).
[138] Gao, L.; McCarthy, T. J. *Langmuir* 23, 9125 (2007).
[139] Miwa, M.; Nakajima, A.; Fujishima, A.; Hashimoto, K.; Watanabe, T. *Langmuir* 16, 5754 (2000).
[140] Richard, D.; Quéré, D. *Europhys. Lett.* 48, 286 (1999).
[141] Yoshida, N.; Abe, Y.; Shigeta, H.; Nakajima, A.; Ohsaki, H.; Hashimoto, K.; Watanabe, T. *J. Am. Chem. Soc.* 128, 743 (2006).
[142] Sakai, M.; Song, J.-H.; Yoshida, N.; Suzuki, S.; Kameshima, Y.; Nakajima, A. *Surf. Sci.* 600, L204 (2006).
[143] Takeda, K.; Sasaki, M.; Kieda, N.; Katayama, K.; Kako, T.; Hashimoto, K.; Watanabe, T.; Nakajima, A. *J. Mater. Sci. Lett.* 20, 2131 (2001).
[144] Takeda, K.; Nakajima, A.; Hashimoto, K.; Watanabe, T. *Surf. Sci.* 519, L589 (2002).
[145] Tadanaga, K.; Morinaga, J.; Matsuda, A.; Minami, T. *Chem. Mater.* 12, 590 (2000).
[146] Notsu, H.; Kubo, W.; Shitanda, I.; Tatsuma, T. *J. Mater. Chem.* 15, 1523 (2005).
[147] Tourovskaia, A.; Barber, T.; Wickes, B. T.; Hirdes, D.; Grin, B.; Castner, D. G.; Healy, K. E.; Folch, A. *Langmuir* 19, 4754 (2003).
[148] Sapsford, K. E.; Ligler, F. S. *Biosens. Bioelectron.* 19, 1045 (2004).
[149] Chapman, R. G.; Ostuni, E.; Takayama, S.; Holmlin, R. E.; Yan, L.; Whitesides, G. M. *J. Am. Chem. Soc.* 122, 8303 (2000).
[150] Ostuni, E.; Grzybowski, B. A.; Mrksich, M.; Roberts, C. S.; Whitesides, G. M. *Langmuir* 19, 1861 (2003).
[151] Thorslund, S.; Nikolajeff, F. *J. Micromech. Microeng.* 17, N16 (2007).
[152] Kim, J.; Chaudhury, M. K.; Owen, M. J. *J. Colloid Interface Sci.* 226, 231 (2000).
[153] Cai, K. Y.; Frant, M.; Bossert, J.; Hildebrand, G.; Liefeith, K.; Jandt, K. D. *Colloids Surf. B* 50, 1 (2006).
[154] Zhang, X.; Bai, R. B.; Tong, Y. W. *Sep Purif Technol* 52, 161 (2006).
[155] Midwood, K. S.; Carolus, M. D.; Danahy, M. P.; Schwarzbauer, J. E.; Schwartz, J. *Langmuir* 20, 5501 (2004).
[156] Yu, X.; Wang, Z.; Jiang, Y.; Zhang, X. *Langmuir* 22, 4483 (2006).
[157] Huwiler, C.; Kunzler, T. P.; Textor, M.; Vörös, J.; Spencer, N. D. *Langmuir* 23, 5929 (2007).
[158] McGovern, M. E.; Kallury, K. M. R.; Thompson, M. *Langmuir* 10, 3607 (1994).

Curriculum Vitae

Name: Zimmermann

First Name: Jan-Helge

Date of Birth: August 15, 1975

Nationality: German

Education and Training:

10/03 – pres.	*PhD Program in Physical Chemistry*
	University of Zurich, Zurich, Switzerland
04/03	*Diploma in Interdisciplinary Sciences*
	ETH Zurich, Switzerland
10/02 – 02/03	*Diploma Work in Physical Chemistry*
	ETH Zurich, Switzerland
	Diploma Thesis: Single Molecules in Thin Crystalline Films
10/98 - 10/02	*Diploma Studies in Interdisciplinary Natural Sciences*
	ETH Zurich, Switzerland
02/96 - 01/98	*Education as Chemical Technical Assistant*
	Lette-Verein-Berlin, Germany
06/95	*Abitur*
	John-F.-Kennedy Highschool, Berlin, Germany
06/95	*High School Diploma*
	John-F.-Kennedy Highschool, Berlin, Germany

““Ducks!” he shoutet.

“What?”

“That’s what water slides off of!”” [7]

[7] The same demon, some considerable while later, in “Good Omens” by Terry Pratchet & Neil Gainman, HarperTorch, 1999